UNIVERSITY OF SOUTHAMPTON

Faculty of Engineering and Applied Science

Department of Electronics and Computer Science

A progress report submitted for continuation towards a PhD

Supervisor: Professor Steve Beeby

Supervisor: Dr Russel Torah

Microengineered ferroelectret materials for energy harvesting

By Mingming Zhang

05/2024

Abstract

Ferroelectrets are thin films of polymer foams which usually store charges in their internal voids and present a strong piezoelectric property after electrical charging. Ferroelectrets exhibit the similar piezoelectric properties, but the mechanism leading to those properties is completely different: in ferroelectrets, the properties is a result of deformation of charged voids, whereas piezoelectric materials rely on ion displacement in a lattice. For ferroelectrets, the interior voids contain opposite polarity charges on the top and bottom void surfaces and each void can be regarded as a dipole. When a ferroelectret material is compressed or expanded in its thickness direction, the dipole moments inside change in magnitude which leads to the changing of the compensation charge on the surface electrodes. Due to its outstanding piezoelectricity and material properties, ferroelectrets are widely utilized as functional materials in electromechanical sensors and actuators.

Compared with piezoelectric materials, ferroelectret materials have several advantages. First, they have a very prominent piezoelectric effect and their piezoelectric coefficient is several times higher than that of traditional piezoelectric materials. Secondly, their production cost is relatively low. Again, most ferroelectrets are mainly composed of non-toxic materials, which do not cause environmental pollution. In addition, a ferroelectret film is light, thin and very soft; it can be made into different shapes and sizes, according to need. Finally, the unique acoustic impedance of ferroelectret materials makes it more useful in areas such as ultrasonic waves and underwater acoustic wave detection. Therefore, ferroelectret materials show great potential in vibration energy harvesting applications.

Energy harvesting technology refers to collecting the energy from surroundings into electricity then supplying power to the system. The working principle of the piezoelectric vibration energy harvester is based on the piezoelectric effect of the piezoelectric materials. Under the action of the external vibration force, the piezoelectric layer in the device generates stress and strain, an electrical signal is formed. The piezoelectric energy harvester has the advantages of simple structure, long-life, high-energy density, and compatibility with the MEMS process.

Polydimethylsiloxane (PDMS) has been demonstrated in the fabrication of ferroelectrets with controlled void layouts and geometries rather than the random voids associated with foams. Its primary advantages include low cost, fast simple fabrication and high levels of flexibility. However, PDMS is not a stable electret material and the surface charge stability on the void surfaces of the PDMS is poor, causing the effective piezoelectric coefficient of most samples to fall below 10 pC/N in one month, therefore some approaches are necessary to extend the charge stability of the PDMS ferroelectrets or find a novel ferroelectret material suitable for achieving a high level of activity over a large period of time.

This report first focuses on some basic definitions and the background related to ferroelectret; This project also tries to use mathematical approach and simulation analysis to find an optimal cellular ferroelectret geometry structure with a high level of piezoelectric activity. This report presents approaches to enhance the surface charge density and stability of a PDMS based ferroelectret device by adding Polytetrafluoroethylene (PTFE) to the PDMS. This report also illustrates a new approach to obtain PDMS ferroelectret with random voids by using mechanical stirring to create cavities.

Contents

List of Figures

List of Tables

Declaration of Authorship

Print name: Mingming Zhang

Title of thesis: Microengineered ferroelectret materials for energy harvesting

I declare that this thesis and the work presented in it is my own and has been generated by me as the result of my own original research.

I confirm that:

1. This work was done wholly or mainly while in candidature for a research degree at this University;

2. Where any part of this thesis has previously been submitted for a degree or any other qualification at this University or any other institution, this has been clearly stated;

3. Where I have consulted the published work of others, this is always clearly attributed;

4. Where I have quoted from the work of others, the source is always given. With the exception of such quotations, this thesis is entirely my own work;

5. I have acknowledged all main sources of help;

6. Where the thesis is based on work done by myself jointly with others, I have made clear exactly what was done by others and what I have contributed myself;

7. Parts of this work have been published as:

Zhang, M., Shi, J., & Beeby, S. Improved Charge Density and Stability in PDMS Ferroelectrets Using PDMS/PTFE Composite Materials. *Sensors and Actuators A: Physical.*Volume, 364, 1 December 2023, 114763.

Zhang, M., Shi, J. and Beeby, S.P., 2019, December. Improved charge stability in PTFE coatings for PDMS ferroelectrets. In *2019 19th International Conference on Micro and Nanotechnology for Power Generation and Energy Conversion Applications (PowerMEMS)* (pp. 1-5). IEEE.

Zhang, M., Shi, J. and Beeby, S.P., 2021, December. A new approach for obtaining PDMS ferroelectrets with random voids. In *2021 IEEE 20th International Conference on Micro and Nanotechnology for Power Generation and Energy Conversion Applications (PowerMEMS)* (pp. 184-187). IEEE.

Signature: Date:

Acknowledgements

I am deeply grateful to my supervisor, Prof. Steve Beeby, Dr. Russel Torah, and my mentor Dr. Junjie Shi. They always supported and guided my research at the University of Southampton. I would like to express my gratitude to my internal examiner Dr. John Tudor.

I am also very grateful to my friends who have helped me a lot in life and in my studies.

Finally, I need to thank my parents for their support in getting me to this point.

Chapter 1

1. Introduction

1.1 Background

In recent years, there has been a rise in the demand for microelectromechanical systems and portable microelectronic devices [1]. The application of these devices has involved various aspects of industry and life. In terms of environmental applications, they can be used to monitor the ecological environment, water levels, crops and pollution. In the field of medicine and health, they can be used to monitor the health condition of patients or implantable medical equipment [1]. In addition, portable electronic devices such as mobile phones and computers have become an indispensable part of people's lives [1] [2].

One of the difficulties in the research on microelectronic devices is solving power supply problems. Depending on factors like location, volume and portability, power supply parts are required to have features such as small size, long working time and high integration. However, at present, most electronic devices still use batteries as power supply, resulting in problems such as limited-service life, difficulty in replacement (in some dangerous working area), and environmental pollution. For example, some large wireless sensor networks consist of hundreds or even thousands of nodes; regular battery replacement for these networks is prohibitively expensive and difficult to implement. This has led to the development of technologies for environmental energy harvesting and it is imperative to study new, environmentally friendly and renewable energy harvesters [3].

Energy harvesting technology presents a great potential in power supply applications. Energy harvesting is a process which can collect energy from human activities or the surrounding environment, then transform it into electrical energy to supply power for the system. The development of energy harvesting technology is closely related to the application environment and how energy is harvested. The energy conversion efficiency of different energy collection methods is also different. The essence of environmental energy harvesting technology is to convert various forms of energy—such as solar energy, thermal energy, vibration energy, etc.—that exist in the natural environment into electrical energy to provide power for electronic devices [4]. From Harb[5] and Ertuck[6], etc, it can be seen that environmental energy has a longer lifecycle than conventional battery energy. Among various kinds of environmental energy sources, the solar energy is strongly affected by the environment, the energy collection rate on cloudy days is less than half that on sunny days [6]. The disadvantage of the thermoelectric device is that the energy conversion density per unit volume is low (10%) when comparing with other energy conversion (solar power: 15% to 20%). Vibration energy is widespread in the existing environment, in addition to converting mechanical energy into electrical energy, it can effectively reduce vibration damage to the system structure in many situations [6].

The output power of the vibration energy harvesting device is typically between μW and mW, which can meet the power needs of low-power electronic devices such as wireless sensors. There are three typical methods for electromechanical energy conversion—electromagnetic induction, electrostatic conversion and piezoelectric conversion [7].

The electromagnetic induction technique is relatively well-established and the energy conversion efficiency is relatively high. However, it generates electrical energy through the relative movement of magnet and coil, so the structure is complex and the volume is large. Electrostatic conversion can directly generate power from 2V to several volts, which can be easily combined with MEMS. However, electrostatic conversion needs to control μm dimensions. Piezoelectric conversion does not require precise control. The piezoelectric material generates charge under the action of an external force. Piezoelectric energy harvesting devices have the advantages of simple structure, no heat generation, no electromagnetic interference, and are thus particularly suitable for various types of sensing and monitoring systems.

Since the discovery of piezoelectric phenomena at the end of the 19th century, its electromechanical properties have attracted the attention of a large number of researchers. Piezoelectric materials such as piezoelectric ceramics, piezoelectric single crystal materials, piezoelectric polymers and piezoelectric films, are widely researched in the energy harvesting field. For most research, the current focus is improving the energy density of piezoelectric materials. Due to the high piezoelectric coefficient and high energy output of lead zirconate titanate (PZT), this material is widely mentioned in many literatures [8]. For other research, piezoelectric polymers with lower Young's modulus, such as polyvinylidene fluoride (PVDF), have also been extensively studied due to the flexible and lightweight structure [9]. However, their piezoelectric coefficient and energy output are far less than those of PZT. Therefore, it is necessary to study and develop a new type of high energy output, lightweight and flexible energy harvesting material.

Ferroelectrets, also known as piezoelectrets, are thin films of, typically, polymer foams. Ferroelectret foams usually consist of a cellular polymer structure filled with air and present a strong piezoelectric property after electric charging. Compared with non-cellular polymer films, these new materials have the advantages of low density, low thermal conductivity, thermal insulation, and sound absorption [10] [11].

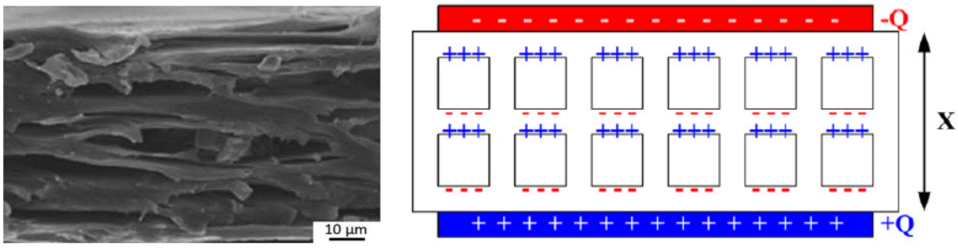

Figure 1. (a) SEM image of a cellular PP film [12], (b) Modelling schematic illustration [13]

Ferroelectrets are usually composed of gas-filled cell structures (Figure 1). The permanent dipole moments consist of positive and negative charges after poling, which are stored on the internal gas polymer interface, respectively [12]. Due to the combination of internal dipole moments and anisotropic cellular polymer structures, ferroelectrics exhibit a strong piezoelectric effect [14] [15] [16]. For most ferroelectric applications, the two outer surfaces of the electrical polymer foam should be metallized to form electrodes. In the process of ferroelectret compression, in order to keep the whole foam neutral, the electric field in the voids is compensated by the induced charge on the electrodes produced by the internal stored charge. It produces a large charge-space deformation when the polymer foam is compressed by mechanical stress. In other words, the distance between the positive charge and the negative charge decreases, resulting in a change in the dipole moment and the amount of compensation charge. If the electrode is short-circuited, the current will be generated [13].

In all ferroelectret materials, cellular polypropylene (PP) is the most investigated material due to its outstanding properties such as large piezoelectric coefficient (up to 600pC/N), light weight and low cost (comparing to piezoelectric materials) [12] [17] [18] [19]. The basic preparation and further optimization of PP foam, as well as the electromechanical performance of PP type ferroelectric sensor, has been extensively studied; several research groups have conducted experimental and theoretical studies on PP and achieved a very high piezoelectric coefficient. PP ferroelectric has been developed for commercial applications such as motion sensors and pressure sensors for different purposes [18].

Polydimethylsiloxane (PDMS) has been demonstrated in the fabrication of ferroelectrets with controlled void layouts and geometries rather than the random voids associated with foams [20]. Its primary advantages include low cost, fast simple fabrication and high levels of flexibility with a Young's modulus that can vary from 0.57 MPa to 3.7 MPa depending upon the degree of cross-linking [21]. However, PDMS is not a stable electret material and the surface charge stability on the void surfaces of the PDMS is poor [22].

In contrast, Polytetrafluoroethylene (PTFE) exhibits excellent charge stability over time [23]. However, PTFE is not as soft or flexible as PDMS and is difficult to mold and shape mechanically. PTFE is typically processed as a powder rather than as a standard plastic, often using compression molding techniques or with the powder mixed with dispersants and applied as a coating by film casting [24]. The effect of adding PTFE particles to PDMS had been described in previous studies [25]. PTFE is a fluorocarbon and, since fluorine is the most electronegative element, PTFE will accept more electrons than PDMS [26]. Therefore, more electrons can be trapped on the surface of the PTFE particles, and as the ratio of PTFE particles within the PDMS increases, the surface charge density of the PDMS/PTFE composite will also increase [27].

This paper explores measures to combine PTFE in the form of a powder with the PDMS to improve the charge stability in the ferroelectret whilst retaining the compliant, flexible mechanical properties of the PDMS. This report also illustrates a new approach to obtain PDMS ferroelectret with random voids by using mechanical stirring to create cavities.

1.2 Aim of this work

This work first tries to verify the results of previous work in the group and external published work, including the fabrication procedures of PDMS ferroelectrets and the related results.

Secondly, this work will use mathematic approach and simulation analysis to find an optimal cellular ferroelectret geometry structure with a high level of piezoelectric activity.

The piezoelectric coefficient of existing Polydimethylsiloxane (PDMS) ferroelectrets [13][20] present a downward trend with time (usually drop very fast in several days after charging), which is a serious limitation. This situation is caused by the escape of inner charges. As a result, the main purpose of this project is to use different approaches to extend the charge stability of the PDMS ferroelectrets or find a novel ferroelectret material suitable for achieving a high level of activity over a large period of time (more than 10 years) to replace the traditional batteries.

This project also focusses on a new approach to obtain PDMS ferroelectret with random voids to find a fast, easy and cost-effective way to make PDMS ferroelectret.

1.3 Outline of the report

Chapter 2

Chapter 2 will describe the literature and is divided into three main parts: introduction of piezoelectric effect, electret and ferroelectric effect, some fundamental background of ferroelectret materials, the vibration energy harvesting and the charge decay mechanism of electret.

Chapter 3

In this part, a simplified ferroelectret cellular model is discussed. ANSYS is used to explore the relationship between piezoelectricity and the geometry structure.

Chapter 4

This chapter will introduce the manufacturing process of PDMS ferroelectret, and different charging processes and parameters (time, voltage and distance) will be applied to find the optimal condition. The different term time of piezoelectric coefficient also be measured to verify the result in the literature.

Chapter 5

This chapter will illustrate and compares approaches to enhancing the surface charge density and stability in PDMS ferroelectrets. Different approaches to adding the PTFE particles to the ferroelectret structure will been explored.

Chapter 6

This chapter will illustrate a simplified method to obtain PDMS ferroelectrets containing a large number of random voids formed using a high-speed stirring process.

Chapter 7

According to the conclusions we drawn in each chapter, a summary of the advantages and shortcomings of the existing materials and processes is presented; future work for the next research years is also discussed.

Chapter 2

2. Literature review

2.1 Introduction

This literature review aims to provide a background of the electret, ferroelectret and the energy harvesting techniques in human body. This review includes ferroelectret properties and fabrication methods as well as looking at examples of the state of the art in human body energy harvesting applications.

2.2 Electret

Electrets are the solid-functional dielectric materials that can store long-term dipoles and space charges, that is, the damping time constants (corresponding to the lifespan of the storage charge) of these materials is longer than the formation time [27]. Although the term “electret” is not as widely known as “magnet”, there are many devices in our daily life that are closely related to it. The electret produces a polarization effect under the action of an external electric field. The electret with good performance can still retain its polarization state for a long range and is difficult to be affected by the external environment following removal of external electric field.

Electret can be prepared by multiple methods, such as corona charging, thermal polarization, photo polarization and magnetic electret [29]. At present, corona charging and thermal polarization methods are in common use, of which corona charging is to bombard the dielectric material with air ionization caused by high-voltage electric field or ion beam produced by breakdown to deposit the ion beam on or near the surface of the dielectric. Electrets with high surface charge density can be made by corona charging. Another common method is thermal polarization. Under the condition of high temperature, high voltage is applied to the dielectric material, which makes the molecular dipoles in material arrange in an orderly manner. By maintaining the electric field, the material is cooled to promote the capture of space charge and freeze the molecular dipole. Early electrets were prepared by thermal polarization.

In 1732, Gary discovered that materials such as rosin, sulphur, and wax have a strong chargeability and studied the electrostatic attraction between them. A century later, in 1839, Faraday [30] proposed the term "dielectric" and described electret as “that which retains an electric moment after the externally-applied field has been reduced to zero”. Faraday believes that under the action of an electric field, there may be two different polarities of charges penetrating into the dielectric, but these charges cannot be moved by large distances. In turn, the British scientist Heaviside [27] started the analogy of dielectric and magnetic in 1885 and proposed the hypothesis of permanent polarization of the dielectric. The above dielectric was defined as “electret” referring to the term “magnet”. In 1919, Japanese researcher Eguchi [27] prepared the world’s first artificial electret through thermal polarization method. At the same time, he pointed out that the charge adjacent to electrodes in the material exhibits the same or opposite polarity as the electrode. These charges are named by Gemant [27] as the homocharge or heterocharge. In his paper, Eguchi called the permanently polarized dielectric as "electret." Since then, the term “electret” has been widely accepted by the world.

2.2.1 The performance of electret

The electret is fundamentally featured with its charge storage performance. According to the different types of stored charge, the charge in electret can be divided into dipole charge and space charge. The dipole charge is formed by applying an electric field to electret material at high temperature to cause the orientation of a large number of dipoles. The space charge is formed by injecting charge carriers directly into the electret material. The injection modes can be directly contacting electrode, or making air and other media produce ionization by corona charging and electron beam irradiation, and the ions can be deposited on and near the surface the surface of material or deep in the body under the action of electric field. According to whether the polarity of surface charge of electret is consistent with that of the applied electric field, the charge in electret can be classified into homocharge and heterocharge, as shown in Figure 2.1 [27].

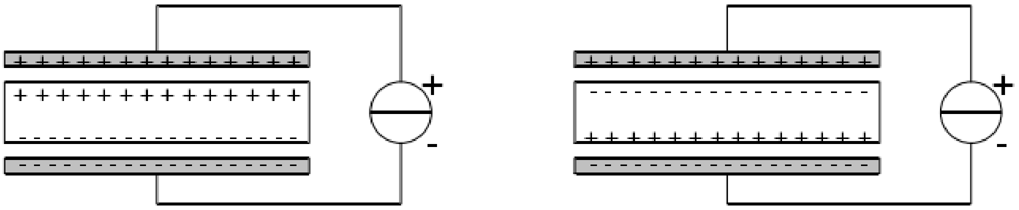

(a) homocharge (b) heterocharge

Figure 2. Homocharge and heterocharge

Electret material can store the charge for a long period, and without metal electrode, it forms an electrostatic field in the surrounding space. When electrode enters the field, the induced charge will produce on the electrode, which is the electrostatic effect of this material. Both electret microphone and electret micro-generator make use of the effect [28~30].

2.2.2 Electret materials

The definition of modern electret was given by Brazilian scientist Gross [31]. He believes that the orientation of the molecular dipole and the space charges injected from the electrodes are two basic ways of forming the electret; the latter present the same physical process that Faraday described 100 years ago, while the former lead to the formation of different polarity of charges. Since then, the research area of electret has been extended. Nowadays, electrets are always associated with fluorocarbon polymer films, which mainly contain long lifespan space charges. They have excellent mechanical properties and flexibility and the application prospect is broad. Prof. Sessler from Germany and Prof. West from the U.S. first proposed the idea of using polymer film electrets to develop acoustic sensors. In 1962, Bell Labs developed the world's first polymer film electret microphone as shown in Figure 3 [32]. The new type of acoustic sensor they developed was first put on the market by Sony Corporation of Japan in 1968. It is estimated that in recent years, the world's annual output of this acoustic sensor has exceeded 2.5 billion; this is one of the most important applications of electrets. Some electret materials and its properties are present in the Table 1 [32-34].

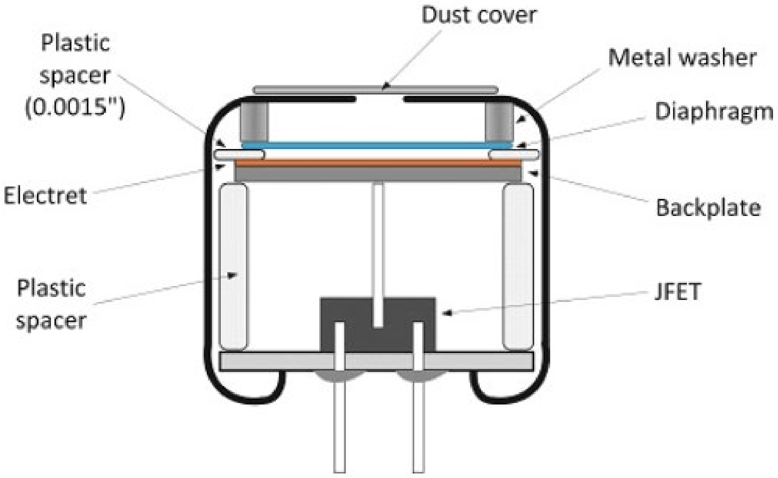

Figure 3. The acoustic sensors developed by polymer film electrets to develop

Table 1. The properties of some electret materials [32-34]

Category	Materials	Properties	Applications
Real-charge electrets	FEP, SiO_2	External electric field and force	Electret microphones, head-phones, air filters, dosimeters
Cellular and porous electrets	PP, PTFE	Strong longitudinal piezoelectric effect	Loudspeakers, ultrasonic transducers, hydrophones

Electret can also be divided into two categories: inorganic electret and polymer-based organic electret. Inorganic electret materials mainly include amorphous silicon nitride (Si_3N_4) films, amorphous silicon dioxide (SiO_2) films, SiO_2/Si_3N_4 bilayer films and other inorganic electret materials. The preparation technique of SiO_2 electret and SiO_2/Si_3N_4 electret is compatible with the processing of Micro-Electro-Mechanical System technology (MEMS). Therefore, compared with other types of electrets, SiO_2 electrets and SiO_2/Si_3N_4 electrets have apparent advantages in the preparation of micro electret sensors [32].

Polymer-based organic electrets mainly refer to polymer materials containing aromatic groups, alkyl groups or halogens, which are all compounds with high molecular weight polymerized by one or more simple low molecular weight compounds. We can understand the polymer from two levels. From the microscopic view, it refers to the molecular structure of the polymer, including its chemical composition and chain structure. Different polymers generally have various monomer types. For example, polyethylene has a relatively simple structure and is composed of repeated arrangements of -CH2- groups. In addition, there are many connection ways for monomers to form macromolecules, and the polymers formed by different connection modes are different in properties. The macrostructure of polymer refers to the spatial structure characteristics of the macromolecules that composes the polymer in the material. For example, the macromolecular chain skeleton can be linear, reticular, branched chain and other geometric shapes. Polymer materials generally include crystalline or amorphous structures, or both. Crystalline structures are usually formed by macromolecules with strong intermolecular forces and simple molecular structures, while amorphous structures are usually produced by macromolecules with complex structures. The macromolecular chains of crystalline polymer materials are arranged in parallel, so they show the characteristics of anisotropy. The molecular of amorphous polymers is not arranged in long-range order, and the macromolecules show irregular arrangement, so they present the characteristics of isotropy. Most polymer materials contain both amorphous and crystalline structures [33].

According to the nature and function of the material, polymer electret films are generally divided into three categories [32~34]:

(1) Highly insulating fluoropolymer electret materials, mainly including Petrafluoroethylene-per-fluoromethoxyethylene copolymer (referred to as PFA), polychlorotrifluoroethylene (referred to as PCTFE), Tetrafluoroethylene-hexa-fluoropropylene copolymer, (FEP), Ploytetrafluoroethylene (PTFE), etc.;

(2) Polar polymer materials, mainly including poly (vinylidene fluoride) (PVDF), Copolymer of vinylidene fluoride trifluoroethylene (P(VDF/TrFE)), Copolymer of vinylidene fluoride tetrafluoroethylene (P (VDF/TFE)), etc.;

(3) Non-fluoropolymer electret materials, mainly including polyethylene (PE), polypropylene (PP), polyimide (PP), parylene Polyethylene terephthalate (PET), etc.

2.2.3 The applications of electret

Electrets have a wide range of applications. Electret capacitive microphone mostly refers to thin film electret capacitive microphone, generally using FEP or PTFE as material. The microphone has stable sensitivity and frequency characteristics, its small size (diameter from a few millimeters to 2 inches), low cost and high sensitivity, which makes it an important component in the field of consumer electronics. It is widely used in professional sound measurement systems, telephones, hearing aids, professional audio recordings, games and toys [35][36]. Electret micro-generator is a research focus at present, and is manufactured by MEMS technology in general. The preparation technology of silicon-based electret materials such as SiO_2 and SiO_2/Si_3N_4 is well compatible with the processing of MEMS technology, thus the materials are widely used in the fabrication of micro-generators [37]. On the other hand, organic electret material that is based on polymer film has higher surface charge density and better stability, and the micro generator using polymer film will have higher output power [38][39]. The piezoelectric electret material like PVDF has high sensitivity, good flexibility, wide frequency response range, good impedance matching and low noise. Therefore, piezoelectric electret materials can be used in the field of physical quantity measurement, and the measurement of mechanical strain, acceleration and structural vibration [39]. Thanks to good biocompatibility, no cytotoxicity and obvious bacteriostatic ability, electret materials such as FEP and PTFE also can be used in biomedical research [40]. In addition, they are widely used in electrostatic copying, air filtering and other fields.

Piezoelectret is electret-based piezoelectric polymer with a foamed structure. Piezoelectret has been used to harvest vibrational energy, human motion energy and sound energy. The vibrational energy harvesters based on piezoelectret are utilized to harvest medium frequency vibrational energy generated by factory machines, aircrafts, automobiles, and so on. Human motion energy harvesters are generally used to power wearable sensors [41]. These applications will be described in detail in later chapters.

2.3 Ferroelectret

Piezoelectrets are polymer-foam based space-charge electrets with strong piezoelectric effect.

Since it has the characteristics of both a piezoelectric material and an electret. It is named piezoelectret, also known as ferroelectret.

Piezoelectricity is a description which presents the relationship between pressure and electricity. According to Jaffe [21], piezoelectricity, also known as the piezoelectric effect, is ‘the ability of certain crystalline materials’ which can transform ‘an electric charge proportional to a mechanical stress’. This phenomenon was first found by French J. and P. Curie in 1880 [22][23]; they occasionally put several stones on top of quartz crystals and found the existence of ‘electric charge’ in the quartz. Continuing with the research, these brothers found that the amount of charge regularly changed with the mass of stones. This phenomenon presents the relationship between ‘mechanical stress’ and ‘electrical charge’ in piezoelectric materials, which normally presents a proportional relation. In the following decades, with the application of piezoelectric mechanism in many different areas, piezoelectric effect was widely discovered in many solid materials (such as crystals, ceramics, and so on) [24][25][26]. Studies on piezoelectric materials are increasing enriching their application and improving these properties.

The piezoelectric effect is well understood and is classified as two types: direct piezoelectric effect and indirect piezoelectric effect. Direct piezoelectric effect is the internal electrodes polarization of piezoelectric materials when external force is applied on the surface of the materials. On the contrary, indirect piezoelectric effect is the process regarding to the applied electric field may cause mechanical force. The more general situation is: when the force is expressed as a vibration, the piezoelectric materials will generate a current due to the direct piezoelectric effect. Similarly, when applying a high-frequency electrical signal to piezoelectric materials, these materials will create a high frequency acoustic signal (also known as ultrasound signal— a kind of mechanical shock) because of indirect piezoelectric effect. Figure 4 gives us the mechanism of the direct piezoelectric effect (a) and indirect piezoelectric effect (b). Piezoelectric coefficients are used to describe the strength of the piezoelectric effect.

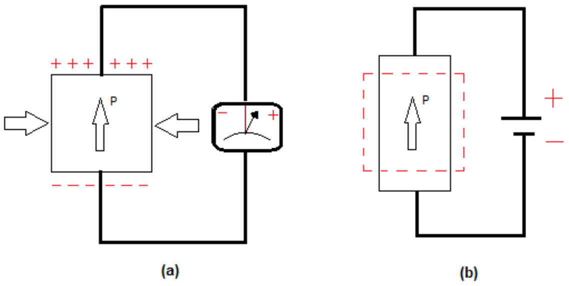

Figure 4. The mechanism of direct piezoelectric effect and indirect piezoelectric effect

The development of ferroelectret materials began in 1990. At the time, Kari Kirjavainen [43] and his colleagues at Tampere University of Technology, later at the Technical Research Centre of Finland (VTT), performed the first corona-charging experiments on cellular films which made by standard plastics as polypropylene [43], and finally found that this kind of porous polymer film has a prominent piezoelectric effect.

In 1999, the International Symposium on Polar Materials was held in Delphi, Greece. Some research teams reported the theoretical and experimental research progress of ferroelectret materials [44]. Since then, ferroelectret materials have attracted experts in various fields of research. It involves many branches of academic knowledge, including physics, chemistry, dynamics, materials science and engineering.

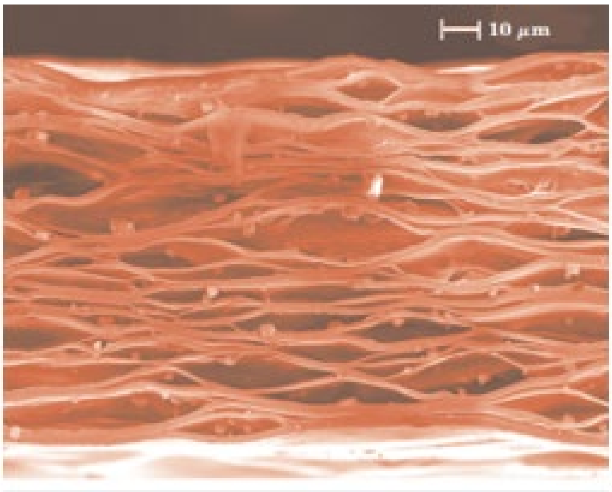

Figure 5. A cellular polymer with oval-shaped voids structure [45]

Ferroelectret material is a polymer film with oval-shaped voids structure, as shown in the Figure 5 [45]. The thickness of the film is about several ten to one hundred micrometres, and the thickness of the void is about ten micrometres. After charging, the upper and lower inner surfaces of the voids are full of electric charges with same magnitude but opposite polarity (as present in the Figure 6). Then the upper and lower surfaces of the film are plated with electrodes and finally, a ferroelectret material is made. Because of its outstanding piezoelectric properties, it is also called piezoelectret.

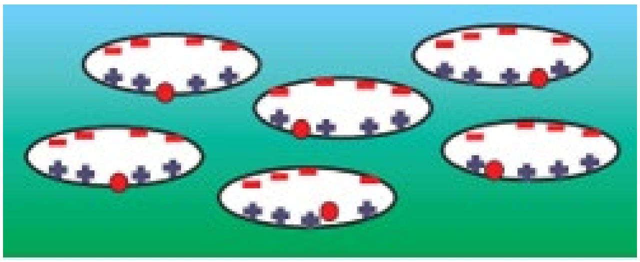

Figure 6. A cellular polymer after charging [45]

Ferroelectrets have the basic characteristics of electret materials, that is, the ability to store charges for a long term [44]; the charges in the void exists stably for a long time at room temperature. Under the action of external voltage, there is an S-shaped circuit between the electrical displacement D and the external voltage V, as shown in Figure 7. This S-shaped circuit is similar to the relationship between the magnetic induction intensity and the magnetic field strength of a ferromagnetic material; so, this material is called ferroelectret.

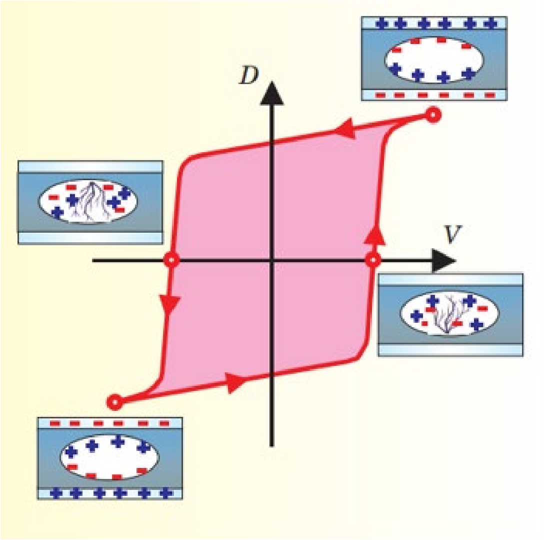

Figure 7. The S-shaped circuit of ferroelectret [45]

The reason why ferroelectret has a hysteresis loop is that when the external voltage increases to a certain value, the electric field strength inside the voids exceeds the breakdown electric field strength of air, and the air in the voids of the ferroelectret is broken by the electric field at this time. The charges with opposite polarity move in the opposite direction under the action of the external electric field, and finally adhere to the inner wall of the voids. The direction of electric field induced by the charges in the voids is opposite to the electric field of the external voltage, so that the actual electric field in the voids is lower than the critical electric field of the air inside the voids, and the breakdown is terminated [46].

Compared with traditional piezoelectric materials, ferroelectret materials have a number of advantages. First, it has a very prominent piezoelectric effect, and its piezoelectric coefficient is several times higher than that of traditional piezoelectric materials. Secondly, its production cost is relatively low, so it has a price advantage. Again, most ferroelectrets are mainly composed of non-toxic materials, and the most common preparation material is the porous polypropylene film, which does not cause environmental pollution. In addition, ferroelectret film is light, thin, and very soft and can be made into a variety of shapes and sizes according to need. Finally, the unique acoustic impedance of the ferroelectret material makes it more advantageous in areas such as ultrasonic waves and underwater acoustic wave detection [47].

Due to these advantages, ferroelectret materials are widely concerned by researchers in various fields. For a long time, the researchers around ferroelectret materials have mainly focused on the following aspects [47~49]:

1. The fundamental mechanism of the piezoelectricity of ferroelectret materials;
2. How to improve the piezoelectricity of ferroelectret;
3. How to improve the thermal stability of ferroelectret materials;
4. The material preparation of ferroelectrets;
5. The measurement and characterization of ferroelectret materials;
6. The application scalability of ferroelectret materials.

In the past decades, the study of ferroelectret materials has made significant progress. The understanding of the piezoelectricity of ferroelectret has been explored in depth, from qualitative analysis to quantitative research gradually. The preparation method of ferroelectret has also been greatly improved, the piezoelectricity and thermal stability of ferroelectret materials had significantly improved as well. In addition, ferroelectret made by different materials have also been prepared experimentally to study their piezoelectric properties and thermal stability. Various applications of ferroelectret materials are illustrated constantly, showing the broad application prospects of ferroelectret materials.

2.3.1 The mechanism of ferroelectret

Compared with traditional piezoelectric materials such as quartz crystals, piezoceramics and ferroelectret polymers, ferroelectret polymer films present a more pronounced piezoelectric effect. Table 3 describes the piezoelectric coefficient d_{33} of these four materials [45].

Table 2. Piezoelectric coefficients of several useful materials [45]

Piezoelectric material	$\mathbf{d_{33}(pC/N)}$
Quartz (silicon dioxide)	2
Lead zirconate titanate (PZT-4)	295
Polyvinylidene fluoride (PVDF)	20
Cellular polypropylene [17]	600

The large differences of piezoelectric coefficient presented in the table are related to their different piezoelectricity mechanisms.

For ferroelectret materials, the upper and lower surfaces of each void are holding charges with opposite polarity after poling, which can be treated as a dipole, as shown in Figure 6. And for the normal ferroelectric polymers PVDF, the dipole moment comes from molecular dipoles [45]. Under the influence of external force or electric field, due to the softness in the thickness direction, the voids of the ferroelectret are more likely to be deformed, and therefore its piezoelectric coefficient is much larger than normal ferroelectric polymers.

In addition, the macroscopic piezoelectric effect of ferroelectret and ferroelectric polymers is different. When a tensile stress is applied in the thickness direction, the thickness of these two materials will increase. For ferroelectret, the thickness increase mainly occurs by the deformation of the voids, therefore the dipole moment will increase, and the induced charge on the electrode will increase as well, so the piezoelectric coefficient is positive. And for ferroelectric polymers, because the interaction between the long chains of the polymer is much less than the effect of the covalent bond in the chains, the deformation is mainly due to the structure change of the long chains of the polymer, resulting in a lower density of the dipoles. And the relative displacement of the positive and negative charges inside the dipole is very small—the dipole moment can be considered as unchanged—so finally the induced charges on the electrode will decrease and the resulting piezoelectric coefficient will be negative. The macroscopic piezoelectric effect of ferroelectret is similar to that of quartz ceramics and piezoelectric ceramics (PZT), but their microcosmic mechanisms are completely different. The former is due to the deformation of charged voids, and the latter is due to the relative shift of ions on the crystal lattice [45].

2.3.2 Formation method of ferroelectret

The conventional method for the formation of micropores inside piezoelectret films is melt foaming. As shown in Figure 8, melt foaming is the stretching of a polymer with organic or inorganic particles added at melt temperature [50]. Due to the large difference in mechanical properties between the electret film and the added particles, flattened lenticular micropores are formed inside the film during the stretching process. The formation of micropores can also be achieved by chemical or physical methods. Chemical foaming uses the thermal decomposition of the blowing agent at high temperatures to produce gas and form a microporous structure; physical foaming generally uses a high-pressure inert gas as the blowing agent, which dissolves the physical blowing agent into the polymer matrix in a saturated state, and then creates pores by rapid external pressure relief. Compared to chemical foaming, physical foaming is usually more environmentally friendly because it does not use chemicals that pollute the environment [50].

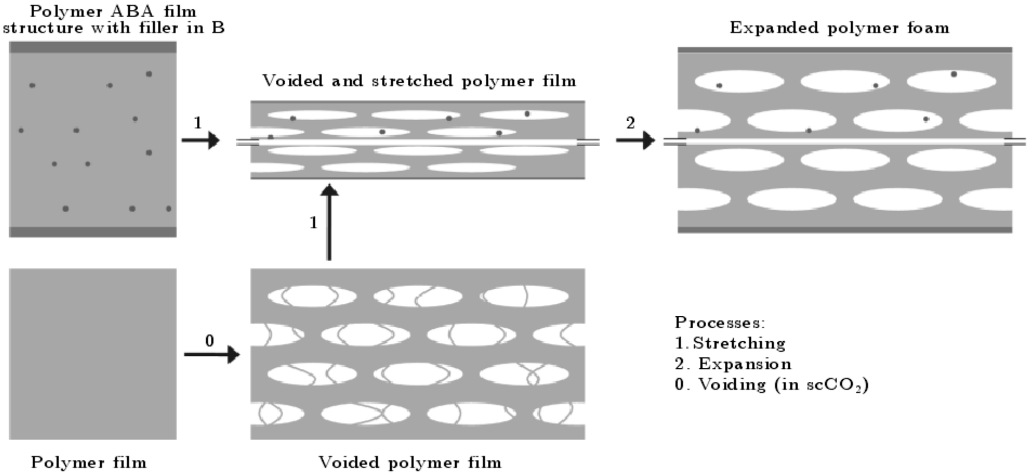

Figure 8. Schematic diagram of preparation of cellular piezoelectrets based on melt stretching (top) and foaming agent foams (bottom)processes [50].

Obviously, it is difficult to achieve fine tuning of the microstructure of the films by the above-mentioned preparation processes. Since the pore shape, size and porosity of piezoelectret films have a significant effect on the piezoelectric activity [48], many research groups have worked on the preparation of piezoelectret films with controlled microporous structures. Two samples of FEP films with circular electrodes on one side were stacked together and placed in a mould (with a vacuum chamber on one side) and heated to about 200°C. Since the temperature used is much lower than the melting temperature of FEP, the adhesion between the two layers is mainly based on electrostatic forces. A schematic diagram of the sample obtained in the above way is shown in Figure 9.

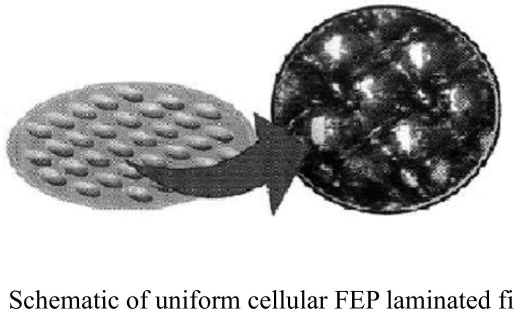

Figure 9. Schematic of uniform cellular FEP laminated film [51].

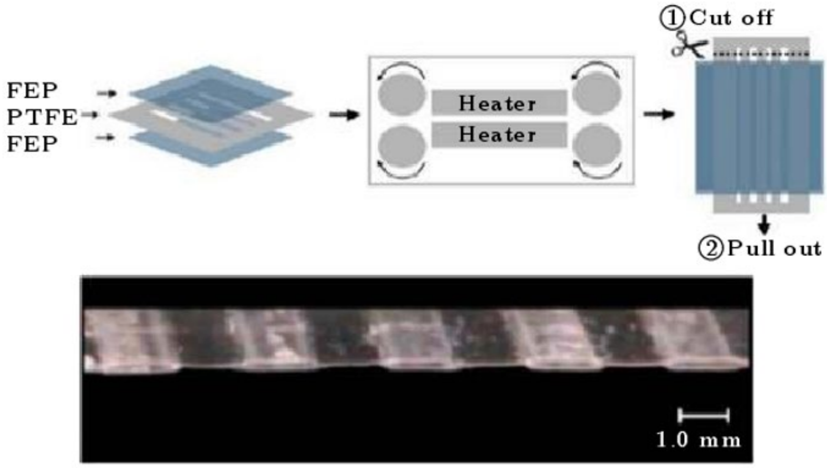

Figure 10. The schematic illustration of the fabrication process with a PTFE template with parallel rectangular openings to prepare a two-layer FEP film with tubular channels and the SEM image of the air voids [52].

In 2009, Altafim et al [52] developed another template method for the preparation of tubular channel FEP composite films: a PTFE template with multiple parallel rectangular openings (1.5 mm*30 mm) was prepared by laser cutting and then inserted into two layers of FEP films and heated to 300°C under pressure. After cooling, the FEP films at the rectangular openings of PTFE are fused together. Due to the anti-adhesive property of PTFE, the PTFE template can be easily removed after one end is cut, and the FEP laminated film with tubular channels is obtained as shown in the scanning electron micro-scope (SEM) image in Figure 10 [52].

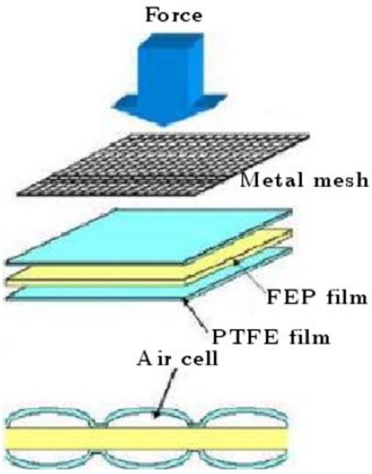

Figure 11. The schematic of PTFE-FEP-PTFE laminated film prepared by metal mesh patterning [53].

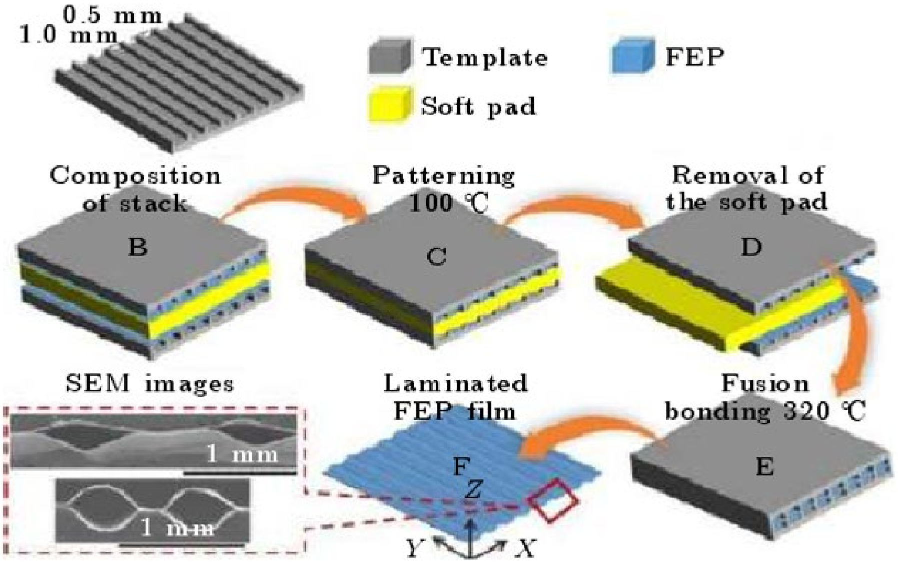

Figure 12. The schematic of template patterning fabrication process of FEP laminated film with parallel-tunnel structure [54].

Zhang et al. have proposed grid embossing [53] and stencil embossing [54] since 2006. As shown in Figure 11, the grid imprinting method consists of alternating layers of FEP and PTFE films on a flat plate and then bonding the multilayers at high temperature by applying force through the grid. Under the action of the grid, the FEP and PTFE films in the grid region are firmly bonded together at high temperatures, while a certain amount of gas remains between the films in the grid region, thus forming a microporous structure between the stacked films [48]. This process can be used to artificially regulate the microporous structure by changing the structural parameters of the grid. In addition, another stencil imprinting method can be used to regulate the microporous structure, and ordered microporous structure films with square pore arrays [55][56], circular pore arrays [57], cross tunnelling [58] and parallel tunnelling (Figure 12) [54] have been obtained. A soft pad is sandwiched between two stencils with parallel groove structure, and a layer of FEP film on the top and bottom surface of the pad (Figure 12-B), which is hot pressed as a whole (Figure 12-C), and then the pad is removed (Figure 12-D). The stencil was clamped symmetrically to thermally bond the contacting parts of the two FEP films at high temperature (Figure 12-E), and the stencil was removed after the temperature dropped to room temperature to obtain a FEP film with a parallel tunnel structure (Figure 12-F).

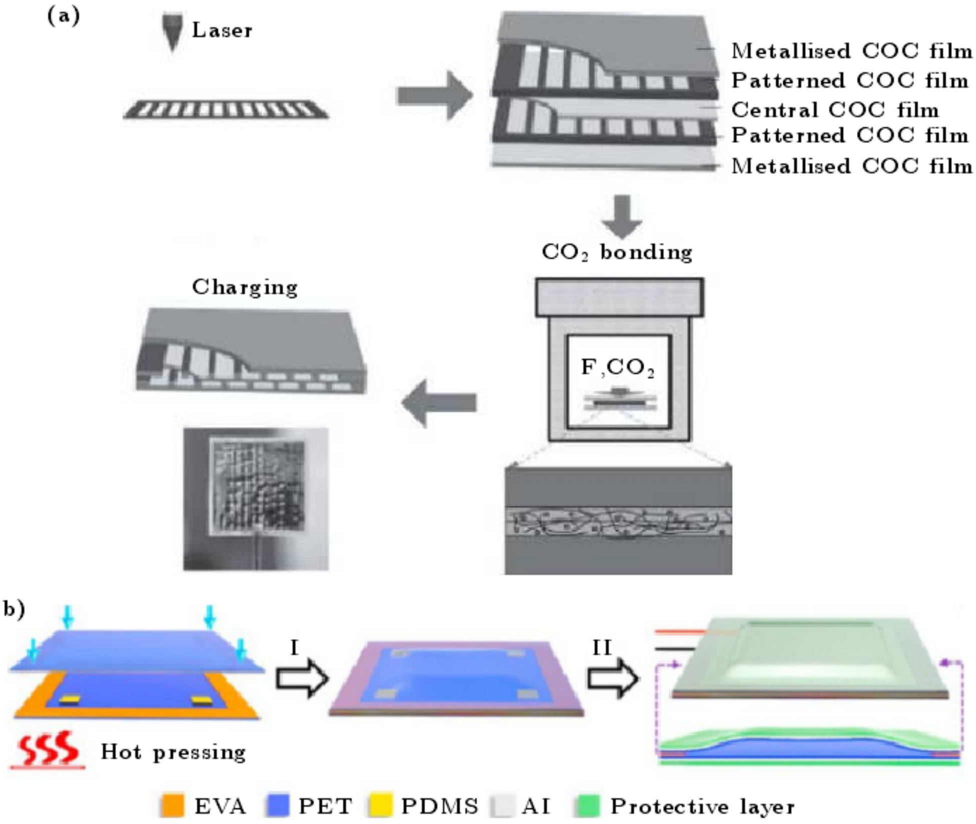

Figure 13. Schematic preparation process of other typical cellular piezoelectrets:(a) Schematic of COC laminated film prepared by supercritical CO2-assisted low temperature assembly method [59]; (b) schematic of preparing arched bubble PET/EVA/PET composite film.

Li and Zeng [59] reported a supercritical carbon dioxide (CO_2)-assisted low-temperature preparation of rectangular channel COC laminates. As shown in Figure 13(a), two layers of COC films were laser etched to form an array of rectangular channels, which were then stacked alternately with three other layers of normal COC films. The layers were bonded to each other at a temperature of 120°C with the assistance of supercritical CO_2. Kachroudi et al [60,61] proposed a low-cost microcavity mold: the mask was attached to a photosensitive film (Riston MM540) and cured in a UV lithography system, where the photographic film was developed into a cylindrical array mold of a certain size. A porous polydimethylsiloxane (PDMS) film was prepared on the mold by spin-coating, and then alternately laminated with two others dense PDMS layers and bonded by plasma bonding technique to form a porous structure. The piezoelectric electret was prepared by a hot-pressing method. As shown in Figure 13(b) [62], a ring-shaped EVA adhesive layer, called EVA/PET laminate, was applied at the boundary of the flexible PET electret film. Four PDMS films are fixed on the four corners of the EVA/PET laminate as spacers, and then another EVA/PET laminate is placed on the top and bonded by hot pressing to form an arch-shaped air-gap PET/EVA/PET laminate with a height of 0.5-1 mm.

The above laminated film is polarized to obtain a bipolar piezoelectric electret. In addition, some progress has been made in the study of unipolar piezoelectret electrodes [63][64]. In 2014, Rychkov et al [63] proposed and prepared unipolar piezoelectret for the first time, and in 2019, Ma et al [64] used unipolar FEP piezoelectret for vibrational energy harvesting studies for the first time. Since the polarity of the charge can be selected, unipolar piezoelectret materials can have better thermal stability. The experimental results showed that the surface potential of the sample remained more than 80% of the initial value when stored at room temperature for 8 days.

In 2014, a PDMS ferroelectret is fabricated as presented in reference [65]. First liquid PDMS and curing agent (Sylgard 184 from Dow Corning, MI, USA) should be mixed at a 10:1 weight ratio. Then this mixed gelatinous liquid will be degassed in a vacuum desiccator. Then the degassed PDMS was poured into the moulds and were degassed again and then baked at 80 °C in the oven for two hours. The PDMS in the moulds should be at a suitable fluid level when pouring, which may affect the thickness of samples. After the PDMS in the moulds was dried, the polymerized PDMS was detached from the moulds. An oxygen plasma treatment was applied to bond the two PDMS parts together. The bonded PDMS was then baked in oven at 80 °C for 1 hour. The schematic of PDMS casting and bonding processes, and the final bonded sample by plasma treatment are illustrated in Figure 14. Figure 15 shows the SEM image of cross-section view of single layer PDMS ferroelectret foam.

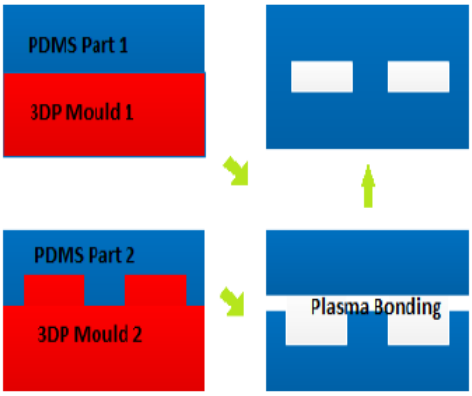

Figure 14. The fabrication processes of PDMS ferroelectret [65]

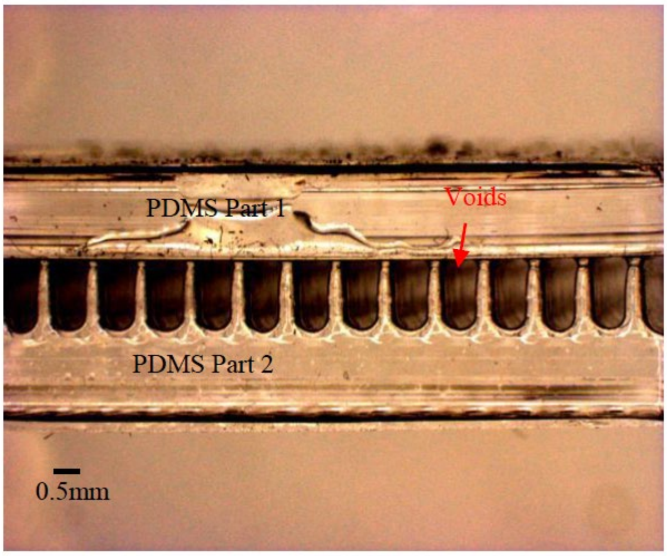

Figure 15. Image of cross-section view of single layer ferroelectret foam [65]

2.3.3 The electrical charging of ferroelectret materials

The polarization of the cellular polymer film is an important step in the formation of ferroelectret material. Corona charging is the more commonly used method, and the experimental device is shown in Figure 16 [68]. The cellular polymer film is placed on a metal plate as an electrode, and a certain distance of 3 cm is maintained between the pin and the plate. Applying a very high voltage to the needle, such as 30 kV, for a certain period of time, such as 120 seconds, completes the charging process. Finally, depositing electrodes on the upper and lower surface of the film, such as a 50 nm aluminium, completes the preparation of the ferroelectret.

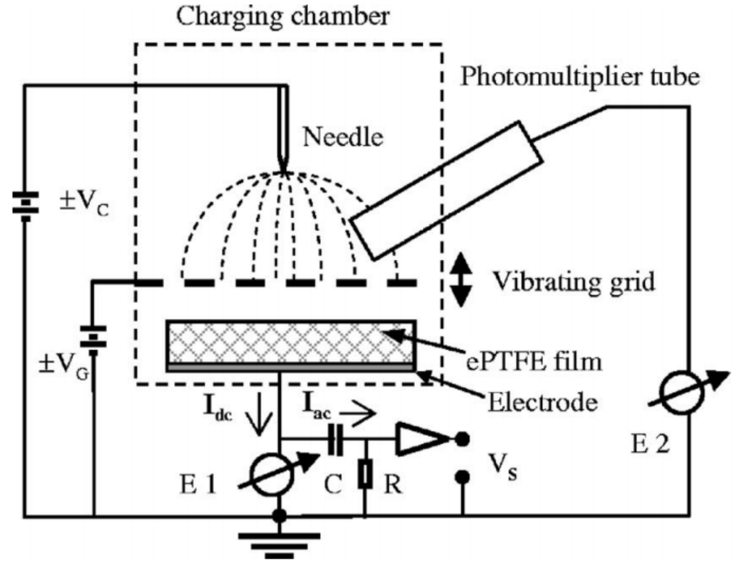

Figure 16. The experimental device of corona charging [68]

In addition to corona charging, there are other charging methods such as electrode charging and electron beam charging. For the electrode charging method, firstly the upper and lower surface of the ferroelectret film is plated with electrodes, and then a very high electric field is applied between the two electrodes. A strong electric field is formed in the voids of the polymer, which causes the breakdown of air in the voids and eventually forms charges with opposite polarity in the surface of the voids. Therefore, the basic mechanism of electrode charging is the same as that of corona charging. For electron beam charging, although the mechanism is different from the first two methods, the resulting charged void structure is similar.

According to experimental research, the thickness of ferroelectret film is usually reduced after the charging process [66]. Therefore, the optimal method is processing the expansion treatment by high pressure gas again when finishing the charging process of the ferroelectret film; this can further improve the coupling between the electrical and mechanical properties.

2.3.4 Some typical ferroelectret materials

Ferroelectret not only has a strong piezoelectric effect equivalent to ceramic materials, but also has the characteristics of low acoustic impedance, flexibility, low density, environmental friendliness, large-area film formation, and low cost [69], has great potential in piezoelectric energy harvesting. The most studied and most common piezoelectric electrets are bipolar piezoelectrets based on non-polar polymers, including polypropylene (PP) [70, 71], polytetrafluoroethylene (PTFE) [72,73], fluorinated polyethylene propylene (FEP) [74], cyclic olefin copolymer (COC) [75], polyethylene naphthalate (PEN) [76] and other ferroelectret.

Polypropylene (PP) is a thermoplastic resin and prepared by the polymerization of propylene. PP have a strong impact strength and the impact strength of PP increases by the ethylene content. Due to the high degree of crystallinity, the surface stiffness and scratch resistance of this material is outstanding. This material is mainly used in the field of household appliances, plastic pipes and high permeability areas.

PP film has a very high piezoelectric activity, but because of the limitation of its charge thermal stability, its operating temperature is generally not more than 60 degrees. PP cellular structural materials are inexpensive, and have a low density and excellent mechanical properties, so they have been widely used for insulation, packaging, electrical insulation and sound insulation area [70,71].

Polyethylene terephthalate (PET) is milky white or light yellow, with a smooth and shiny surface. Presenting an excellent physical and mechanical property in a wide temperature range, it has an excellent electrical insulation and its electrical performance is still good even at high temperature and high frequency [77].

Cyclic olefin copolymer (COC) is an amorphous polymer. It is very resistant to attack from acids, bases and most solvents except non-polar solvents and it has exceptional optical properties. COC is mainly used in the applications of packing films, lenses and medical devices. [75].

Polydimethylsiloxane (PDMS) is the most widely used silicon-based organic polymer [78]. PDMS is inert, non-toxic, and non-flammable. Its applications range from contact lenses and medical devices to elastomers; it is also present in shampoos (as dimethazone makes hair shiny and slippery), food (antifoaming agent), caulking, lubricants and heat-resistant tiles. It is a common ferroelectret material in many researches because of it is easy to use and very cheap.

Since the discovery of the piezoelectric properties of PVDF, in order to improve the piezoelectric properties and thermal stability of the material, people have conducted extensive research on PVDF and its additions. Yag discovered the piezoelectric properties of trifluoroethylene (TrFE) and PVDF polymer PVDF-TrFE in 1979 [79]. Wang et al. studied the piezoelectric properties of hexafluoropropylene (HFP) and VDF polymer PVDF-HFP [79]. The research results show that the addition of HFP monomer greatly improves the mechanical flexibility of the copolymer. The elastic modulus of the copolymer is much smaller than that of PVDF. They used a laser vibration analysis experimental system to measure the piezoelectric coefficient d_{33} of the coaxial cable. When the content of hexafluorophenyl in the material is 5.9%, the radio frequency coefficient d_{33} is only 20pC/N, which is equivalent to the piezoelectric coefficient of PVDF; when the content of hexafluorophenyl in the material replaces 4.7%, the polycoefficient d_{33} is 133pC/N is much higher than the fluorination coefficient of PVDF. Wang Feipeng et al. first studied the carbonization characteristics of PVDF-TFE-HFP/PTFE composite membranes [80]. In order to ensure the uniformity of the charging effect, the material is grid-controlled corona polarization. By adjusting the thickness of PVDF-TFE-HFP and other methods, the piezoelectric coefficient d_{33} of the composite film is as high as 47 pC/N. The heat treatment process can improve the piezoelectric stability of the P (VDF-TFE-HFP) film, and can significantly improve the piezoelectric stability of the composite film [80].

The spatial micro-electret material represented by polytetrafluoroethylene has a porous structure, and a large number of pore structures in the earlier. This structure increases the contact area between the polymer and the air, and may form a lot of more complex. At the same time, this structure exerts external force in the thickness direction of the film, and the film is deformed. When the pore structure in the film is reduced, the pores inside the material will gradually accumulate with opposite polarities. The space in the middle produces a non-uniform displacement relative to the upper and lower surfaces of the film. The film overlaps polyimide up and down, and the slenderness forms the piezoelectric effect of this type of material.

The metal electrode is vapor-deposited on the end. When an external force is applied to the material, the open circuit voltage signal can be detected when the material is separated. Due to the stable displacement storage capacity of PTFE, porous membranes containing PTFE usually have a higher piezoelectric coefficient and good piezoelectric performance stability.

Xia Zhongfu and others studied the piezoelectric properties of PTFE porous membranes [81]. The porous membrane is prepared by mechanical stretching, and a pore structure is generated during the mechanical stretching. The coefficient d_{33} is 103pC/N. After high temperature and high temperature treatment, the tubular coefficient d_{33} of the porous PTFE membrane with a porosity of 70% only attenuates by 15%. Wang et al. studied the piezoelectric properties of PTFE/PVDF-HFP bilayer membranes [80]. They calculated the piezoelectric coefficient of the double-layer composite film by analyzing the dielectric resonance spectrum. The research results show that the piezoelectric coefficient d_{33} of the material after charging from the side containing PTFE is 31pC/N. Xiao Huiming and others studied the piezoelectric properties of PVDF/PTFE double-layer composite membranes [82]. The composite membrane was prepared by spin-coating PVDF on the surface of the porous PTFE membrane. The research results show that when the composite film is corona charged at a high temperature of 80℃, the piezoelectric coefficient d_{33} of the composite film reaches the highest value, which is 75 pC/N. Under the best charging conditions, the piezoelectric performance of the composite film is stable and will not cause significant attenuation.

2.3.5 The applications of ferroelectret

The advantages of ferroelectret materials make it have a broader application when comparing to these traditional piezoelectric materials.

Ferroelectret materials can be used to measure pressure. Combining the ferroelectret material with an alarm can be used to monitor the safety of the room. Placing a ferroelectret on the bottom of the shoes can be used to measure the pressure of the foot when the person walks or moves. Similarly, placing the ferroelectret under the cushion of chair can be used for pressure detection, and further improving the design of the chair according to the measurement results. Figure 17 is a seat sensor L-3030SL from Emfit, placing it under the cushion, pressure can be measured, especially suit for the childcare.

Figure 17. The seat sensor L-3030SL from Emfit

Ferroelectret materials have a wide range of applications in vibration energy harvesting field. Placing the ferroelectret material under the bed can detect whether the patient's breathing and muscle movement are normal during sleep, and also can check whether the patient has rested on the bed in time. Because of the high piezoelectricity of the ferroelectret, it is possible to measure a very small force. Figure 18 present a dynamic pressure measurement experiment, the ferroelectret sensor is placed under the dog's limbs when the dog walking.

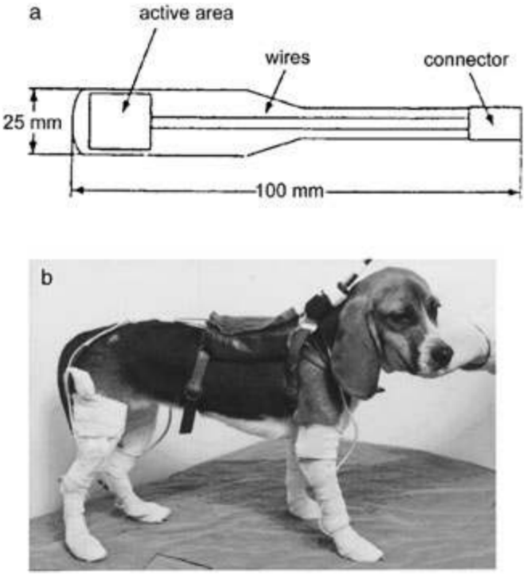

Figure 18. (a) The schematic diagram of ferroelectret sensor (b) The ferroelectret sensor is fixed with an elastic bandage

Due to the high sensitivity of the ferroelectret, the ferroelectret sensor can be placed under the protective layer, to prevent wear or other damages and extend the service life. In addition, the ferroelectret material is very soft, can be bended flexibly. Therefore, it can also be covered on the curved surface according to needs, as shown in Figure 19 [83].

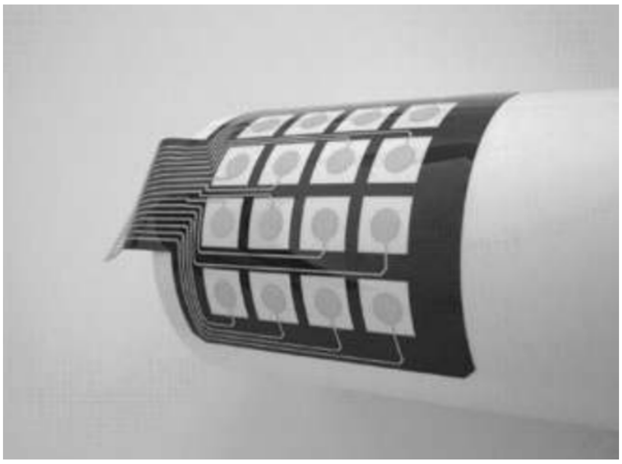

Figure 19. The ferroelectret sensor covered on the curved surface, the circular sheet is the ferroelectret film [83]

The extremely high sensitivity of the ferroelectret has made it widely applicable to the keyboard, touch panel and the like applications. Combining it with other electronic component such as transistors, a pressure sensor, pressure switch or microphone is made (as shown in Figure 20).

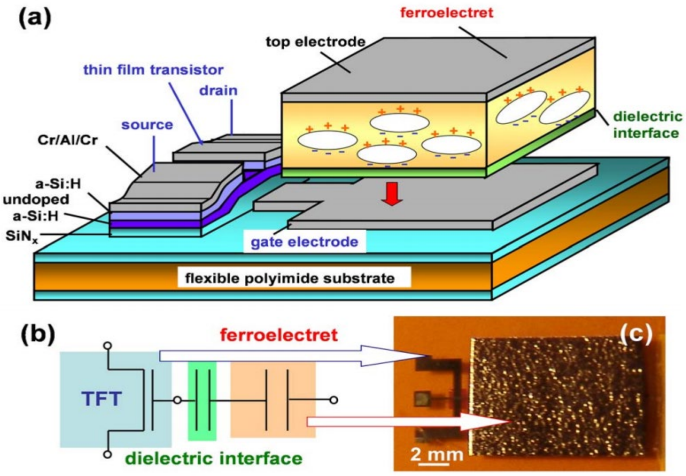

Figure 20. (a) Sketch of the transducer arrangement for the investigation of the ferroelectret field effect (b) Photograph of one transducer element and (c) equivalent circuit diagram [84]

In addition, the unique acoustic impedance of ferroelectret materials makes it have a huge application prospect in the fields of ultrasonic wave emission and detection under water.

2.4 Energy harvesting based on ferroelectret

2.4.1 Overview of energy harvesting

Energy harvesting technology refers to collecting the energy from surroundings into electricity then supplying power to the system. These energies mainly include kinetic energy, light energy, electromagnetic energy, and heat energy. Micro-energy harvesting is mainly used in wireless sensors, health monitoring, implantable medical monitoring, and active RF sensors identification and so on. These markets are currently developing rapidly, and in these applications, there is an inevitable bottleneck in battery maintenance and replacement, which also makes energy harvesting indispensable. It is foreseeable that, in the near future, energy harvesting will become an important technology in the field of Internet of Things [84]. The energy harvesting phenomenon was first recorded by Thomas Johann Seebeck in 1821, which is a kind of thermoelectric effect that he found when putting two different metals at different temperatures then connecting them as a closed loop circuit, and this circuit will generate current [85]. In 1831, the electromagnetic phenomenon was found by Michael Faraday and Joseph Henry. Michael Faraday invented the first direct current dynamo in the world by this mechanism [85][86]. In 1839, Edmund Becquerel discovered the photovoltaic effect, and Charles Fritts invented the first solar cell by utilizing the mechanism of the photovoltaic phenomenon in 1883 [85][86]. And at the end of the 19 century, Pierre and Jacques observed the piezoelectric effect that some materials can produce electricity under pressure [86][87].

Photoelectric energy harvesting is one of the most well-established technologies. According to Soitec, CEA-Leti, France and Fraunhofer ISE, Germany in 2014[85], high quality monocrystalline silicon solar cells can achieve a high conversion efficiency of 46% with the output power from microwatts to kilowatts. These solar cells are widely applied in MEMS electrostatic actuators, satellite, and heaters. However, this conversion is limited by light conditions.

Thermal is another energy that is widely distributed in nature. Most examples of thermal energy harvesting are based on the thermal strain material. These materials have the ability, when the temperature changes within a certain range, a phase transformation process will have occurred, and the thermal expansion coefficient will significantly increase. Therefore, combining thermal strained material and electrical activity materials, the conversion from heat power to electrical energy is achieved. However, thermoelectric conversion efficiency is very low. Generally, the theoretical conversion efficiency is only 5.5% [87], and it requires a large temperature difference, which is difficult to adopt in a general application environment.

Mechanical energy is ubiquitous in daily life and is easier to utilize than other energies. Therefore, the conversion of mechanical energy is a research hotspot in the energy harvesting field. There are three typical methods for electromechanical energy conversion, electromagnetic induction, electrostatic conversion, and piezoelectric conversion. Piezoelectric energy harvesting devices have the advantages of simple structure, no heat generation, no electromagnetic interference and are particularly suitable for various types of sensing and monitoring systems.

The working principle of the piezoelectric vibration energy harvester is based on the piezoelectric effect of the piezoelectric materials. Under the action of the external vibration force, the piezoelectric layer in the device generates stress and strain, an electrical signal is formed. Compared with the electrostatic and electromagnetic energy harvester, the piezoelectric energy harvester has the advantages of simple structure, long-life, high-energy density, and compatibility with the MEMS process. Since the piezoelectric material has a high energy density, only a slight deformation can obtain a large electrical output power. Therefore, piezoelectric vibration energy harvesting is considered the most promising alternative to the battery for supplying power to micro systems, such as wireless sensor nodes.

Compared with piezoelectric ceramic PZT and ferroelectric polymer PVDF, it is relative late for the research of energy harvesting technology based on ferroelectret. However, since Anton and Farinholt [88] firstly reported the preliminary experimental results of an energy harvester based on PP ferroelectret film in 2012, more and more scholars have joined the relevant research.

2.4.2 Ferroelectret energy harvesting

According to the different energy harvesting objects, the energy harvesting of ferroelectret including vibration energy harvesting and human motion energy harvesting, and it is summarized. Vibration energy harvesting is used to harvest mechanical vibration energy generated by the machines of factory, airplanes, automobiles, and the others. The human motion energy harvesting is used to harvest the kinetic energy generated by the human body in daily activities, and the frequency is low, it is generally below 10 Hz.

2.4.2.1 Vibration energy harvesting

There are a large number of vibration sources in daily life, such as millwork, airplanes, automobiles, and the others, the vibration energy generated during working is dissipated in the environment, resulting in energy waste. The energy harvesting of ferroelectret can collect part of the waste vibration energy without affecting the normal operation of the machine. Therefore, the research based on vibration harvesting of ferroelectret has become a focus in the academic circle.

In 1996 [89], Umeda, a researcher from Niigata University in Japan, studied the conversion efficiency of the piezoelectric energy harvesting device. The test device consisted of a steel ball and a simply supported beam made of piezoelectric ceramic plate. Bending deformation will have occurred, and electrical signals will have generated when the steel ball hits the piezoelectric ceramic plate. The electrical signals are used for evaluating the influence of different factors to the power generation efficiency of piezoelectric ceramics. The experiment found that the peak frequency conversed by the piezoelectric ceramics was the same as the frequency of the applied vibration. The obtained voltage waveform was similar to the vibration waveform. Changing the height of the steel ball, the power output of the piezoelectric ceramic changed with the input mechanical energy and showed an effective curve. Tests have shown that, as the mechanical energy of the steel ball increases, the conversion efficiency decreases [89].

However, this type of device is mostly found in the early piezoelectric energy harvester research. From the reported literature, it is difficult to use MEMS technology to achieve batch processing and miniaturization in devices driven by mechanical impact.

Anton and Farinholt [88] first explored the feasibility of using porous PP ferroelectret to harvest vibration energy. In the experiment, the dynamic piezoelectric coefficient of the sample is 35 pC/N, and the active area is 2.54cm*2.54cm. As shown in Figure 21, a vibrator with a mass of 1 kg is placed in the active area of the film, and the acceleration peak is set to ± 0.5g (g is the acceleration of gravity) and a sinusoidal excitation with a frequency of 500 Hz, when the load resistance increases from 10 k W to 400 k W, the corresponding output power increases from 2.5 nW to 40 nW. It is worth noting that the active area of the sample used in the experiment is only 6 cm^2. Considering that the mass density of the porous PP ferroelectret film is only about 5% of that of PZT, as well as the characteristics of flexibility and large-area film formation, the active area can be greatly increased in order to increase the output power so that it can achieve the purpose of powering low-power electronic devices. In 2014, Anton and the other persons [90] increased the piezoelectric activity and active area of the sample, and changed the vibration mode to 31-mode transverse sinusoidal excitation, and again studied the vibration energy harvesting based on the porous PP ferroelectret. It shows that, based on the PP ferroelectret energy harvester with piezoelectric coefficient d_{33} and active area A of 175 pC/N and 15.2cm*15.2cm, when the sample transverse stretch length and working frequency are ± 73 μm and 60 Hz, respectively, then charging a 1 mF storage capacitor for 30 minutes, which can make the voltage reach 4.67 V and the average output power reaches 6 μW. This experimental result proves that the ferroelectret energy harvester has the ability to power small electronic components, but there is a big gap between its output power and PZT ferroelectret energy harvester.

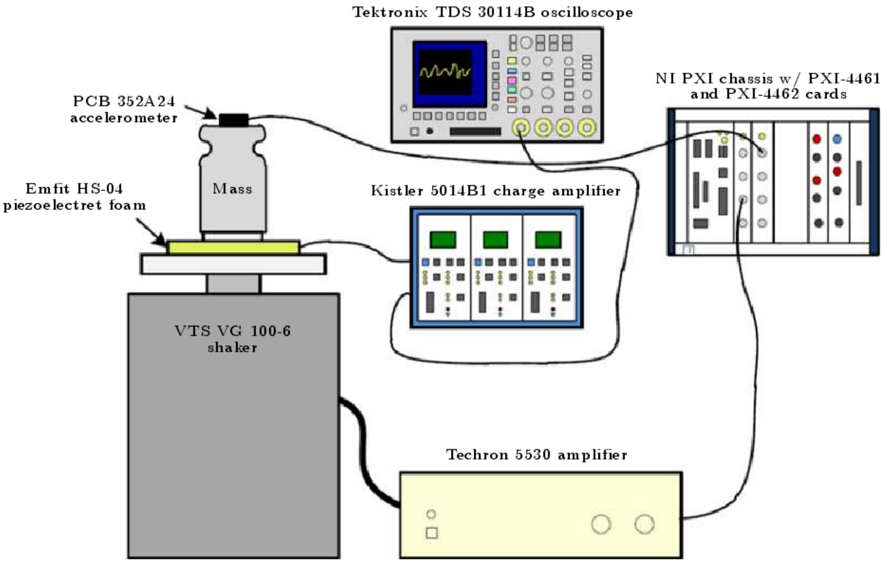

Figure 21. Schematic of experimental setup used for dynamic d33 testing and energy harvesting [88].

In another article by Pondrom et al. [91], the active area of the single-layer PP piezoelectric electret film used in the experiment is 25 mm^2, and the number of layers n = 9 (the number of electrical series The number of layers p in parallel with electricity is 3). When the mass of the vibrator is 8 g and the acceleration is 9.81 m/s^2, the maximum output power of 1.3 µW can be obtained at the harmonic frequency of 140 Hz [92]. The theoretical prediction and experimental results have good consistency.

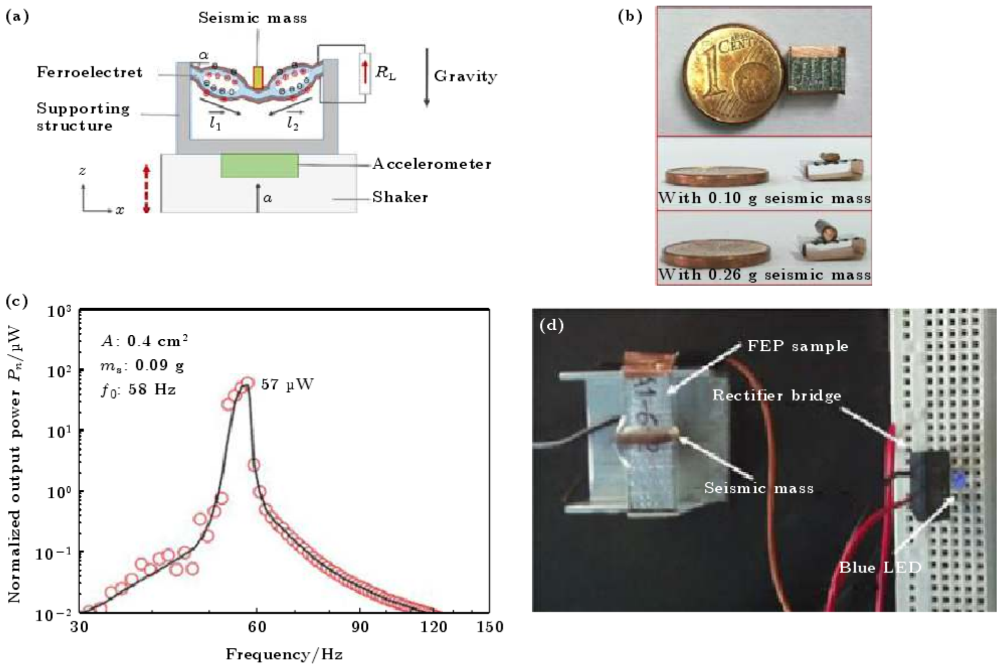

Figure 22. (a) Schematic of energy harvesting setup; (b) FENG; (c) measured normalized power generated by a FENG; (d) setup of energy harvester to power LED [96].

In order to increase the output power, Ray and Anton [93] increased the number of PP ferroelectret layers to 20 and 40 layers, and the active area of the single-layer ferroelectret film was increased to 25.4cm*25.4cm and an energy harvesting is used to charge the capacitor. The 20-layer device is exerted with an acceleration of 0.5g at the harmonic frequency, and a 100 μF capacitor can be charged to 1.45 V within 15 minutes, and a peak power of 0.45 μW is generated; The 40 layers device is exerted with an acceleration of 0.5g at the harmonic frequency, and a 100 μF capacitor can be charged to 1.7 V within 15 minutes, and a peak power of 0.89 μW can be generated.

Sessler and the others [94] also prepared a cross-linked polypropylene (IXPP) ferroelectret vibration energy harvester using stacking and folding methods, and it is systematically analyzed the dependence of output energy and resonance frequency on parameters such as vibrator quality and sample layer number. Three layers of circular IXPP ferroelectret with a diameter of 20 mm are stacked and connected in series, and vibration energy harvesting experiments are performed under different vibrator masses. The experiment shows that the output power and resonance frequency are related to the number of layers. The advantages of this kind of stack and folded ferroelectret energy harvester in practical applications are that it is designed for an energy harvester suitable for specific situations by changing the corresponding parameters while the output charge, capacitance and voltage of the device can be changed along with it. Moreover, the impedance matching can be achieved by adjusting the load resistance. The experimental results show that by using 8 layers of circular IXPP samples with a diameter of 20 mm, when the mass of the vibrator is 20 g, the best output power is 80 μW.

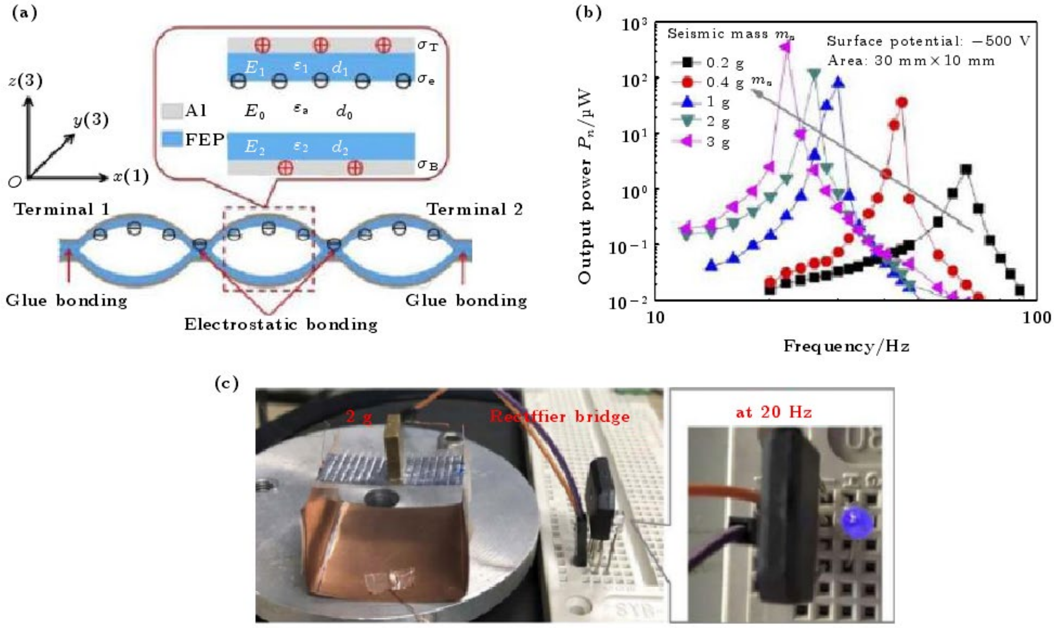

Figure 23. (a) Schematic cross-sectional view of the structure of the FEP unipolar ferroelectret (The upper layer is negatively charged and the lower layer is not charged); (b) normalized output power vs. frequency; (c) setup of energy harvester to power LED [97]

Zhang and the others [95] used cross-tunnel structure FEP ferroelectret to conduct vibration energy harvesting research. The quasi-static piezoelectric coefficient d_{33} of the sample used in the experiment was as high as several thousand pC/N, and the active area A was 7.1 cm^2, when the oscillator mass, acceleration and working frequency are 69.5 g, 0.2g and 120 Hz, the best output power can reach 73 μW. In order to demonstrate the energy harvester's ability to charge low-power electronic devices, an active area of 3.1 cm^2, a vibration energy harvester with a vibrator mass of 54 g is used as a power supply, at a vibration frequency of 150 Hz, the LED light can be fully lit. In 2018, Zhang and the others [96] prepared a ferroelectret energy harvester using FEP ferroelectret film with significant lateral ferroelectret activity. As shown in Figure 22(a), the parallel tunnel structure FEP ferroelectret film is fixed on the two ends of the support structure, the mass of the vibrator causes the film to undergo a slight static deformation, the resulting angle amplified tensile force on the sample to take full advantage of the large piezoelectric activity of the film in the transverse direction (g_{31} = 3.0 V•m/N). For a small-sized energy harvester (Figure 22(b)), when the mass of the vibrator is 0.09 g, the output power of 57 μW can be obtained (Figure 22(c)). Connecting this device to a rectifier bridge as a power supply can successfully light up the LED light (Figure 22(d)). In 2019, according to the structural design idea of this device, Ma and the others [97], studied a vibration energy harvester based on parallel tunnel FEP unipolar ferroelectret. As shown in Figure 11, this is a parallel tunnel structure FEP unipolar ferroelectret. on one side of the FEP film is negatively charged by corona polarization, on the other side is not charged (Figure 23(a)). The 31-mode energy harvester prepared based on this material can obtain a normalized output power of 355 μW at a resonant frequency of 22 Hz and a load of 3 g (Figure 23(b)). The energy harvester can also be used successfully lit the LED light (Figure 23(c)). Recently, Ben Dali and the others [98] introduced a large distance air gap between the parallel tunnel structure FEP piezoelectric film and the 3D printed support substrate, and made an energy harvester with the air-gap single-arm cantilever beam structure, which not only enhances the structural stability of the device, but also significantly increases the output power.

2.4.2.2 Energy harvester and sensing for human applications

Human beings produce a lot of mechanical energy in daily activities (limb movement, pulse, heartbeat, breathing, vocal cord vibration, and the others). This kind of energy is ubiquitous in daily life and is not affected by the natural environment such as light and temperature. The applications of energy harvesters in the field of human energy harvesting mainly include wearable sensors and piezoelectric floors. The main application directions of self-powered wearable sensors based on energy harvesting technology include remote smart medical treatment and smart home. As a dynamic sensor, the wearable sensors are generally attached to people's throat, wrist, abdomen, or soles, and are used to measure people's breathing, heartbeat, pulse, voiceprint, exercise steps and other information, which is the important components of the internet of things. The wearable sensors generally require materials with good flexibility, high sensitivity, excellent stability and self-powered function [99], so ferroelectret are considered to be one of the most ideal materials for wearable sensors. When a person is moving, the ferroelectret can convert the vibration energy of the skin surface into electrical energy. On the one hand, it can be used as a ferroelectret sensor device to obtain various dynamic strain information on the skin surface, on the other hand, it can also supply power to itself, that is, there is no need to add an additional power supply for its power supply, which greatly improves the service life and conversion efficiency of the wearable sensor. The voiceprint sensor is generally placed near the vocal cords of the larynx. When the wearer speaks, due to the content of the speech, the speaker's pitch and loudness are different, the vibration of the vocal cords will also be changed. The voiceprint sensor generates characteristic electrical signals due to receiving different vibration signals, which can distinguish different speakers and different speaking content.

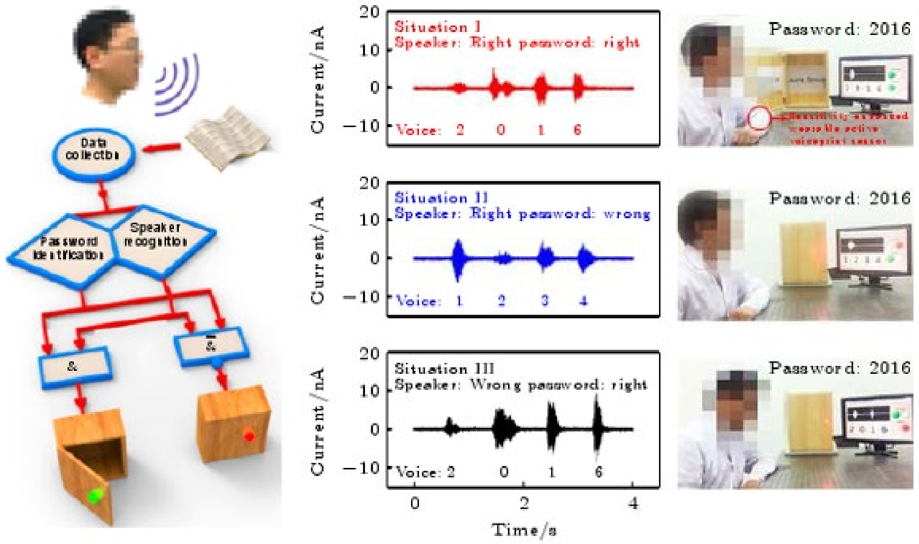

Figure 24. Voiceprint recognition system based on PP films [102].

Li and the others [102] prepared a wearable voiceprint sensor using PP film (as shown in Figure 24). The PP film was treated by thermal expansion, and the PP film was charged by corona polarization, and then the aluminum electrode was deposited on the surface of the sample by magnetron sputtering, a single-layer sample film is prepared. Three pre-processed sample films are laminated together to obtain a p ferroelectret sample for voiceprint discrimination. Based on this sensor, the voiceprint recognition system can use the characteristic current signal to record the speaker’s content and voiceprint characteristics. When someone tries to open the voiceprint password box, the recognition system will recognize the speaker’s voice password for twice, only when the voice password and the speaker’s voiceprint are correct, the password box will only be opened.

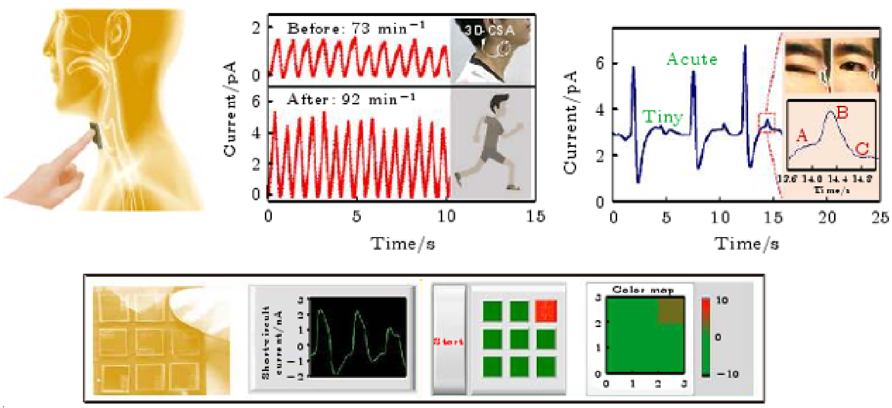

Figure 25. Three-dimensional cellular sensor array (3D-CSA) array for wearable biomedical monitoring based on cellular PP/PZT composite films [103].

Yan and the others [103] used a thermally induced phase separation method to prepare a porous PP/PZT composite frame three-dimensional cell sensor array (Figure 25). This ferroelectret has good biocompatibility and thin thickness (80 μm), light weight and good flexibility. It has shown good prospects in the fields of soft robotics, artificial intelligence, and healthcare monitoring. Placing this cell sensor array in the larynx, it can be used as a voiceprint sensor; It can monitor health information such as pulse and heart rate during exercise when attached to the carotid artery; It can be attached to the muscles near the eyes to detect the blinking frequency of a person, when the driver is in Fatigue driving occurs during driving, and the eye muscle movement is small, which can trigger a warning signal. In addition, this material is also used in a touch imaging system, and a square electret film is made into a 3 × 3 array sensor, when one of them is pressed by a finger, the color of the square LED will be changed, so as to realize the visualization of the touch.

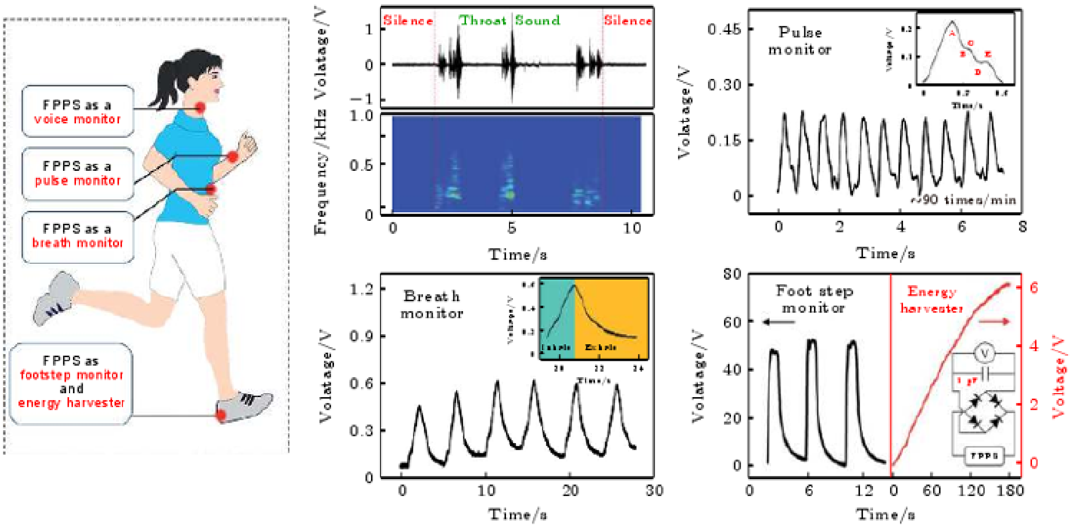

Figure 26. The flexible piezoelectret-based pressure sensors based on PFA films [104].

Wu et al. [104] used hot pressing to press soluble polytetrafluoroethylene (PFA) cube particles and PFA film together to form a flexible ferroelectret with an array structure (Figure 26). Based on this type of flexible ferroelectret, the health monitoring system established not only obtains vital signs information such as pulse, respiration, and heartbeat, but also detect people's walking steps.

Wu et al. [105] also used FEP's spherical protrusion array ferroelectret film (as shown in Figure 27(a)) to prepare a self-powered wireless remote-control system. When the operator presses the electret film, the infrared emitter diode system can be used to send instructions to the fan to control the turn-on and turn-off for fan (as shown in Figure 27(b)).

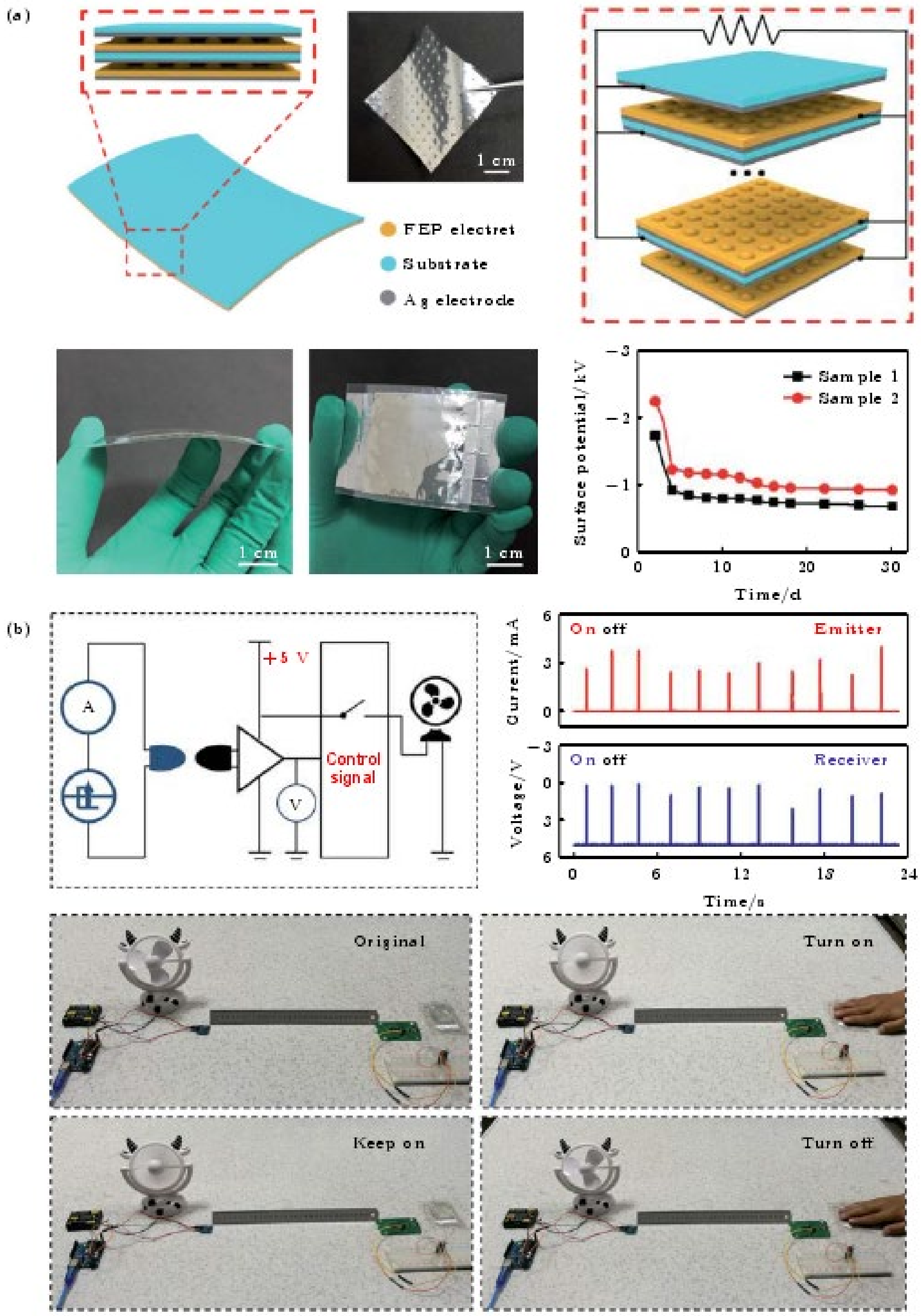

Figure 27. Self-powered wireless remote system: (a) Schematic diagram and photograph of raised bubble shape FEP laminated films; (b) the fan can be controlled by self-powered wireless remote system [105].

Tajitsu and the others [106] designed an energy harvesting floor based on ferroelectret. The FEP film and the porous PTFE film are pressed together to obtain a ferroelectret unit. After the unit is stacked in multiple layers, it can be laid under the floor as a ferroelectret harvester (as shown in Figure 28). When the tester steps on the floor, the instantaneous power can reach 4500 μW.

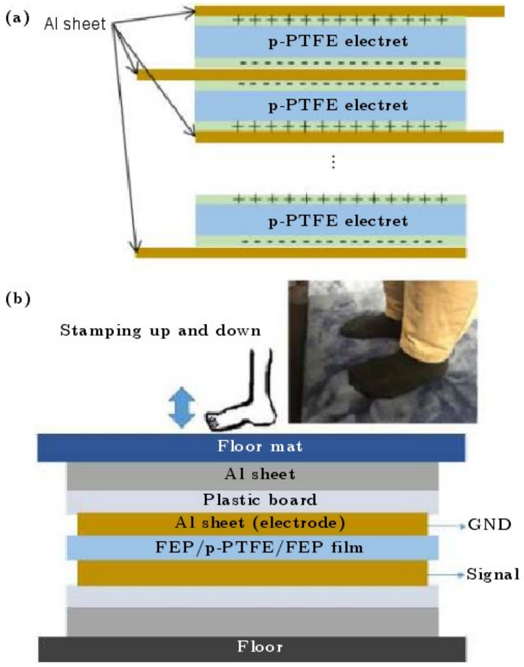

Figure 28. Underfloor energy harvesting system based on piezoelectrets: (a) FEP/PTFE/FEP multilayer films;(b) schematic view and photograph of the system [106].

2.5 The charge decay mechanism of electret

When a certain electric field is applied around the material, the surface of the material will accumulate a certain amount of charge, which is called surface charge.

In recent decades, researchers have conducted a large number of experimental studies on the attenuation characteristics of the surface charge of polymer insulating materials [107~110]. The attenuation characteristics of surface charges are more complicated and affected by many factors.

In terms of attenuation mechanism research, it is generally believed that there are three main ways of attenuation under atmospheric pressure: first, internal transport. The surface charge is affected by the uneven distribution of material conductivity, polarization and other processes, injected into the dielectric body and transported to the ground electrode by means of the allowable band. This is a dynamic process. The reaction process is affected by the migration rate, sinking, and de-trapping of carriers under an electric field. Most theoretical models established in the literature believe that this approach is the dominant mechanism of surface charge decay. Second, surface conduction. Due to the uneven distribution of surface charges, a tangential electric field will be formed on the surface of the material. Under the influence of the tangential electric field, the surface charge will migrate along the surface of the material. The migration rate is affected by surface conductivity and surface state, as well as by air humidity. The impact is relatively large. The charge migration along the surface will cause local charge redistribution, but the total surface charge will not change. Third, gas neutralization. The charges accumulated on the surface of the material will form a local electric field on the surface and nearby spaces. The free particles in the air migrate to the surface of the material under the action of the electric field, and a neutralization reaction occurs [108]. In the gas phase reaction, the nearby electric field strength and the energy level of the surface state will affect the efficiency of the gas phase reaction. Since there are many factors affecting the electric field distribution, the mechanism is more complicated.

The study [111] found that the voltage waveform, gas composition and pressure, surface treatment, adding additives and other factors in the experiment will all affect the surface charge attenuation. These factors are introduced below. The existence of surface charge has an important impact on the performance of the material. It can not only change the electric field around itself, but also provide discharge charges and discharge channels for creeping discharge. The attenuation characteristics of the surface charge of the material will directly determine whether a stable and good electret can be formed.

2.5.1 Voltage

During the polarization process of the electret, the long-term stability of the charge will vary depending on the applied voltage waveform. According to the different applied voltage waveforms, it can be roughly divided into three categories: AC voltage, DC voltage and pulse voltage. Early research focused on AC voltage. In recent years, with the development of UHV DC transmission, more and more insulating materials are used in the DC transmission process. Therefore, studying the dynamic characteristics of surface charges under DC voltage has great practical significance and industrial applications. In the literature [112], three forms of DC, AC and pulse voltage are used to study the discharge of the plane electrode to the epoxy resin and the breakdown field strength of the material after discharge. The results show that the material under direct current has the highest breakdown field strength, followed by alternating voltage, and the smallest is pulse voltage. In the literature [113], DC voltage and AC voltage were used to pre-corona discharge HTV silicone rubber sheets. After the discharge is over, the effect of pre-discharge under different waveform voltages on the charge decay is studied by applying pulse voltage. The results show that in the air, the attenuation characteristics of the surface charge of the silicone rubber with DC preload are similar to those of the non-preloaded material, and the decay rate of both is much lower than that under the AC preload. The surface conductivity and bulk conductivity of the material were tested, and it was found that the conductivity under the action of AC increased significantly. The reason analysis is that because the dissipation of surface charges includes surface transport and transport into the material body, as the conductivity increases, both attenuation pathways are enhanced, and the attenuation rate becomes larger. Therefore, the use of charge decay can be used to characterize the surface conductivity of polymer materials.

It is generally believed that polymer tends to accumulate surface charges more easily under DC voltage [113]. Some scholars have carried out a large number of experimental studies on the influence of surface charge characteristics on insulators, GIS and other power equipment. In [114], in order to study the law of surface charge dissipation under DC voltage, a self-built surface charge test system was used. The experiment measured that the surface charge dissipation process of insulators approximately decayed exponentially. Based on the experimental results, three ways of dissipating the surface charge of the insulator are analyzed, and it is believed that the surface charge is mainly dissipated inside the insulator. Feng [115] studied the influence of the voltage polarity on the surface charge characteristics by applying DC voltages of different polarities when studying the surface charge of the DC gas insulated switchgear medium. The surface charge distribution diagram of the insulator under positive and negative polarity is shown in Figure 29 [115].

It can be seen from Figure 29 that the accumulation of negative charges is stronger than that of positive charges, indicating that negative charges are more likely to accumulate on the surface of the insulator. It can be seen from the above research that the voltage type has a greater impact on the attenuation characteristics of the surface charge. In fact, the attenuation of surface charge is affected by factors such as voltage waveform, amplitude, polarity, application time, and frequency. Therefore, the appropriate voltage waveform should be selected according to the type of material and the application site.

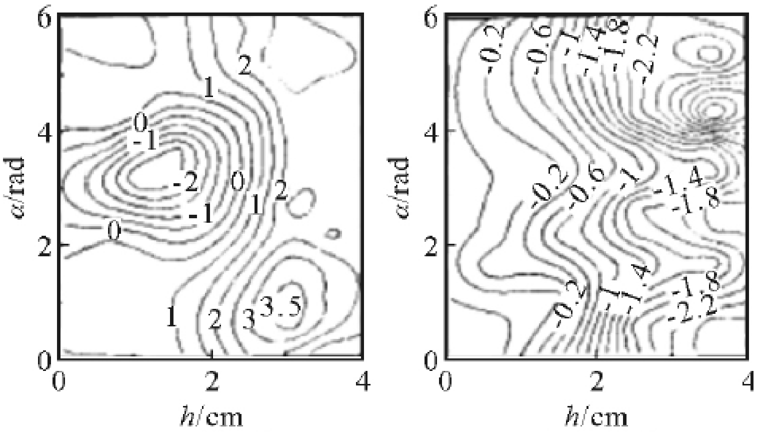

Figure 29. Surface charge distribution under positive and negative polarities [115].

2.5.2 Gas pressure and composition

During the polarization process of the electret, if the pressure in the chamber where the electret is located can adjust, the dynamic characteristics of the surface charge of the material are different. The article [116] studied the process of the change of the surface charge of silicone rubber by changing the pressure under the reaction atmosphere, and found that as the pressure decreases, the surface charge decays slowly. Analysis believes that as the pressure decreases, the concentration of charged particles in the air decreases, so the intensity of the neutralization reaction with the surface charge of the material becomes weaker. The decrease in pressure suppresses the attenuation of surface charges. In [117], when studying the influence of different pressures on the surface charge density, it was found that when the pressure increased from 0.1 MPa to 0.13 MPa, the absolute value of the surface charge density increased significantly, and then the pressure continued to increase to 0.5 MPa, and the absolute value of the surface charge density increased. It's not obvious. Affected by the surrounding gas atmosphere, the dynamic characteristics of the surface charge are significantly different under different gas atmospheres. In [118], the electrostatic probe method was used to measure the surface charge distribution of basin insulators under different gases. In the experiment, the decay process of the insulator surface charge in the air and SF_6 was measured. Analysis believes that the diffusion of surface charges into the material is one of its main attenuation ways, and the attenuation speed is related to the volume resistivity and surface resistivity of the material. The dissipation of surface charge in the air is greater than the dissipation rate in SF_6. The reason is that the moisture in the air increases the surface conductivity of the insulator, thereby speeding up the dissipation of the charge along the surface of the insulator.

2.5.3 Surface treatment

At present, part of the treatment of insulating materials is artificial modification treatment to improve the electrical properties of the material, and some are affected by natural conditions. For example, a spacecraft flying in space is radiated by high-energy rays of the universe, which will cause surface charges. The accumulation of large amounts. In [119], a mixture of F_2/N_2 was used to fluoride the surface of epoxy resin in the reaction chamber to study the effect of fluorination on the dynamic characteristics of surface charges. As the fluorination time increases, the thickness of the fluorinated layer increases and the surface micro-roughness increases. The surface conductivity has increased significantly due to the shallowing of surface charge traps and surface adsorption of water. Surface charge current measurements show that surface charge decays faster than unfluorinated materials. In [120], chemical vapor deposition modified polytetrafluoroethylene film and low-density polyethylene film were used, and phosphorus trichloride vapor was used to treat LDPE film. The results show that phosphorus-containing groups can be attached to the surface of polymer materials to form nanoclusters. These nanoclusters can reduce surface fluidity, form new charge traps, and have a good effect on the formation of stable electrets. In [121], gamma rays were used to irradiate epoxy resin materials to study the surface charge attenuation characteristics. The results show that the surface charge dissipates in a double exponential law, and the chemical reaction caused by gamma radiation increases the number of carbonyl and hydroxyl groups on the surface of the sample, and the surface trap energy level becomes shallower, thus increasing the dissipation rate of the charge. It can be seen from the above research that the use of fluorination or chemical vapor deposition to treat the surface of the material can cause changes in surface roughness and the depth of charge traps, which in turn affects the changes in the dynamic characteristics of surface charges. In fact, the influence of the surface of the material is mainly caused by the physical and chemical changes on the surface of the material, such as the introduction of some elements, macromolecular groups or changes in the surface roughness, etc., will affect the attenuation characteristics of the surface charge. Shao [122] uses atmospheric pressure dielectric barrier discharge to generate plasma to treat polymethylmethacrylate (PMMA) materials. The study found that the surface roughness of the treated material increases, new traps are introduced on the surface, the ability to capture carriers is enhanced, and the surface resistivity increases, thus increasing the material's surface flashover voltage under vacuum.

2.5.4 Addition agent

In recent years, there have been more studies on adding additives to improve the electrical properties of materials. Additives mainly include various organic and inorganic additives. Among them, the inorganic nano additive is added to the polymer material to form a nano composite dielectric. Compared with traditional polymer dielectrics, the electrical, thermal and mechanical properties of nanocomposite dielectrics have been greatly improved [123,124]. Commonly used additives are SiO_2, ZnO, TiO_2. The paper [125] studied the trap energy level density distribution characteristics of alumina ceramics doped with different additives, as well as the surface charging and flashover characteristics in vacuum under the action of negative pulse voltage. The results show that the trap distribution in the medium has a strong influence on its surface charging characteristics and flashover behavior along the surface. The greater the number of trapped charges, the greater the surface charge density, and the lower the corresponding vacuum flashover voltage, which proves the role of the carrier trapping and de-trapping mechanism in the vacuum flashover process of the insulator. In [126], nano-particle boron nitride particle with different mass fractions was mixed into epoxy resin to study the effect of additives on the charge decay of the material surface. With the increase of the added mass fraction, the change of the charge density curve slows down. When it reaches 30wt%, the curve is the slowest and continuing to increase the additive mass fraction to 40wt% causes the charge decay rate to accelerate.

Polytetrafluoroethylene (PTFE) exhibits excellent charge stability over time [16]. However, PTFE is not as soft or flexible as PDMS and is difficult to mold and shape mechanically. PTFE is typically processed as a powder rather than as a standard plastic, often using compression molding techniques or with the powder mixed with dispersants and applied as a coating by film casting [17, 18]. The effect of adding PTFE particles to PDMS had been described in previous studies [19]. PTFE is a fluorocarbon and, since fluorine is the most electronegative element, PTFE will accept more electrons than PDMS [20]. Therefore, more electrons can be trapped on the surface of the PTFE particles, and as the ratio of PTFE particles within the PDMS increases, the surface charge density of the PDMS/PTFE composite will also increase [20].

2.5.5 Charge storage performance of fluorine polymer electrets

Prior to the polarization of the fluorine polymers, the orientation of the molecules is random. Even though the molecules have electrical moments, the sum of the electric moments is zero at the macro level. Fluorine polymers are electrically neutral, instead of showing an electric field. Fluorine polymer materials are a kind of dielectric substance with wide applications.

As is known to all, there are three kinds of polarization of dielectric substance: (1) displacement polarization of electrons, atoms and ions; (2) polarization of space charge; (3) orientation polarization of dipoles. Electronic polarization refers to the displacement of the outer valence electrons of the atomic nucleus relative to the nucleus caused by a high voltage electric field. Electron polarization costs a very short period of time. When a polymer forms a covalent bond, some or all of the atoms in the polymer carbon chain have positive or negative apparent charges. The high voltage electric field will cause the relative displacement of the atoms in the polymer carbon chain, which is known as the displacement polarization of atoms. The polarization arising from the displacement of the positive ions and negative ions in polymer materials at different directions in the high voltage electric field is called ionic polarization. In addition to the electric charges bound in atoms and molecules, there are also real charges in fluorine polymer materials, such as free space charges formed by conduction electrons and holes, as well as bound charges directly injected into the near surface of the material or deep inside the material. In the high voltage electric field, the bound or injected space charge in the materials is trapped inside the material upon displacement, and there will be a more long-lasting polarization, which is known as the polarization of space charges. In addition to the above-mentioned particles, there will also be dipoles in the material. Prior to the polarization, the dipoles in the material are arranged randomly, and the vector sum of the dipole moment is zero at the macroscopic level. The high voltage electric field will cause the dipoles to be arranged in an orderly manner. The dipole moments of a large number of dipoles are in superposition, as a consequence, the dipole moment is no longer zero macroscopically, but basically remains the same direction as the electric field, which is known as the orientation polarization of dipoles.

As the atomic nucleus binds the surrounding electrons, the polarization of electrons generally occurs at the outermost layer of the electron cloud of atoms. Generally speaking, the apparent charge of atoms is very small with low polarization intensity, which is only about one tenth of the electronic polarization. Electronic polarization is extremely weak in the high voltage electric field with general intensity. The intensity of ionic polarization is much lower than that of electronic polarization, therefore, ionic polarization makes less contribution to the polarization of materials at the macroscopic level. Compared with the displacement polarization of electrons, atoms and ions, the polarization of space charge and the orientation polarization of dipoles make more contribution to the polarization of materials at the macroscopic level.

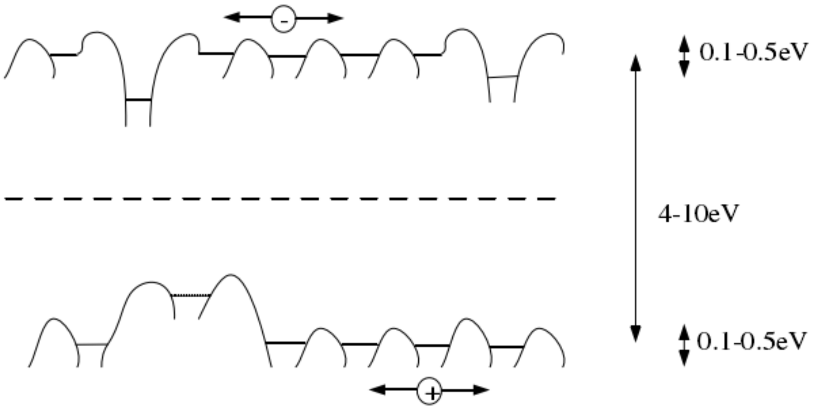

Figure 30. Schematic diagram of energy levels of polymer materials [27]

As shown in Figure 30, the energy band gap of polymer electrets is about 4~10eV, which is relatively wide [27]. The part between the conduction band and the valence band is known as a localized state, and the conduction band and the valence band are called an extended state (also called a non-localized state). The traps in polymers generally include hole traps and electron traps. Hole traps lie close to valence band while electron traps lie close to conduction band. Space charges are stored in the trap energy level between valence band and conduction band. In the case that there is no electron in the electron trap contains, the electron trap is electrically neutral. However, in case of electrons in the electron trap, the electron trap has negative polarity. When there are electrons in the hole trap, the hole trap is electrically neutral. After electron liberation, the hole trap shows positive polarity. The energy bands in electrets can be classified into multiple discrete energy levels, which has been proved by the TSD current spectrum of electrets as well as relevant experimental results [127]. The charge carrier is able to move between different traps with the energy provided by thermal activation, nevertheless, considering that the gap between conduction band and valence band is too large, the energy provided by thermal activation can hardly enable the charge carrier to move between conduction band and valence band.

Polymer electrets usually consist of surface traps and in vivo traps, and the trapped charges can be stored near the surface of the material or deep in the material. Surface traps are related to such factors as surface oxidation, chain scission, molecular adsorption, chemical impurities, and differences in short-range order constitutional units. In vivo traps, however, are influenced by such factors as the irregularity of molecular chains, the deformation of crystals, the defects of the monomers as well as the impurities in materials. Given that the corona charging technology is widely adopted to prepare electrets, the distribution of surface traps plays a significant role in the production practice of electrets. According to the results of TSD current spectrum experiments, the surface shallow traps account for a large proportion in some relatively important polymer electrets, such as FEP, PTFE, and PCTFE [128].

In general, there are two kinds of dipoles in electrets, namely, induced dipoles and permanent dipoles. The electric field between the two charges in the induced dipoles is in the opposite direction of the externally applied field and the more the induced dipoles, the weaker the externally applied electric field. In case of the cancellation of the externally applied external electric field, the induced charge will soon disappear. There are quite a few polar molecules in polar materials, and the center of positive charges do not coincide with that of negative charges polar molecules, which is equivalent to an electric dipole, also known as a permanent dipole. High voltage electric field will enable the permanent dipole to generate a specific orientation. On condition that the permanent dipole is frozen under the condition of maintaining the electric field, the orientation of the permanent dipole will basically remain unchanged in spite of the cancellation of the high voltage electric field, and the material still remains polarized. In case of the polarization, the dipole charges are usually unevenly distributed in the material, and only under some special polarization conditions can the dipole charges be evenly distributed in the material.

It is difficult for the space charges and dipole charges to coexist in polymer electrets for a long time. Materials with low conductivity usually belong to non-polar materials, which are applicable to store space charges, but have less dipole charges. Materials with higher conductivity usually belong to polar materials, which have more dipole charges, however, higher conductivity is not good for the storage of space charges.

Upon polarization, the materials will show varying degrees of depolarization. Space charges and dipole charges make the greatest contributions to the polarization of electrets, as a consequence, the research on the characteristics of polymer electrets mainly focuses on the types of the charges stored in materials, the density of space charges, and the stability of storage of charges. The research on the electret characteristics of fluorine polymers also involves whether the material is a polar material or a non-polar material, and the piezoelectric properties of the material. This research mainly aims to discuss the electret properties other than piezoelectric properties.

PVDF is a kind of semi-crystalline polymers whose degree of crystallinity is about 50%. In 1969, Japanese scholar Kawai discovered the piezoelectric properties of PVDF, followed by more in-depth studies on PVDF conducted by other scholars [129]. At room temperature, the longitudinal piezoelectric coefficient d_{33} of PVDF is about 15pC/N, which is relatively stable. Priced cheap, PVDF can be used as material to make thin films on a large scale. PVDF film is characterized by lower dielectric loss, lighter weight, good mechanical strength, and lower acoustic impedance. However, the polarized PVDF films will show obvious depolarization at 80°C, and its poor thermal stability makes them unable to be used in a high-temperature environment. Therefore, the research on VDF (vinylidene fluoride) and copolymers composed of other monomers through copolymerization is of great significance. It is likely that the addition of other monomers will enable the copolymers not only to have benign piezoelectric properties but also to have good stability of charge storage.

PCTFE is one of the fluorine polymers with a variety of excellent properties developed by Hearst of Germany. It is wear-resistant, aging-resistant, non-flammable, and ultraviolet ray-resistant, with sound dielectric properties and excellent chemical stability. Benefiting by its large charge storage density and sound charge storage stability, it will still remain stable polarization state, neither will it show obvious depolarization, even if the temperature is above 80°C. It is the first time that Qui et al. have studied the electret characteristics of the copolymer of VDF and CTFE, namely, P(VDF/CTFE) [130], in which they polarize the material by means of positive corona and negative corona charging methods.

As present in the Figure 31, According to the research results, the charge storage stability of P (VDF/CTFE) has been obviously enhanced. Raising the charging temperature within certain limits can increase the proportion of deep trap charges in and reduce the proportion of shallow trap charges, thereby significantly promoting the charge storage stability of copolymers. The analysis results of TSD current spectrum show that the copolymer P (VDF/CTFE) is a polar material, and there will be both dipole charges and space charges in the material upon polarization. The transfer law of mean charge depth shows that the free face attachment of such material has deep trap charges with higher concentration than that of deep layer in the material and the geometric distribution of trap levels of the material mainly depends on the components of CTFE.

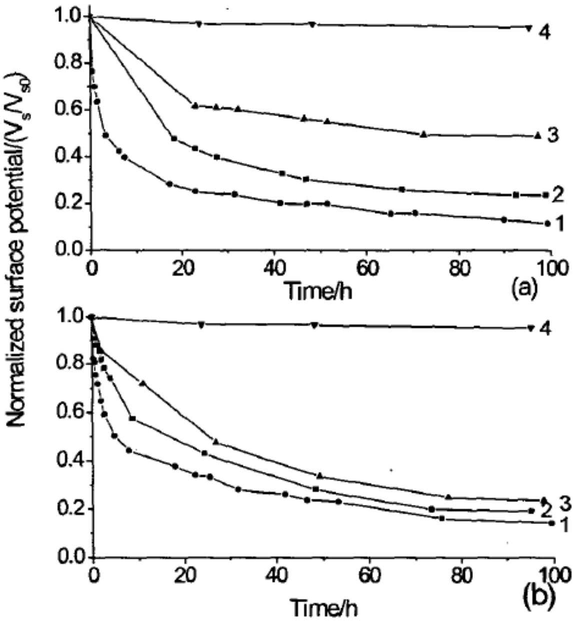

Figure 31. Surface potential decay of PVDF, P(VDF/CTFE) and PCTFE:(a) positively charged; (b) negatively charged.1. PVDF charged at 120°C, 2. P(VDF/CTFE) charged at RT, 3. P(VDF/CTFE) charged at I 20°C, 4. PCTFE charged at RT

In recent years, there are quite a little research on the copolymer P(VDF-HFP) of HFP and VDF [131]. Gorokhovatsky et al. proposed a novel thermal stimulus method for surface voltage recovery, based on which they measured the thermal stability of the P(VDF-HFP) copolymer containing 5% HFP after corona charging [132]. According to the research results, in case of the negative corona charging in low polarization electric field (5-10MV/m), there will be a transition from α nonpolar phase to δ polar phase in the material. The injected charge is trapped in the deep trap between crystals and non-crystals, and the thermal stability of charge storage can be greatly enhanced in the way of forming a specific crystal structure. Wang et al. carried out a study on the electret characteristics of P(VDF-HFP) [133], in which two different P(VDF-HFP) materials with 5.9% and 4.7% hexafluoropropylene respectively were prepared with the casting method. The research results show that mechanical stretching is conducive not only to enhancing the storage density and stability of space charge, but also to increasing the concentration of dipole charges. Positive corona has a significantly better polarization effect on P(VDF-HFP) than that negative corona. The decrease of the HPF content increases the concentration of dipole charges and enhances the capability of space charge trapping. P(VDF-HFP) belongs to a kind of polar material before and after mechanical stretching. After polarization, the material contains both dipole charges and space charges.

In addition to the monolayer films of copolymers, the electret properties of laminated films have also been studied extensively. In the midst of the polarization of laminated films with two or more layers, as there are different parameters for different materials in terms of the dielectric constant and conductivity, there will be charge accumulation between the interfaces of different materials, and the charge density at the interface can be calculated through formula (2.2).

$$\sigma = \left(\varepsilon_2 - \varepsilon_1 \frac{\gamma_2}{\gamma_1}\right) E_2 = (\varepsilon_2 \frac{\gamma_1}{\gamma_2} - \varepsilon_1) E_1 \tag{2.2}$$

Of which, σ refers to the charge density at the interface; γ_1 and γ_2 refer to the conductivity of the dielectric; ε_1、ε_2 refer to the dielectric constant of dielectric; E_1 and E_2 refer to the electric field intensity in different dielectric. The trap generated at the interface of the laminated films can trap charges, making them have good capacity of charge storage. The charge accumulation at the interface makes the polarization process more complex, and the laminated films also show electret properties that are different from those of monolayer films. PTFE is characterized by higher mechanical strength, fire resistance, chemical inertness and excellent dielectric properties. What's more important, PTFE has the best charge storage stability and high temperature resistance among the fluorine polymer electrets. TSD experiment results show that the surface potential of PTFE films through negative corona charging falls by only 6% when the temperature rises to 200°C. Therefore, laminated films usually contain PTFE.

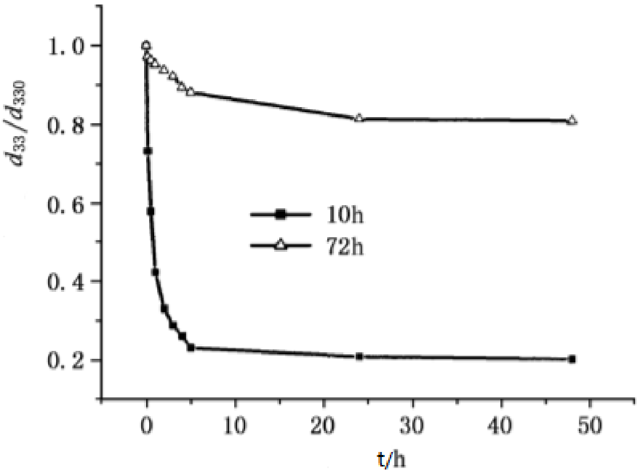

Figure 32. The influence of films with different aging time on d_{33}

Wang et al. carried out the research on the electret characteristics of polyporous PTFE/P (VDF-HFP) bilayer film and studied the electret characteristics of P(VDF-TFE-HFP)/PTFE bilayer film for the first time [133]. The research results prove that in terms of PTFE/P (VDF-HFP) bilayer film, the surface potential of the material decreases at a quicker speed in case of charging from P (VDF-HFP) surface, while the material has sound charge storage stability and the surface potential decreases at a lower speed through charging the PTFE surface. In terms of P (VDF-TFE-HFP)/PTFE material, the charge storage stability in case of charging from the PTFE surface is better than that through charging from the P (VDF-TFE-HFP) surface, in addition, the charge storage capacity of the material under the condition of charging from the PTFE surface is obviously better than that of the PTFE monolayer film, and the thermal stability is significantly better than that of the PVDF monolayer film. The appropriate ageing treatment of the material within certain limits is conducive to the enhancement of the capability of charge storage. Yanhai Zhao et al conducted a study on the electret properties of PTFE/ THV /PTFE three-layer laminated films [134], the research results of which show that when the temperature is below 100°C, the laminated film has good charge storage stability without obvious decrease. It is good for the enhancement of the charge storage stability of the film to appropriately raise the charging temperature within a certain range. The laminated films have relatively stable surface potential, in addition, the laminated film is able to quickly restore itself to its original state after being scrubbed with alcohol.

2.6 Conclusion

In this chapter, electrets, ferroelectrets and methods of forming ferroelectrets and their application to energy harvesting technology are described in detail. As discussed in the applications, ferroelectrets have good piezoelectric properties and are considered to be one of the most suitable materials for wearable energy harvesting device. Comparing existing ferroelectret materials, we find that the piezoelectric performance is limited by the random void geometry and irregular overall cell structure, which is due to their fabrication process. The piezoelectric properties of ferroelectret are determined by the geometry of the voids. Therefore, in the following chapter, simulations investigating the optimization of void geometry and cell structure will be discussed.

In comparison to the existing methods of fabricating ferroelectret, PDMS has been demonstrated in the fabrication of ferroelectrets with controlled void layouts and geometries. Its primary advantages include low cost, fast simple fabrication and high levels of flexibility. However, PDMS is not a stable electret material and the surface charge stability on the void surfaces of the PDMS is poor, to improve the charge stability of PDMS ferroelectret, other electrets (PTFE.FEP) offer much greater charge stability but their combination with PDMS has yet to be investigated, which will be explored in the later chapters.

Chapter 3

3. Mathematical models and Simulation

3.1 Introduction

In this chapter, the simplified mathematical model of the relationship between piezoelectric coefficient d_{33} and the geometry and the distribution of the inner voids of the ferroelectret is summarized firstly, and ANSYS simulation tools are used to simulate the cellular PDMS structure of different sizes and different distribution of voids and the corresponding piezoelectric properties are calculated. After that, the theoretical results are compared with the simulation results to verify the correctness of the theoretical results.

3.2 Mathematic model for d_{33}

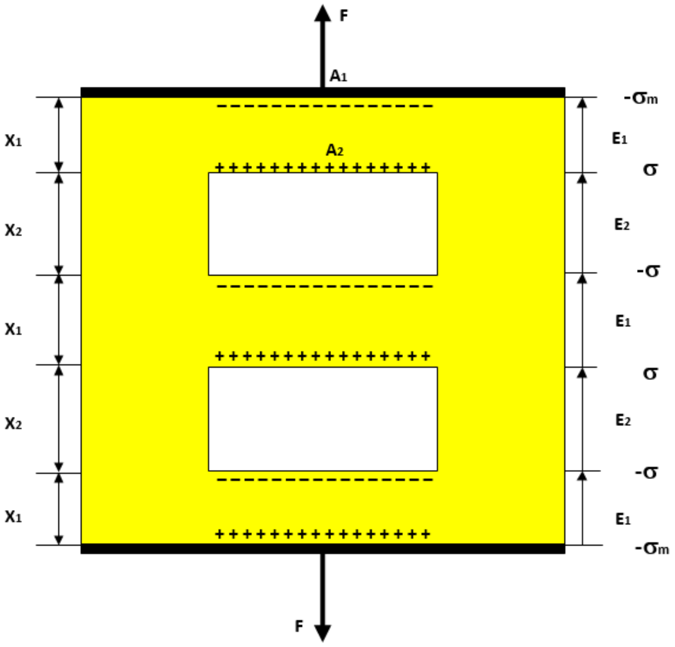

Figure 33. A simplified model of cellular structure [18][31]

As mentioned in the chapter 1, a simplified model of a cellular structure with charge-implanted ferroelectret cellular polymer is present as the Figure 33. There are electrodes (black one) in the cellular surfaces and several solid and void layers between the top and bottom electrode. To simplify this model, inside voids are considered as a same size and all the solid layers are designed in same thickness and width. Therefore, this model can be discussed as a 2D model. This model is used to explore the influence of piezoelectric properties with different size of voids and different layer numbers [31].

Then an assumption can be present: all the cellular structure includes n void layers and n + 1 solid layers (Figure 33 have 2 void layers and 3 solid layers), according to the Gauss' law, the electric field of the solid layer interface (E_1) and void layer interface (E_2) can be written as:

$$E_1 = \frac{\sigma_m}{\varepsilon_1 \varepsilon_0} \text{ and } E_2 = \frac{\sigma_m - \sigma}{\varepsilon_0} \tag{3.1}$$

Where σ_m is the charge density on the electrodes, σ is the charge density on void surfaces, ε_0 and ε_1 are the dielectric constant of air and the relative dielectric constant of the cellular material, and the electric potential (V) across the top electrode and bottom electrode can be obtained according to Kirchhoff's second law:

$$V = \int E\,dx = (n+1)x_1E_1 + nx_2E_2 = 0 \tag{3.2}$$

Where $x_1$and x_2 are the thickness of the solid layer and void layer respectively. Combined equation 3.1 and 3.2, the charge density on the electrodes can be described by:

$$\sigma_m = \frac{n\varepsilon_1\sigma x_2}{[(n+1)x_1 + n\varepsilon_1 x_2]} \tag{3.3}$$

The variation of the charge density on the electrodes $\Delta\sigma_m$ can be illustrated by the function related to the thickness variation Δx_1 and Δx_2:

$$\Delta\sigma_m = \frac{\partial\sigma_m}{\partial x_1}\Delta x_1 + \frac{\partial\sigma_m}{\partial x_2}\Delta x_2 = \frac{-n(n+1)\varepsilon_1\sigma x_2}{[(n+1)x_1 + n\varepsilon_1 x_2]^2}\Delta x_1 + \frac{n(n+1)\varepsilon_1\sigma x_1}{[(n+1)x_1 + n\varepsilon_1 x_2]^2}\Delta x_2 \tag{3.4}$$

Assumed that an external force is applied in the structure surface, and the relationship between stress and strain can be obtained as:

$$\frac{F}{A_1} = c_{33}\frac{\Delta x_1}{x_1} \text{ and } \frac{F}{A_2} = \frac{F}{s_r A_1} = c_{33}\frac{\Delta x_2}{x_2} \tag{3.5}$$

Where F is the external force, c_{33} is the elastic modulus of the cellular material, A_1 and A_2 are the effective areas of the solid and void layers, s_r is the ratio of A_2 to A_1. Since the charge area is a certain portion of electrode surfaces, the effective charge density $(\Delta\sigma_m)_{eff}$ can be described as:

$$(\Delta\sigma_m)_{eff} = (1 - s_r)\Delta\sigma_m \tag{3.6}$$

Combined equations 3.4 to 3.6, the piezoelectricity can be obtained by:

$$d_{33} = \frac{(\Delta\sigma_m)_{eff}}{F/A_1} = \frac{n(n+1)\varepsilon_1 t_r (1-s_r)^2 \sigma}{s_r\,[(n+1)+n\varepsilon_1 t_r]^2 c_{33}} \tag{3.7}$$

Where t_r is the ratio of x_2 to x_1. To a certain material, the charge density on void surfaces σ, the relative dielectric constant ε_1 and the elastic modulus c_{33} are constant, as a result, the piezoelectricity of a cellular material can be influenced by the geometry structure (t_r, s_r, n).

To explore the relationship between the different geometry parameters and piezoelectricity, first mathematic theory proof will be used to calculate the optimal value.

To any positive real number a and b, there is an inequation will be set up as:

$$a + b \geq 2\sqrt{ab} \tag{3.8}$$

Assumed $n + 1$, $n\varepsilon_1 t_r$ take the place of a and b,

Then $$(n + 1) + n\varepsilon_1 t_r \geq 2\sqrt{(n + 1)n\varepsilon_1 t_r},$$

$$[(n + 1) + n\varepsilon_1 t_r]^2 \geq 4n(n + 1)\varepsilon_1 t_r \tag{3.9}$$

And

$$d_{33} = \frac{n(n+1)\varepsilon_1 t_r (1-s_r)^2 \sigma}{s_r\,[(n+1)+n\varepsilon_1 t_r]^2 c_{33}} = \frac{(1-s_r)^2\sigma}{s_r c_{33}} \frac{n(n+1)\varepsilon_1 t_r}{[(n+1)+n\varepsilon_1 t_r]^2} \leq \frac{1}{4}\frac{(1-s_r)^2\sigma}{s_r c_{33}} \tag{3.10}$$

Only when $n + 1 = n\varepsilon_1 t_r$, $d_{33} = \frac{1}{4}\frac{(1-s_r)^2\sigma}{s_r c_{33}}$ can take the maximum value.

To any certain material, the charge density on void surfaces σ, the relative dielectric constant ε_1 and the elastic modulus c_{33} are constant. To illustrate this result clearly, PDMS will be taken as example. Therefore, the charge density on void surfaces σ is equal to 100 $\mu\mathrm{C}/m^2$, the value of elastic modulus c_{33} is 360KPa and the relative dielectric constant of PDMS ε_1 is 2.5[100][101].

For a single layer (One layer includes one solid layer and one void layer) PDMS ferroelectret, d_{33} will achieve the maximum value when t_r is equal to 0.8 according to the equation 10. Figure 34 present the relationship between t_r, s_r and d_{33} when a single layer is applied.

When the thickness ratio of the solid layer to void layer t_r is increased, the piezoelectric properties of the PDMS ferroelectret is improved and the optimised point has been demonstrated at around 0.8, with a peak piezoelectricity of 220 pC/N.

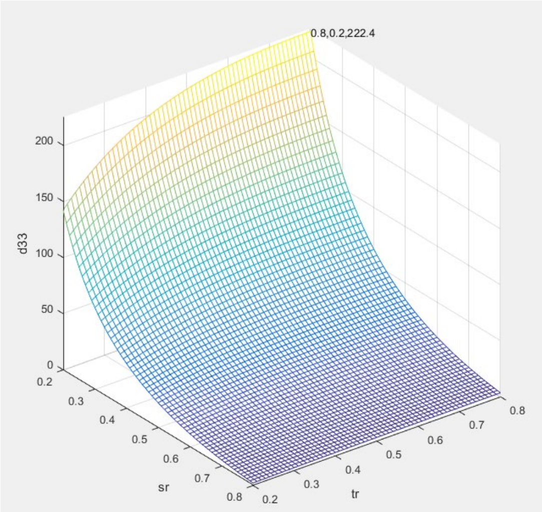

Figure 34. The relationship between t_r, s_r and d_{33}

For the multilayer PDMS ferroelectret structure, the maximum d_{33} of ferroelectret structure only varies with the values of s_r when t_r take the optimal value. The optimal value of t_r is determined by the void layers n only from the equation 10. It is found that with the increase of layer number, the optimal value of the ratio of t_r decreases gradually and finally stabilized at around 0.4 when n is larger than 10. Therefore, to achieve higher piezoelectric properties for multilayer ferroelectret, one should increase the void area as much as possible and guarantee the thickness ratio of the solid layer to void layer t_r equal 0.4.

To a multilayer ferroelectret cellular material, the relationship between the optimal value of t_r and layer number n is present as the following Table3.

Table 3. The optimal value of tr and the related layer number n

layer number n	optimal value of t_r
2	0.6
3	0.54

4	0.5
8	0.45
10	0.43
…	…
≥ 10	0.4

3.3 ANSYS simulation processes

ANSYS is a large-scale and general-purpose finite element analysis (FEA) software developed by ANSYS company in USA. It is the fastest growing computer-aided engineering (CAE) software in the world. It can interface with most computer-aided design (CAD) to achieve data sharing and exchange. The finite element software package in ANSYS is a computer design program with multi-purpose finite element method, can be used to solve the structure, fluid, electricity, electromagnetic fields and collision problems. Hence ANSYS is used to simulate the influence of the void geometry of the ferroelectret cellular structure to the piezoelectric coefficient. The Software version used here is ANSYS 17.1. For this model, static structural is the analysis type used. When a static structural project is creating in the Workbench, system will generate 6 following steps automatically, which includes Engineering Data, Geometry, Model, Setup, Solution and Results.

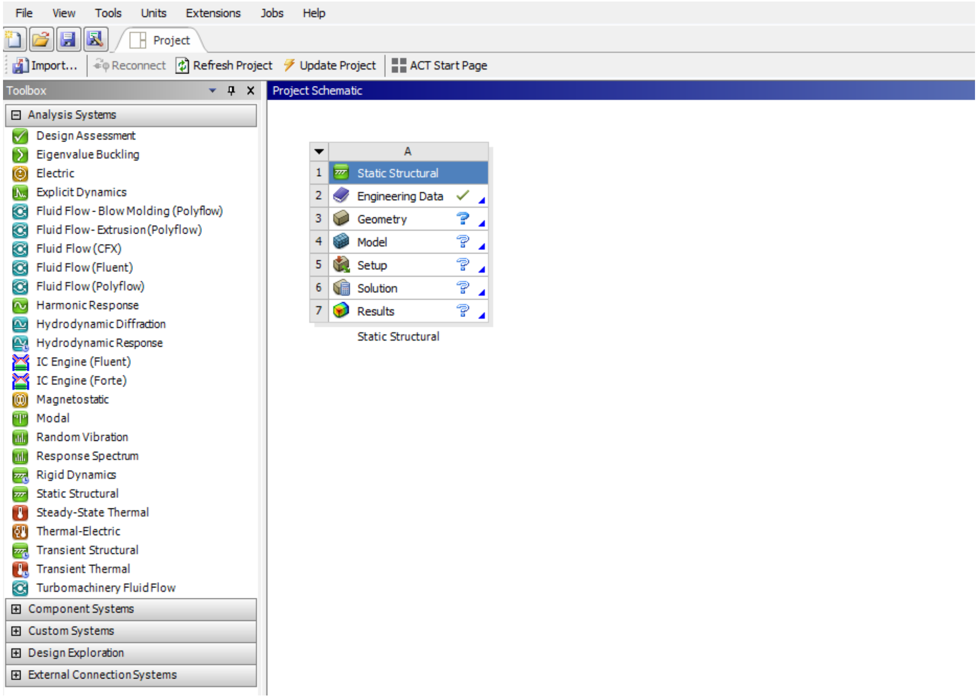

Figure 35. The operation interface of ANSYS Workbench

3.3.1 Engineering Data

The Engineering Data step is use for set some basic data of material. Some basic engineering data such as density, Poisson's ratio and so on can be adjusted in this step. For this project, the parameters of PDMS are shown in the Table 4.

Table 4. The parameters which need be changed and the related value [58]

Density	Young's modulus	Poisson's ratio
0.97kg/m^3	360-870 KPa	0.5

3.3.2 Geometry

The Geometry step is the process to establish the mechanical structure. ANSYS can interface with most computer-aided design (CAD) package to achieve data sharing and exchange. Hence the model can be built in many CAD software (Solidworks, UG NX and so on). A one layers with 10 voids PDMS cellular ferroelectret simplified model is established as Figure 36 and 37.

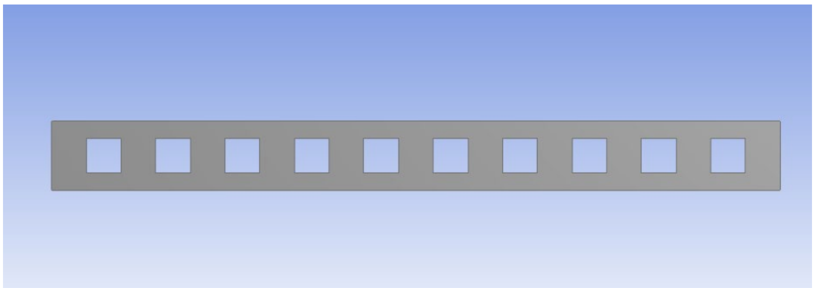

Figure 36. The cross section view of Geometry

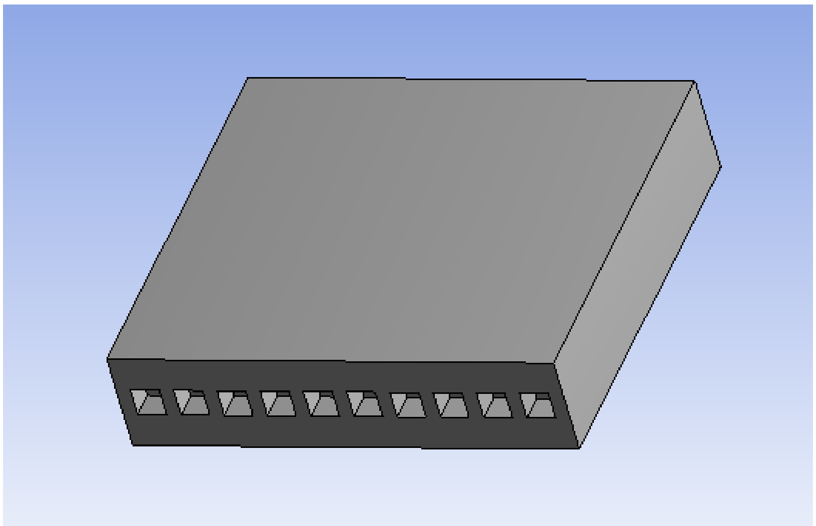

Figure 37. The overall view of Geometry

In this model, the thickness ratio of the solid layer to void layer t_r and the effective areas ratio of the void layer to solid layer s_r are set as 0.4. As mentioned in the literature part, the size of the inner void of ferroelectrets is on the order of magnitude about 100×100 μm^2.To simplify the model, the length of this model is 550 μm. The size of void is a 50 $\mu m \times$ 50 μm^2.

3.3.3 Model

When the Geometry step is finished, a solid cellular ferroelectret structure is generated. The next process is dividing this structure into elements. The accuracy of the final result is decided by the element size. The element size should be considered as a suitable value. Small element size will make system to take a very long time to finish the solution process. Large element size may generate an incorrect result. This is a trade-off between the accuracy and time.

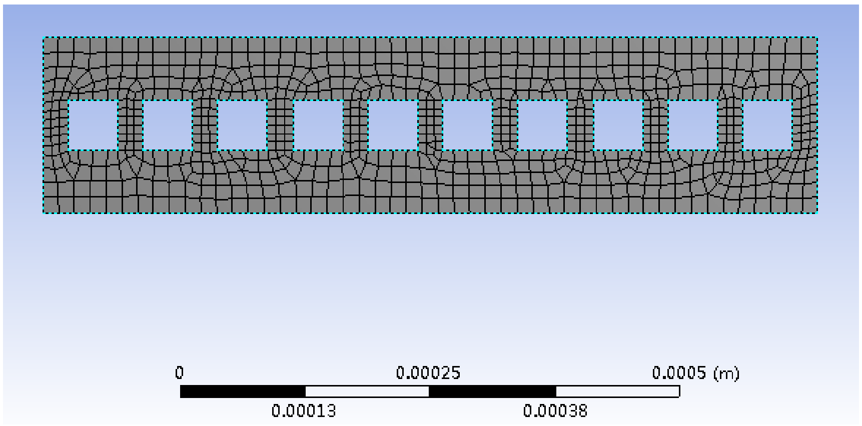

Figure 38. The Mesh result and the element size

In this model, considering this is a simple model, the automatic mesh process can be used. In the mechanical window, the “detail of Mesh” setting, can use to define the generating method and size of the elements. The size function is changed to “Proximity and Curvature”. The final mesh result and the local details are present as Figure 38.

3.3.4 Setup

In this step, some boundary conditions are set to help the software build the mathematical model. In this model, there are only two boundary conditions: surface pressure and the fixed support. That means a pressure is applied on the top surface, and the model cannot move in the vertical direction. These two boundary conditions applied as shown as Figure 39. The application pressure is 1KPa, which is equivalent to the foot pressure of a preson during walking.

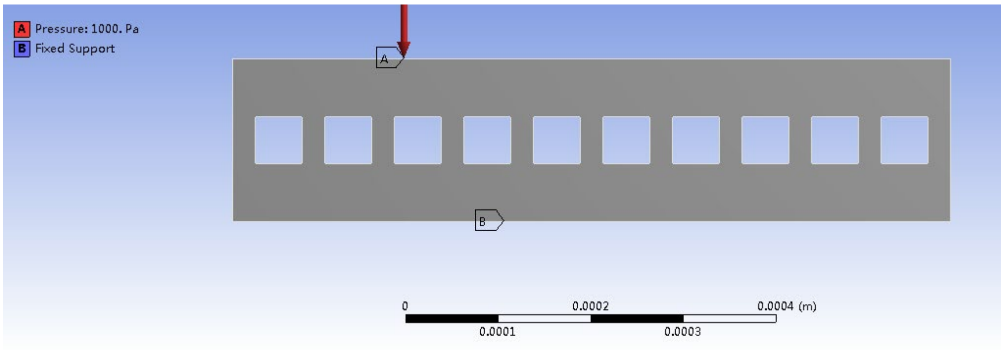

Figure 39. The boundary conditions applied in the ANSYS

3.3.5 Solution and Result

When all the boundary conditions are defined, the solution can be generated. There are many different results can be present, for example, stress, deformation and strain. The deformation result is present as the Figure 40.

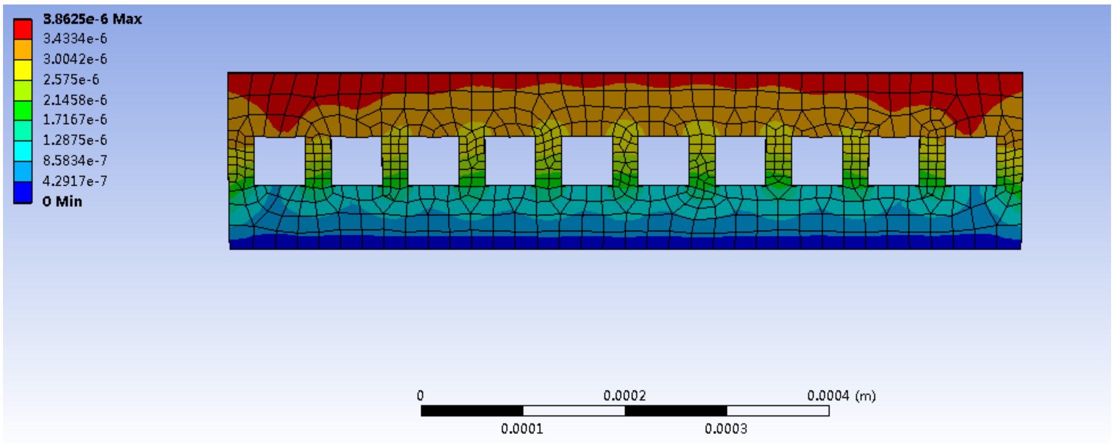

Figure 40. The deformation result in ANSYS

Assumed that the charge density of the whole void surface is the same, the piezoelectric coefficient d_{33} can be calculated by:

$$d_{33} = \frac{(\Delta\sigma_m)_{eff}}{F/A_1} \tag{3.16}$$

And

$$\Delta\sigma_m = \frac{\partial\sigma_m}{\partial x_1}\Delta x_1 + \frac{\partial\sigma_m}{\partial x_2}\Delta x_2 = \frac{-n(n+1)\varepsilon_1\sigma x_2}{[(n+1)x_1+n\varepsilon_1 x_2]^2}\Delta x_1 + \frac{n(n+1)\varepsilon_1\sigma x_1}{[(n+1)x_1+n\varepsilon_1 x_2]^2}\Delta x_2 \tag{3.17}$$

Combining equation 11 and 12, the piezoelectric coefficient d_{33} can be illustrated by:

$$d_{33} = 2\varepsilon_1\sigma(x_2\Delta x_1 + x_1\Delta x_2)(2x_1 + \varepsilon_1 x_2)^{-2}P^{-1} \tag{3.18}$$

Where ε_1 is the dielectric constant of air and the relative dielectric constant of PDMS; σ is the charge density on void surface, x_1 and x_2 are the thickness of solid and void layers, respectively; Δx_1 and Δx_2 are the variations of the thickness and P is the external pressure. Finally, the simulation piezoelectric coefficient can be calculated by equation 3.18, which can be compared with the theoretical value by equation 3.10.

$$d_{31} = \frac{(\Delta\sigma_m)_{eff}}{F/A_3}d_{31} \tag{3.19}$$

The deformation can be written by:

$$\Delta x = \frac{(n+1)\Delta x_1 + n\Delta x_2}{\mu} \tag{3.20}$$

Combining equation 11 and 12, the piezoelectric coefficient d_{33} can be illustrated by:

$$d_{31} = \frac{\mu + \mu^2}{1-\mu^2}\mu\varepsilon_1\sigma(2x_2\Delta x_1 + 2x_1\Delta x_2)(2x_1 + \varepsilon_1 x_2)^{-2}P^{-1} \tag{3.21}$$

Where ε_1 is the dielectric constant of air and the relative dielectric constant of PDMS; σ is the charge density on void surface, x_1 and x_2 are the thickness of solid and void layers, respectively; Δx_1 and Δx_2 are the variations of the thickness and P is the external pressure. Finally, the simulation piezoelectric coefficient can be calculated by equation 3.21, which can be compared with the theoretical value by equation 3.17.

3.4 Simulation result and evaluation

According to the mathematic analysis, to achieve a higher piezoelectric property for a ferroelectret cellular material, the void area should be as large as possible (s_r as small as possible), and the ratio of the thickness of the solid and void layer t_r should be maintained at an optimal value depending on the layer number n.

3.4.1 The simulation result of t_r

To verify the conclusion drawn by mathematic model, 7 model with different values of t_r (from 0.2 to 0.8) but the same geometry structure (one layer with 10 voids, the length is the same) and same s_r (0.4) is established. The Figure 41 present the piezoelectric coefficient d_{33} of analytical model and the ANSYS simulation. It is clear that to a monolayer PDMS cellular structure, the optimal value of t_r is 0.8 when s_r is uniform, which is fit the mathematic analysis. This result matches the literature [18].

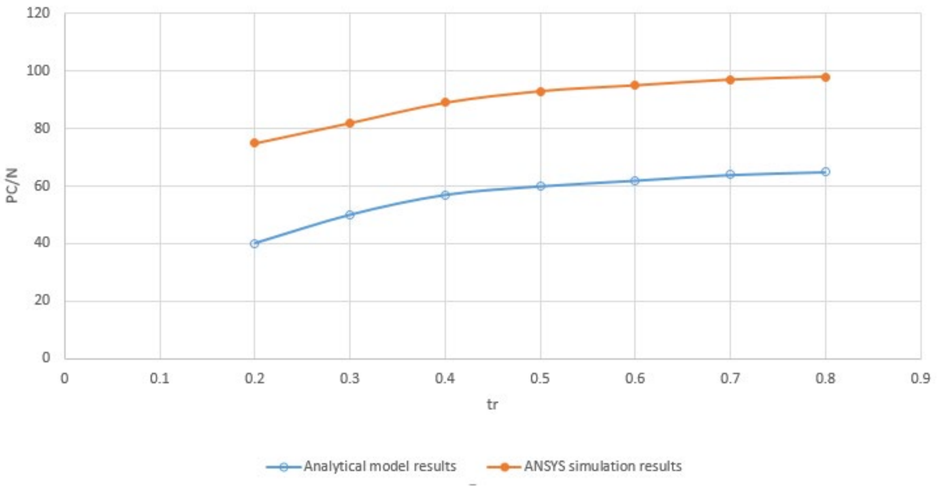

Figure 41. The piezoelectric coefficient d_{33} of different value of t_r and same s_r

3.4.2 The simulation result of different void area

To explore the influence of different void area, 3 models with different void area are established. The overall structure is present as the Figure 42.

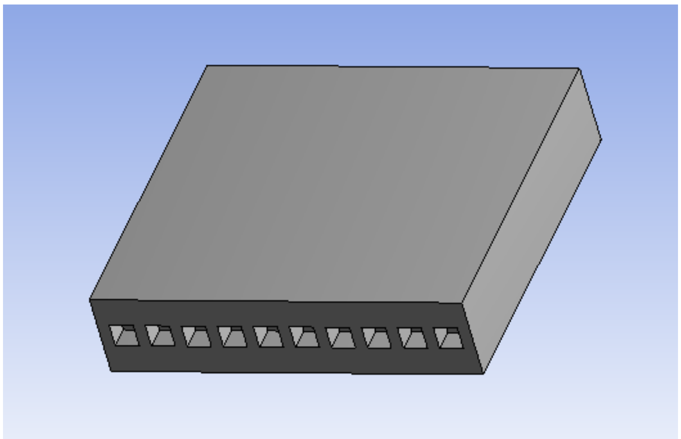

Figure 42. The overall structure

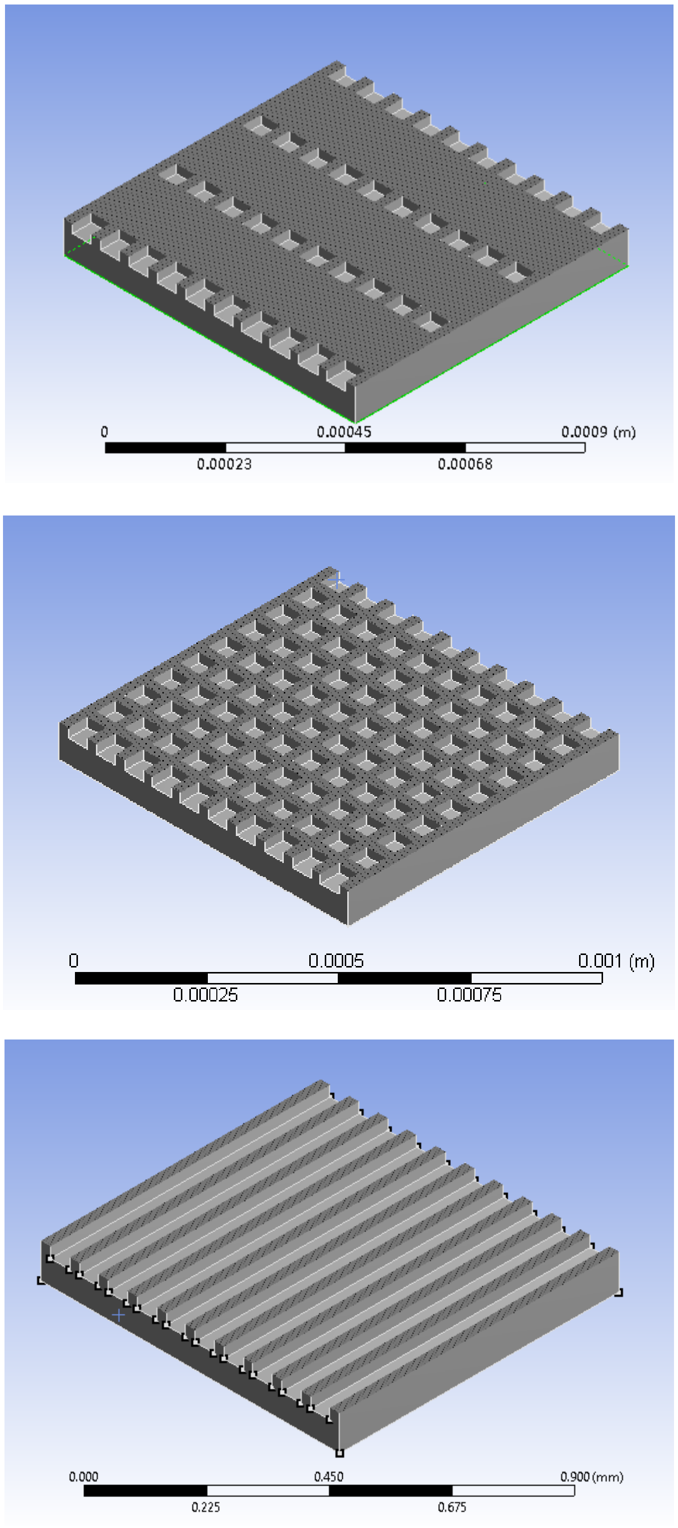

Figure 43. The section view of the three models

Figure 43 give out the section view of the 3 different models. They have a uniform value of t_r (0.4) but different void area, from top to bottom, with the increase of the void area. The corresponding results are present as the Figure 46 and 47. In this figure, the results of void area

1, 2 and 3 are correspond to the models from top to bottom in the Figure 43.

As a result, when t_r is uniform, increase the void area, a higher piezoelectric property will achieve, which is also fit the mathematic analysis. To an optimal geometry structure, the piezoelectric coefficient d_{33} will reach the maximum at the same time.

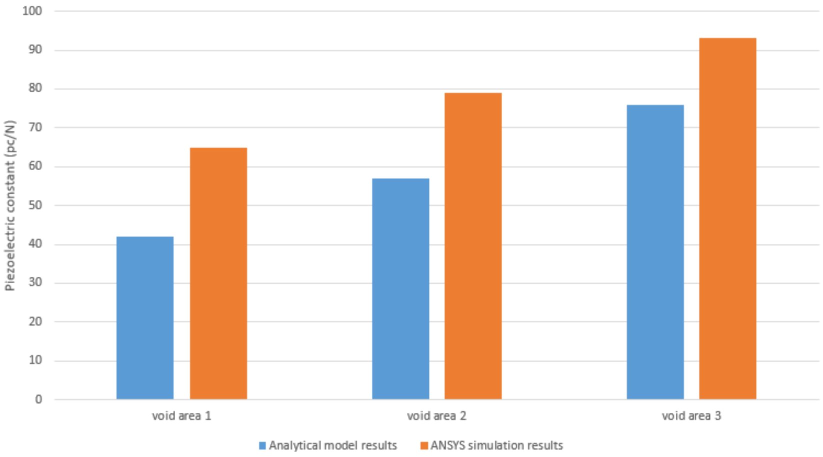

Figure 44. The piezoelectric coefficient d_{33} of different void area

3.5 Charge decay estimation

The charge stability in electrets is of great importance for the long-term application of electret and ferroelectret materials. For some electrets, it is very difficult to directly measure the life of electrets under normal temperature and humidity conditions within a reasonable time span. However, by using the isothermal depolarization procedure, experimental results obtained by increasing temperature to accelerate the attenuation of the electret's stored charge combined with suitable data processing, it is possible to describe the rate of charge decay. The electret charge decay has an approximately exponential relationship with time and temperature [135]:

$$\sigma(t,T) = \sigma_0(0,T)exp\left(\frac{-t}{\tau}\right) \tag{3.1}$$

Here $\sigma(t,T)$ represents the equivalent surface charge density related to time and temperature where τ represents the charge decay time constant at temperature T. In this way, the decay of most real electret charges can be approximately estimated.

In the selected temperature range from 200°C to 300°C, by adjusting the aging time, the equivalent surface charge density can be attenuated to a certain value, and the change over time under isothermal conditions can be measured. According to the measurement data, the effective time constant at each set depolarization temperature can be determined by:

$$\tau|_{T=T_i} = -\frac{dt}{d\, ln\sigma}|_{T=T_i} \tag{3.2}$$

If, during the depolarization process, the charge trapped in the sample to be tested does not undergo significant migration, the following relationship can also be used:

$$\tau|_{T=T_i} = -\frac{dt}{d\, lnV_S}|_{T=T_i} \tag{3.3}$$

Here V_S is the equivalent surface potential. The effective decay time constant of the charge in the electret shows a relationship with the temperature as below:

$$\tau(T) = \tau_0 exp\left(\frac{E}{kT}\right) \tag{3.4}$$

Here, E is the activation energy of the charges trapped in various traps, where k is Boltzmann's constant and τ_0 is a constant. From (1),

$$ln\sigma(t,T) = -\frac{t}{\tau} + ln\tau_0(0,T) \tag{3.5}$$

And

$$lnV_S(t,T) = -\frac{t}{\tau} + lnV_{S0}(0,T) \tag{3.6}$$

Since the charge migration of PTFE in the temperature range is not obvious, in the isothermal depolarization procedure, the measurement of $\sigma(t,T)$ may be directly replaced by the measurement of $V_S(t,T)$. According to formula (4),

$$ln\tau(T) = \frac{E}{k} \times \frac{1}{T} + ln\tau_0 \tag{3.7}$$

The electret charge decay has an approximately exponential relationship with time and temperature as given by equation (3.7), The parameter τ(T) in equation (3.7) represents the charge decay time constant at temperature T, where k is Boltzmann's constant and E, τ_0 is a constant. In the selected temperature range from 200 °C to 300 °C, by adjusting the ageing time, the equivalent surface charge density can be attenuated to a certain value, and the change over time under isothermal conditions can be measured. From this measured data, the effective time constant at each set depolarization temperature can be determined by equation (3.7). From (3.7), $\ln\tau$ and $1/T$ show a linear relationship and E, k, $\ln\tau_0$ can be considered as constants. Since the charge decay time constant of electrets at high temperatures are relatively short [108], this can be obtained by experimental measurements and the charge decay time constant at room temperature can be extrapolated from these results.

The linear relationship between charge decay and temperature for the ferroelectret materials with ratios of PTFE and PDMS varying from 1:10 to 1:2, the PTFE/water solution ferroelectret and the pure PDMS ferroelectret are shown in Figure 45. These ratios were selected to enable the exploration of the effect of increasing the PTFE content on charge stability and on the physical properties of the PDMS. It is anticipated that the more PTFE added, the greater the charge stability but this will reduce physical properties such as the maximum strain the composite can survive. The maximum ratio of PTFE to PDMS was 1:2 which was limited by the viscosity of the formulation and the ability to mix it and evenly disperse the PTFE particles within the PDMS. The charge decay time constants for the electret at 200 °C, 250 °C and 300 °C were experimentally determined by isothermal depolarization. By extrapolating the plot to room temperature (25 °C, corresponding to 1/T equalling 0.00335 in Figure 45 the storage life of the surface charge at room temperature can be obtained where the charge storage life is defined as the time taken for the surface charge density to fall to 20%. The storage life at room temperature of the ferroelectret materials with ratios of PTFE and PDMS varying from 1:10 to 1:2 ranges from 270 years to 1097 years respectively (corresponding to $\ln\tau$ values of 5.6 and 7 in Figure 45. The charge storage life of the ferroelectret with the PTFE/water solution is around 55 years ($\ln\tau=4$). In contrast, the storage life of pure PDMS is only one month ($\ln\tau=-2.4$). This demonstrates the ability of the PTFE additive to enhance the charge stability in a PDMS ferroelectret.

It should be noted that in a typical use case scenario, the electret lifetime actually observed is shorter than the predicted value because of the influence of environmental factors such as ambient radiation-induced conductivity and recombination with opposite-polarity ions deposited on the free surface of the samples attracted by the external field effect of the electrets

[108].

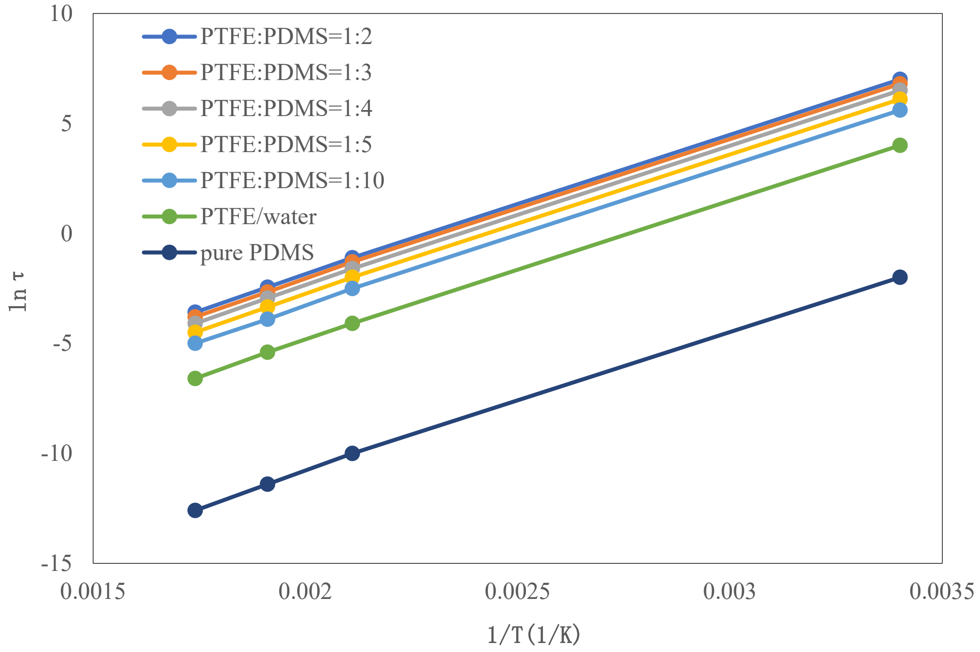

Figure 45. The charge decay time-temperature graph of electrets

3.6 Conclusion

In this chapter, a simplified model of a cellular structure with charge-implanted is present. Mathematic approach and simulation approach are applied to explore the relationship between the piezoelectric coefficient and the inner voids size. And finally, both of these two approaches prove that, to achieve a higher piezoelectric property for multilayer ferroelectret cellular material, two geometry parameters should be targeted. The void area should be as large as possible and the value of the ratio of thickness of the solid and void layer t_r should be maintained at 0.4 for 10 or more layers.

To a certain material, the charge density on void surfaces σ, the relative dielectric constant ε_1 ,the elastic modulus c_{33} and the Poisson's ratio are constant, as a result, the piezoelectricity of a cellular material can be influenced by the geometry structure $(t_r, s_r, n,)$.

From the result of charge decay estimation, the ability of the PTFE additive to enhance the charge stability in a PDMS ferroelectret. However, it should be noted that in a typical use case scenario, the electret lifetime actually observed is shorter than the predicted value because of the influence of environmental factors such as ambient radiation-induced conductivity and recombination with opposite-polarity ions deposited on the free surface of the samples attracted by the external field effect of the electrets [135]. These factors can lead to a reduction in the observed charge storage lifetimes compared with the estimated lifetimes as calculated above.

Chapter 4

4. Sample preparation and charging conditions optimization

4.1 Introduction

This chapter begins by repeating the previous work to fabricate the PDMS ferroelectret with open channel cellular structure, using 3D printing technology to complete the moulds and create a fixed void structure ferroelectret material.

4.2 Sample development

As discussed in chapter 3, the cellular structure with open channel (as shown as Figure 45) and the thickness ratio of the solid layer and void layer t_r is equal to 0.8 (for monolayer) will achieved the highest piezoelectricity. Therefore, the size of this structure can be calculated. When the size of sample is confirmed, the size of related moulds is determined as well. In this experiment, t_r is equal to 0.8, solid layer thickness is 1 mm and void layer thickness is 0.8 mm, which present as the Figure 46.

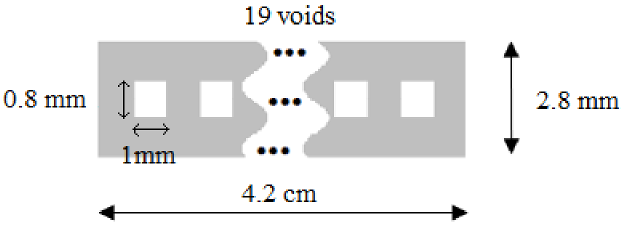

Figure 46. The overall and section view of conceived structure

For this experiment, a Connex350 TM 3D printer (Stratasys, MN, USA) was used to fabricate the 3D- moulds. The model of the mould structure was built by the software Solidworks (Dassault System, MA, USA) and saved as an STL-format file for uploading model to the printer. The mould material used is VerClear^{TM}. After the moulds has been fabricated by the 3D printer, a water gun is used to clean the moulds. Then degassed PDMS is used as glue to bond the moulds to a clear glass. Then the moulds were baked in oven at 80 °C for 24 hours. After this step, the glass-backed moulds should be exposed to a silane vapor for 1 hour to be coated with a thin layer of trichloro (1H,1H,2H,2H-perfluorooctyl) silane (Sigma Aldrich, MO, USA) [18]. As a result, these moulds will no longer inhibited with PDMS.

When finish the moulds, the PDMS ferroelectret can be fabricated as below, which was described by previous work [18]: first liquid PDMS and curing agent (Sylgard 184 from Dow Corning, MI, USA) should be mixed at a 10:1 weight ratio. Then this mixed gelatinous liquid was degassed in a vacuum desiccator. Then the degassed PDMS was poured into the moulds and were degassed again and then baked at 80 °C in the oven for two hours. The PDMS in the moulds should be at a suitable fluid level when pouring, which may affect the thickness of samples. After the PDMS in the mould was dried, the polymerized PDMS was detached from the moulds. An oxygen plasma treatment was applied to bond the two PDMS parts together (as present as Figure 47). The bonded PDMS was then baked in oven at 80 °C for 1 hour. The finished samples are present as the Figure 48.

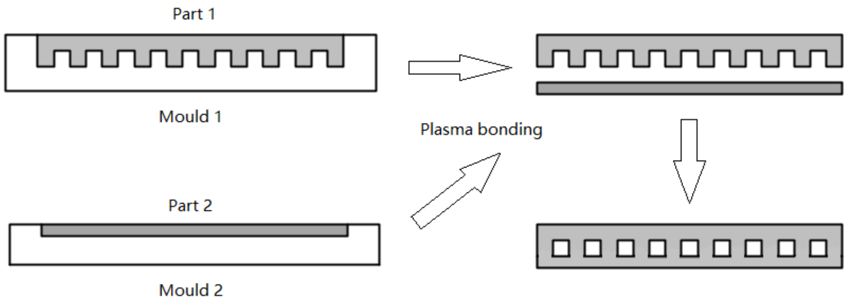

Figure 47. The fabrication processes of PDMS ferroelectret

Figure 48. The PDMS ferroelectret samples

4.3 Charging condition optimization

4.3.1 Experiment design

As present in chapter 2, the polarization process is always using corona charging technology, the ferroelectret material is placed on a metal plate as an electrode, and a certain distance was maintained between the needle and the plate. Applying a very high voltage to the needle, for a certain period of time, completes the charging process.

The purpose of the designed experiment is tried to find the influence caused by different charging conditions (charging time, charging voltage and charging distance). The entire samples used here is fabricated with the same geometry and size.

For this experiment, the corona poling process is described in [188]. The corona charging was applied at room temperature and normal atmospheres pressure. The voltage supply for needle and metal plate can provide from 0 to 30 kV voltages. The standard charging time is 120 seconds and thus 2 to 4 minutes are established. The charging distance is the distance from the needle to the plate which can adjust from 2 to 4 cm. Every experiment will test 5 samples.

The different charge conditions for the 5 samples will be been monitored by measuring the effective d_{33e} using a PiezoMeter Systems (PM300, Piezotest Ltd). For PDMS ferroelectret with the same structure, the energy harvesting performance is proportional to the piezoelectric coefficient. Therefore, the measured piezoelectric coefficient can characterize the final energy harvesting performance of each PDMS ferroelectret.

Control variable method is used here. That means in every different experiment, only one parameter will be changed. To evaluate the influence of the different charging conditions on the final piezoelectricity, the following experiments were designed as the Table 5. For the experiment 1,2 and 3, the only variable is the charging voltage; for the experiment 2,4 and 5, the only variable is the charging time; for the experiment 2, 6 and 7, the only variable is the charging distance.

Table 5. The designed experiments

Experiment number	Charging conditions		
	Charging time	Charging voltage	Charging distance
1	2 minutes	20 kV	4cm
2	2 minutes	25 kV	4cm
3	2 minutes	30 kV	4cm
4	1 minutes	25 kV	4cm
5	3 minutes	25 kV	4cm
6	2 minutes	25 kV	2cm
7	2 minutes	25 kV	3cm

4.3.2 Results and optimization

Five samples will be prepared for each experiment. When finishing the charging process, the whole fabrication process of the ferroelectret cellular is finished and the piezoelectric property can be measured. The piezoelectric constant d_{33} is always measured to reflect the piezoelectric activity of the material. Generally, we will measure the value of d_{33} in five different areas and calculate the mean value.

The best charging conditions are the conditions which can achieve the best piezoelectric properties. In these experiments, all the measurement is in the room temperature and the same time (just after finishing the charging process). The following Table 6 present the results of the different experiments.

Table 6. The result of designed experiments

Experiment number	Charging conditions			Result
	Charging time	Charging voltage	Charging distance	
1	2 minutes	20 kV	4cm	76 pC/N
2	2 minutes	25 kV	4cm	102 pC/N
3	2 minutes	30 kV	4cm	117 pC/N, 3 samples breakdown
4	1 minutes	25 kV	4cm	95 pC/N
5	3 minutes	25 kV	4cm	113 pC/N
6	2 minutes	25 kV	2cm	112 pC/N, 2 samples breakdown
7	2 minutes	25 kV	3cm	115 pC/N, 2 samples breakdown

From experiment 1 to 3, with the charging voltage increase, the related piezoelectric coefficient increases as well. Charging voltage shows positive correlation to the piezoelectric coefficient. But when the voltage is increase to 30 kV, 3 samples (5 samples totally) present a breakdown phenomenon. The breakdown means the sample reached the boundary of the limitation. From the experiment 2, 4 and 5, different charging time shows no relevance to the piezoelectric coefficient. And the experiment2, 6 and 7 present that short charging distance may also cause breakdown phenomenon and shows no relevance to the piezoelectric coefficient.

To explore a better charging voltage (no breakdown and higher piezoelectric constant), some more experiments are established. Maintaining the charging time (2 minutes) and the charging distance (4cm), the various charging voltage from 25 kV to 30 kV are established. Five samples will be prepared for each experiment. Table 7 present the experiment result.

Table 7. The result of various charging voltage

Experiment number	Charging conditions			Result
	Charging time	Charging voltage	Charging distance	
1	2 minutes	25 kV	4cm	102 pC/N, no breakdown
2	2 minutes	26 kV	4cm	104 pC/N, no breakdown
3	2 minutes	27 kV	4cm	100 pC/N, no breakdown
4	2 minutes	28 kV	4cm	102 pC/N, 1 samples breakdown
5	2 minutes	29 kV	4cm	109 pC/N, 3 samples breakdown
6	2 minutes	30 kV	4cm	117 pC/N, 3 samples breakdown

As a result, the best charging conditions can be found: the charging voltage is 30 kV, the charging time is 2 minutes and the charging distance is 4 cm, Lowering the charging voltage can effectively reduce breakdown, but will not get the best performance.

4.4 Conclusion

In this chapter, the fabrication procedure for the PDMS ferroelectret is present, the moulds are first made by 3D printing, then a release agent is attached to the surface of the moulds, which can then be used for the manufacture of PDMS ferroelectret. The moulds consist of two parts and eventually the two demolded samples are bonded together and a voids structure ferroelectret is formed.

The related charging conditions are established to optimize the Corona charging conditions. the best charging conditions had been found: the charging voltage is 30 kV, the charging time is 2 minutes and the charging distance is 4 cm, Lowering the charging voltage can effectively reduce breakdown, but will not get the best piezoelectric performance.

Chapter 5

5. The approaches to enhancing the surface charge density and stability in PDMS ferroelectrets

5.1 Introduction

As mentioned in chapter 2, the decay of charge is a typical phenomenon for most electret materials. The charge decay is affected by the material properties and the processing method of the electret. For a certain fabrication process, charge stability is linked to the dielectric properties of the material. In PDMS, the charge distributed on the upper and lower void surfaces after charging are not stable.

As a result, some methods are needed for enhancing the charge stability. Wang [32] describes a recharge method that can improve the charge stability by recharge the sample when finishing the corona charging. Therefore, the piezoelectric property of a recharged sample is expected to be higher than that of a first-time charged one. In the first part of this chapter, some experiment related to recharge method are illustrated.

In other hand, as present in the literatures, some studies on adding additives to improve the electrical properties of materials. And the effect of adding PTFE particles to PDMS had been described in previous studies [18]. More electrons can be trapped on the surface of the PTFE particles, and as the ratio of PTFE particles within the PDMS increases, the surface charge density of the PDMS/PTFE composite will also increase [20]. In the second part of this chapter, Different approaches to adding the PTFE particles to the ferroelectret structure will be described. The different fabrication processes of PTFE/water solution ferroelectret, PDMS/PTFE composite ferroelectret and PDMS/PTFE composite layer ferroelectret will be explored and compared.

5.2 Recharge samples

The life-span of the implanted charges in the existing researches and related experiment result present PDMS ferroelectret is mostly in the range of days to weeks, the piezoelectric coefficient of most samples will drop to half after 24 hours. And all the implanted charges will escape in 1 month. The following Figure 49 gives out the comparison of measured piezoelectric coefficient from 10 minutes to 1 month.

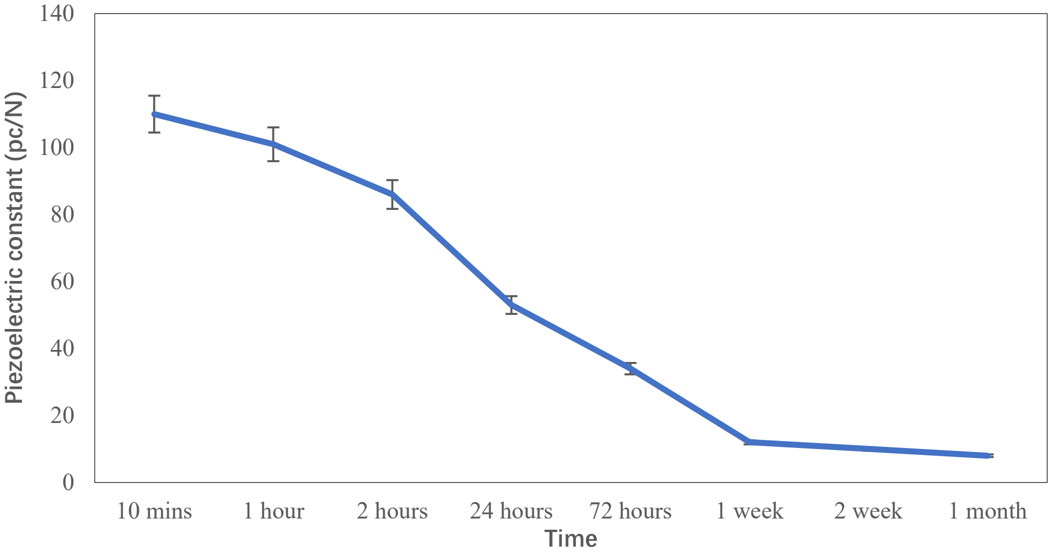

Figure 49. The charge life-span of PDMS ferroelectret after charging

Wang [32] describes that recharging samples have a higher charge density on void surfaces. Therefore, the piezoelectric property of a recharged sample is expected to be higher than that of a first-time charged one. In attention, stable charges accumulate in the recharged sample while unstable charges escape from the sample in the recharging process, it is very likely to have an increasing population of stable (long life-span) charges. By recharging, the electrons that were originally unstable and had a chance of escaping can return to a stable state, thereby improving the overall charge stability.

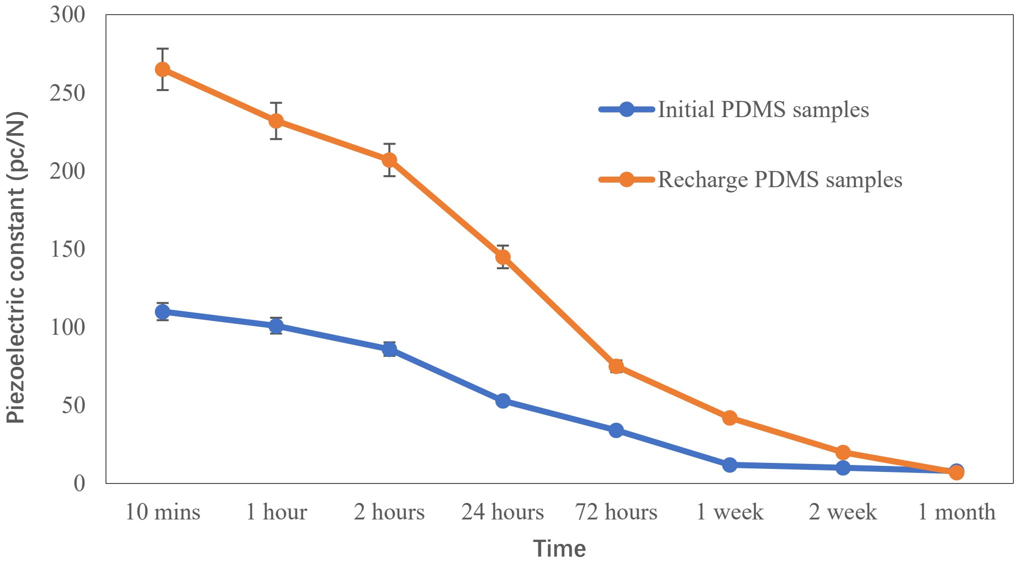

Figure 50. The charge life-span of initial and recharged PDMS samples

The Figure 50 present the charge life-span of initial and recharged PDMS samples (30 kV, 4 cm and 2 minutes with 5 samples). In the short term, repeated charging does improve the piezoelectric properties of the samples. However, although this method effectively increases the piezoelectric coefficient of these samples, the charge stability of samples does not increase significantly for a long time. The charges in the samples does not remain stable after repeated charging and gradually escapes after approximately one month, the piezoelectric properties will eventually remain the same as the sample without repeated charging.

5.3 Improved charge density and stability in PDMS ferroelectrets using PDMS/PTFE composite materials

This part explores measures to combine PTFE in the form of a powder with the PDMS to improve the charge stability in the ferroelectret whilst retaining the compliant, flexible mechanical properties of the PDMS. This work explores several approaches for coating the surfaces of PDMS voids with a PTFE layer and an approach whereby the PTFE is added to the PDMS and the entire ferroelectret device is molded from the combined PDMS/PTFE material. A PTFE/water solution and PDMS/PTFE composite solution have been used to coat the void surfaces and the same PDMS/PTFE composite was used fabricate the whole ferroelectret.

5.3.1 Experiment for PTFE/water solution ferroelectret

The PTFE/water solution was made by mixing 60% by weight of PTFE powder average particle size 1 μm diameter (Sigma Aldrich, MO, USA) to water. Firstly, the dimensional design of a new mould is shown in the Figure 51. As the voids surface will be deposited, it must be considered that the deposited voids still conform to the optimum scale structure of the calculated and simulated ratio. Therefore, the designed dimension of the voids is 1mm*1mm, with the depositing thickness of 0.2 mm, the final void dimensions are expected to remain at 0.8 mm * 1 mm.

The fabrication processes of two PDMS ferroelectret parts are the same. The liquid PDMS and curing agent (Sylgard 184 from Dow Corning, MI, USA) should be mixed at a 10:1 weight ratio. After that, this mixed gelatinous liquid was degassed in a vacuum desiccator. The prepared degassed PDMS was poured into the moulds and were degassed again and then baked at 80 °C in the oven for two hours. The thickness of the samples is controlled by the level of the PDMS poured into the mould. After curing processing, the polymerized PDMS was detached from the moulds. The polymerized PDMS is prepared for coating next.

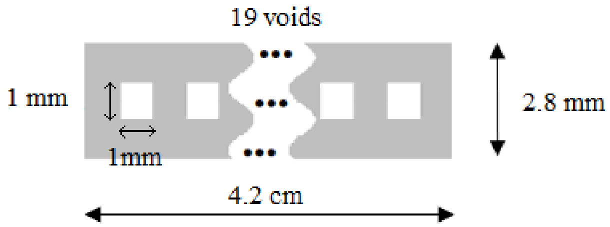

Figure 51. The overall and section view of new structure

The fabrication processes of first attempt are present in Figure 52. PTFE/water solution are spray evenly on the produced PDMS part 1 and 2 (0.7 mm). After 5 minutes of drying, a thin layer PTFE will be formed in the surface of PDMS (as the Figure 52). Then bonding these two parts, a new cellular structure ferroelectret is created. Plasma bonding cannot be used here because the surface is covered by PTFE which cannot bonding by Plasma treatment.

According to the literature, two bonding methods are suggested to use, glue or adhesive by high temperature [18][113]. The separate two parts can be easily and effectively glued up by the contact glue (VA 1401, WEICON, USA). The finished samples present a lower flexible, and its piezoelectric constant equal to zero after charging. The main reason is the liquid glue fills the voids and destroys the original ferroelectret structure.

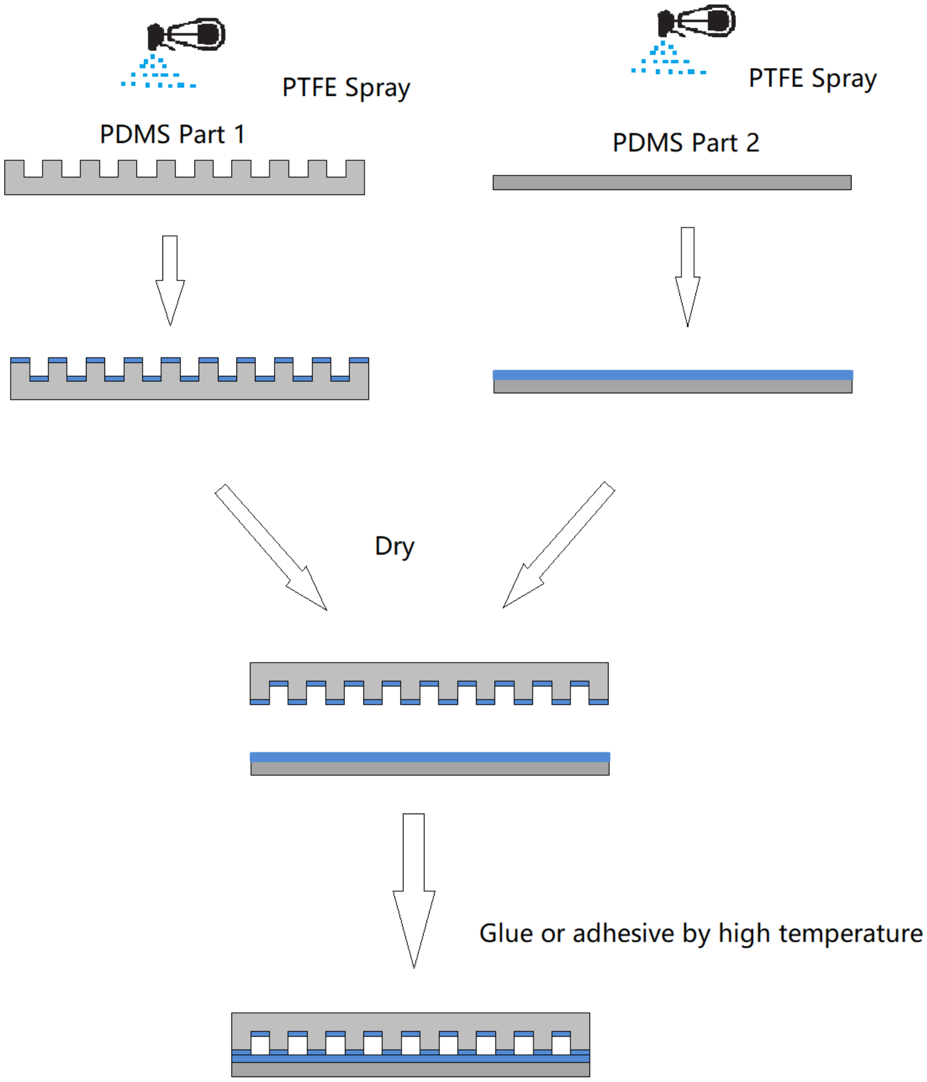

Figure 52. The fabrication processes design A with PTFE/water solution

Therefore, an improved scheme is present as Figure 53. First a mask is made to match the PDMS part 1. This mask allows the PTFE spray deposit to the void only. For PDMS part 2, use the same mask to deposit PTFE at the corresponding position. After dry and clean, plasma treatment can be used to bond these sample because the contact surface is PDMS.

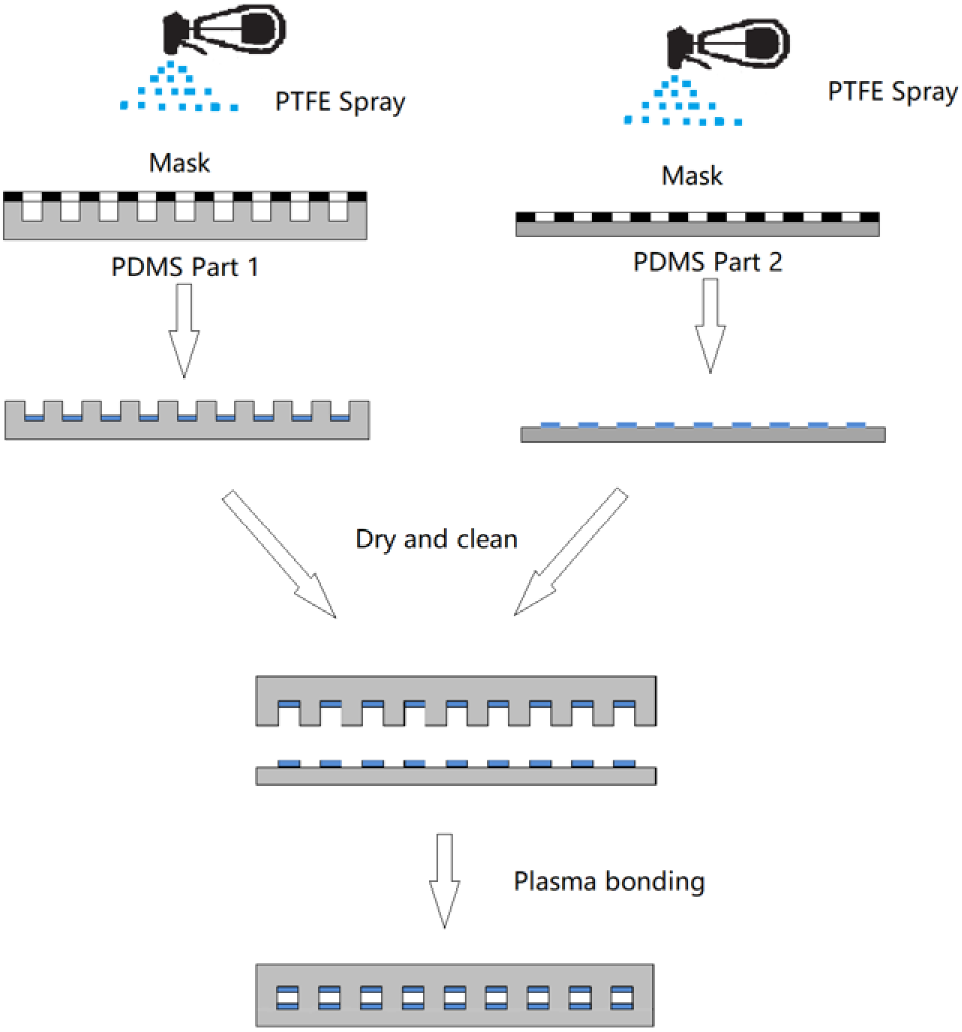

Figure 53. The fabrication processes design B with PTFE/water solution

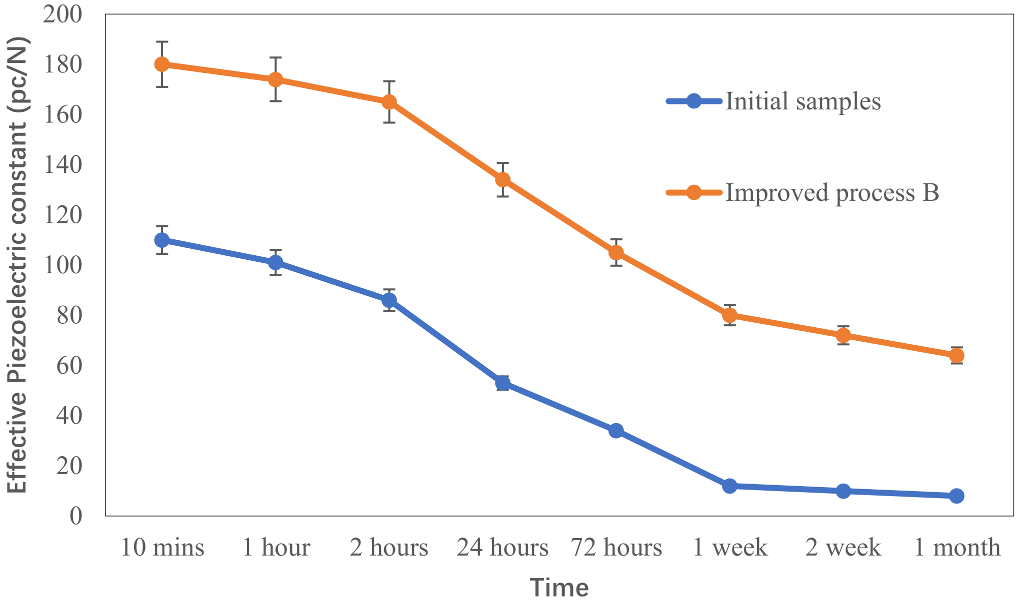

Figure 54. The charge life-span of initial samples and the fabrication processes design B with PTFE/water solution

Then an oxygen plasma treatment (Femto Asher, Diener, Germany, 30S at 35-40W) was applied to bond the two parts together (as shown in Figure 53). The bonded device was then baked in oven at 80 °C for 1 hour.

To explore how the properties of the material are affected by the PTFE coating, a pure PDMS ferroelectret were fabricated which is used for comparison. All the samples were polarized by the corona charging and five samples will eventually be made and each sample will be measured five times. The final statistical average will be used as the result. The charging voltage is 30 kV and the charging time is 2 mins with 4cm charging distance.

The piezoelectric coefficient d_{33} was measured by PiezoMeter Systems. Figure 54 present the charge life-span of initial samples and the fabrication processes design B with PTFE/water solution (30 kV, 4 cm and 2 minutes with 5 samples). From this figure, the charge stability has a promotion. There are 30% charges remain in the void surface after 1 months. However, the bonding process of this method is extremely complex because these two PDMS with PTFE surface parts must be bonded very accurately by position. In the bonding process, it is very difficult to guarantee a good success rate.

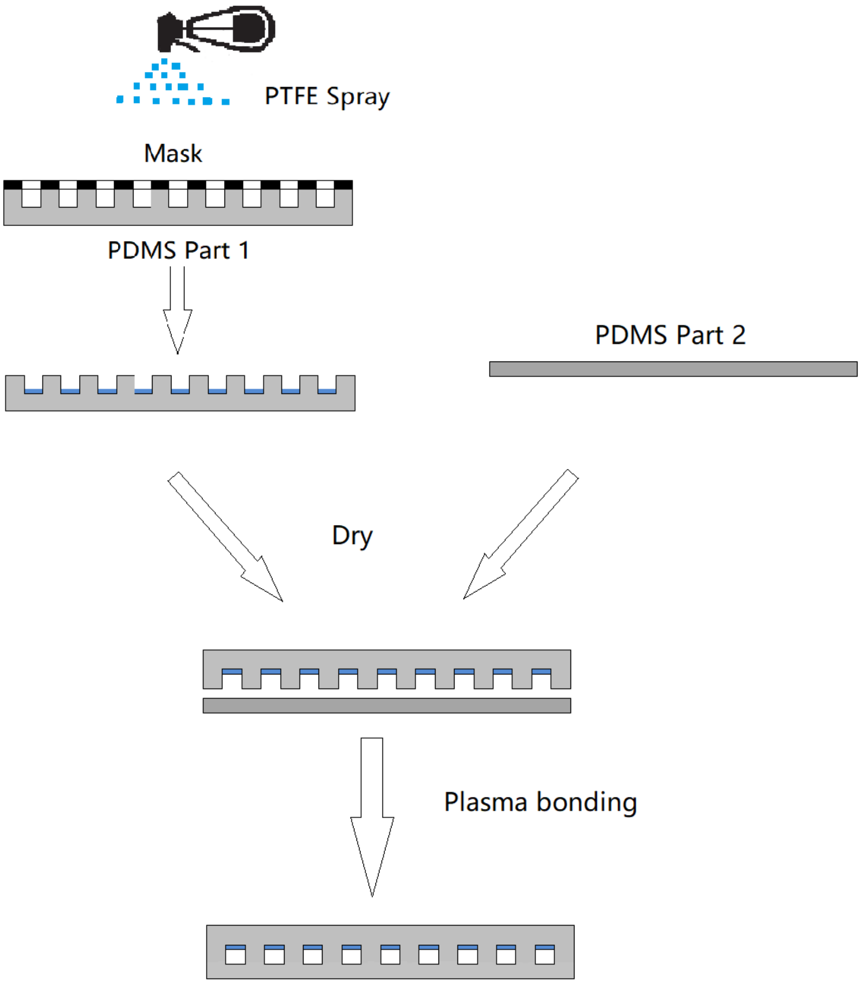

Figure 55. The fabrication processes design C with PTFE/water solution

An improved methods fabrication processes C is present as Figure 55. The fabrication processes design C only deposit PTFE on a single surface of void, makes bonding less of an issue. Figure 56 present the charge life-span of initial samples and the fabrication processes design C with PTFE/water solution (30 kV, 4 cm and 2 minutes with 5 samples). From this figure, the charge stability had improved but only 25% charges remain in the void surface after 1 months.

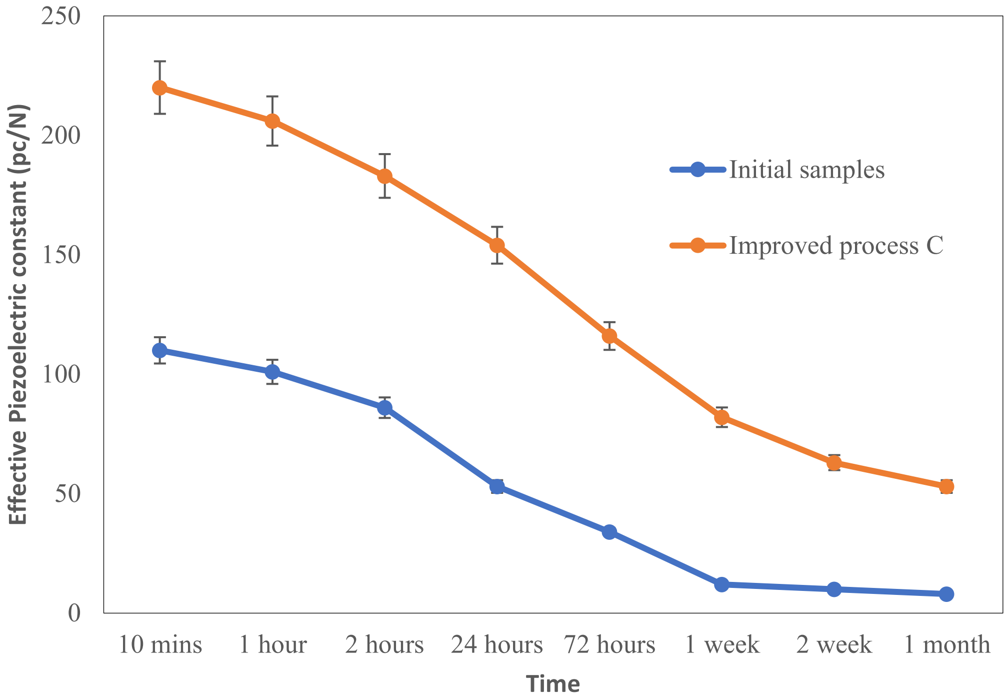

Figure 56. The charge life-span of initial samples and the fabrication processes design C with PTFE/water solution

An improved methods fabrication processes D is present as Figure 57. The fabrication processes D uses two PDMS part 1, the PTFE layer is deposited in the void, thus it is easy to bond them together as well. To maintain the final void dimensions at 0.8 mm * 1 mm, a new mould is designed and fabricated, the PTFE/water solution was sprayed evenly across the PDMS structure through a stencil mask to pattern the deposition, allowing it to coat the void surface whilst preventing the PTFE solution from coating the top, bonding surface of the molded PDMS. The samples were then oven baked at 80 °C for 1 hour leaving a dried, thin PTFE layer (0.1mm) on the void surface.

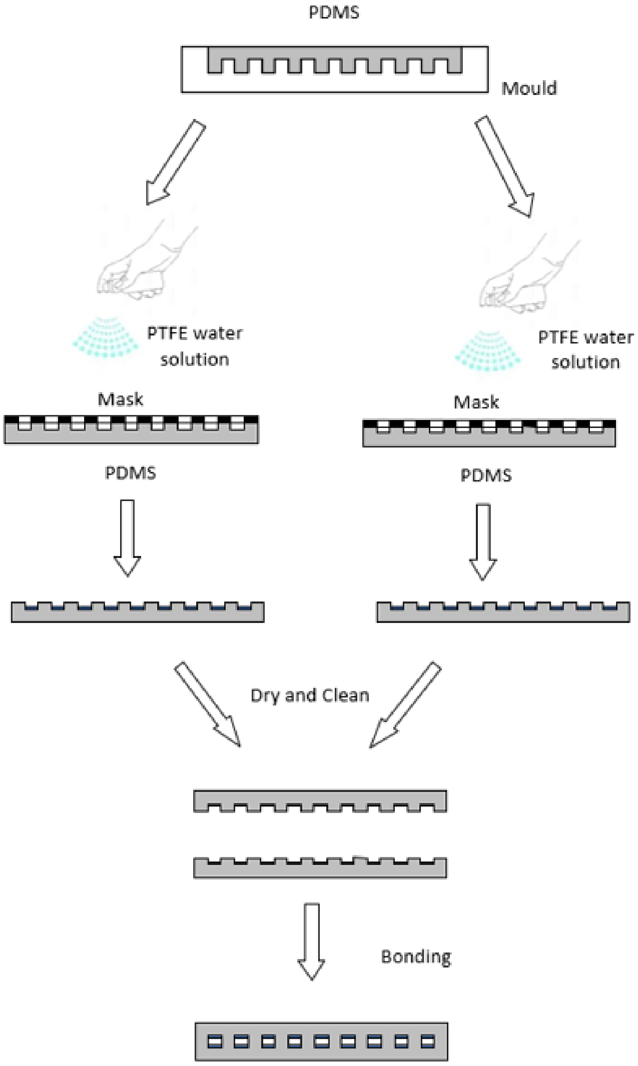

Figure 57. The fabrication processes design D with PTFE/water solution

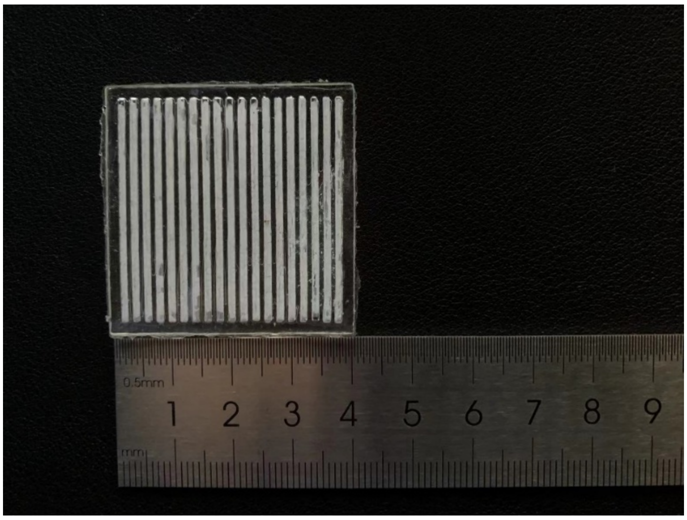

Figure 58. The Photo of samples by fabrication processes design D

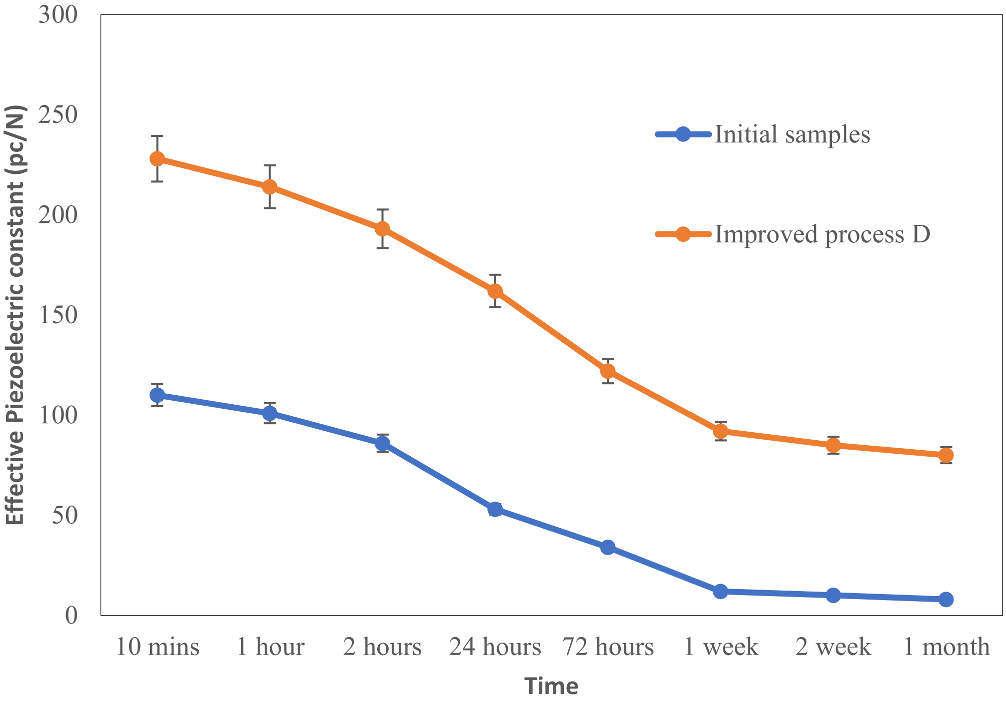

Figure 59. The charge life-span of initial samples and the fabrication processes design D with PTFE/water solution

Figure 58 present the Photo of samples by fabrication processes design D. Figure 59 shows a comparison of piezoelectric performance between PTFE/water solution ferroelectret and pure PDMS ferroelectret (30 kV, 4 cm and 2 minutes with 5 samples). The initial piezoelectric coefficient of PDMS water solution ferroelectret was about 228 pC/N, where the pure PDMS ferroelectret is 110 pC/N. The PTFE/water solution ferroelectret maintained around 35% and the d_{33} of pure PDMS drop to below 10 pC/N in one month. The PTFE particle is not soluble in PDMS, so extremely tiny voids will be formed around the PTFE particle. These voids can also store charges, thereby increasing the overall d_{33}.

To measure the d_{31}, the piezoelectric constant measurer cannot used because the sample cannot be compressed in the radial direction. The measured d_{31} can be divided into two directions as the Figure 60.

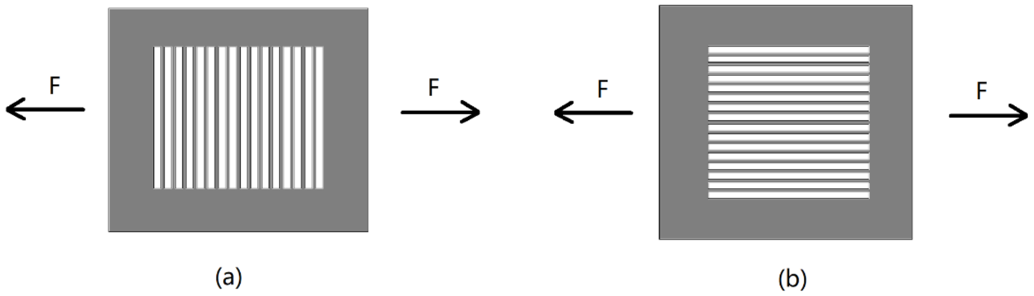

Figure 60. The two directions of d_{31}

Using an Impedance analyzer (6500B, USA) to measure the capacitance of the sample after charging. Aluminum tape is used as the electrodes of the samples. When adjusting the frequency of Impedance analyzer to a suitable range, the capacitance of the sample can be calculated. The value is 60 pF.

As present in the literature, all the ferroelectret materials have a very low value of d_{31}. Therefore, a charge amplifier circuit is designed to enlarge the signal of the d_{31} as the Figure 61.

The amplifier LM741 is characterized by its stability and low noise characteristics. It adopts a high-stability differential amplifier circuit design and can maintain stable operation under different environmental conditions. At the same time, it also has low noise characteristics, which can reduce the noise introduced during the signal amplification process. Secondly, LM741 has a wide operating voltage range. So LM741 is selected as the Operational Amplifier. In this circuit, the gain is equal to 10.

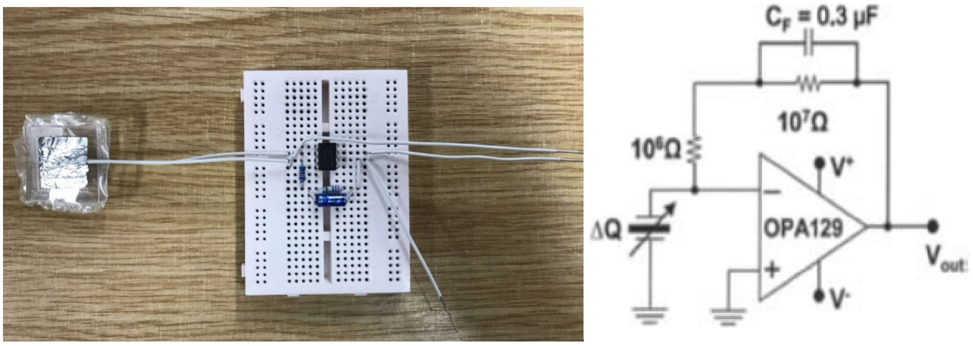

Figure 61. The charge amplifier and its equivalent circuit

The Instron electrodynamic instrument (ElectroPuls E1000) test insttrument is used to apply stress to the sample in radial direction. The power supply is used to supply power for amplifier. The oscilloscope is used to collect the output signal. The device structure is present as the Figure 62.

First an initial sample without PTFE deposition is measured. The test insttrument provide a 500N force in the direction as the Figure 60(a) at the frequency of 1Hz with 10 circles. The output singnal is present as the Figure 63.

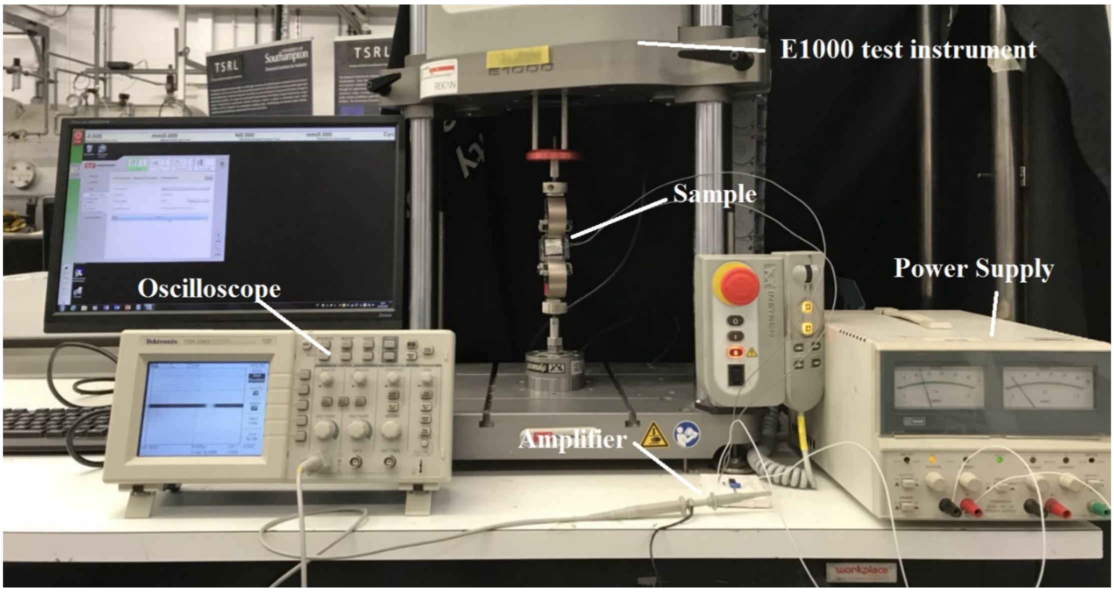

Figure 62. The oscilloscope used for measuring d_{31}

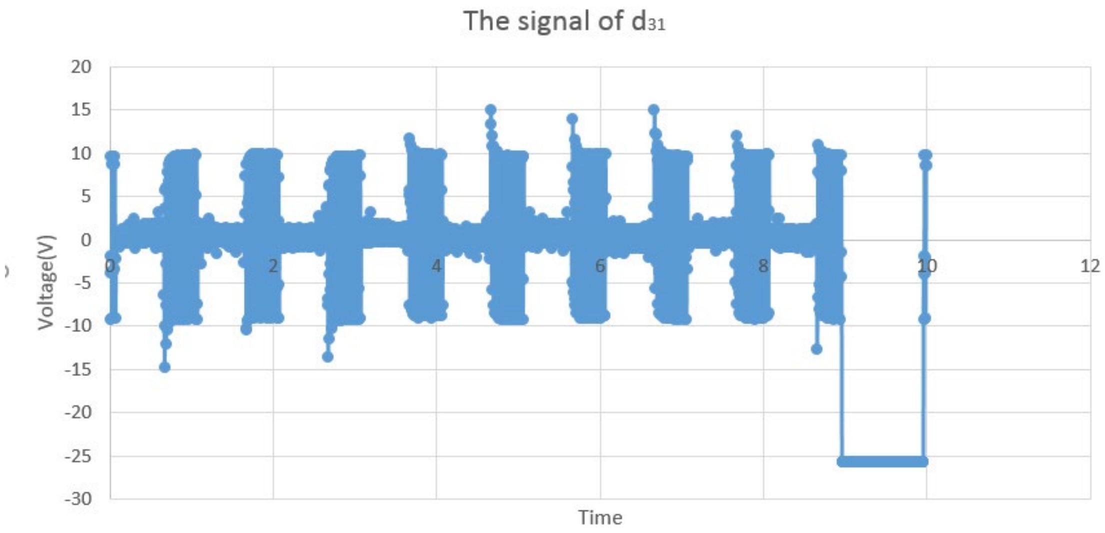

Figure 63. The The output singnal of d_{31a} from oscilloscope

From the Figure 63, it can be seen that the output voltage is 10V at the force of 5N. Considering the amplifier gain is 10, the capacitance is 60 pF, therefore the d_{31a} can be writen by:

$$d_{31a} = \frac{\mathrm{Q}}{\mathrm{F}} = \frac{60pF*10V}{10*5N} = 12pc/N \tag{4.1}$$

Similarly, the d_{31} in the direction 78(b) can be writen by:

$$d_{31b} = \frac{\mathrm{Q}}{\mathrm{F}} = \frac{60pF*6V}{10*5N} = 7.2pc/N \tag{4.2}$$

Where the 6V was also recorded by the oscilloscope. Figure 64 present the charge life-span of d_{31a} and d_{31b} of the initial PDMS sample without PTFE deposition.

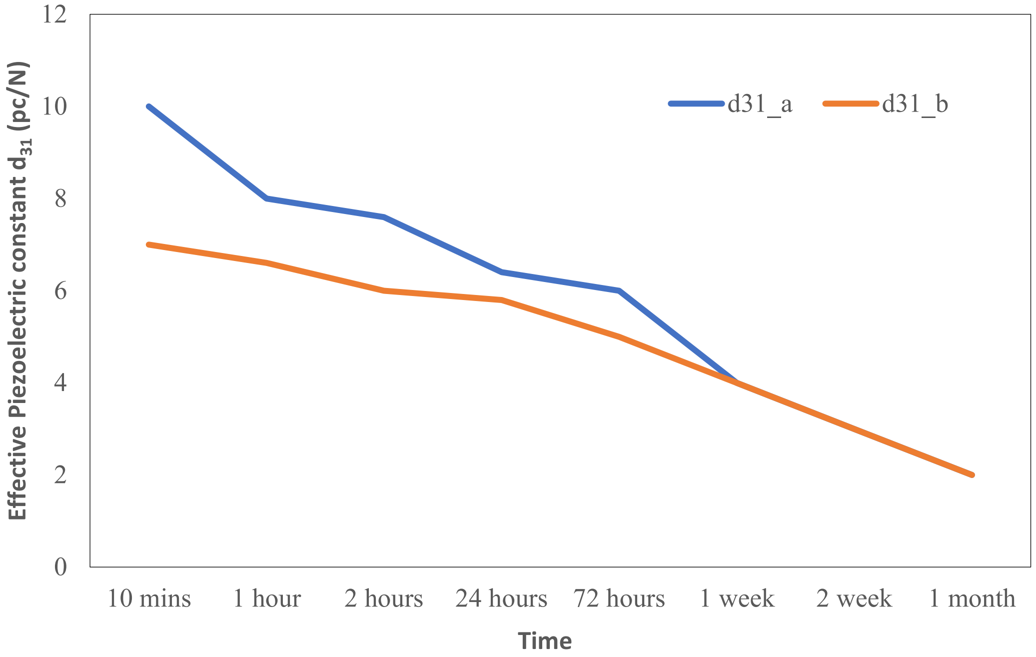

Figure 64. The charge life-span of d31a and d31b of the initial PDMS sample

Figure 65 and 66 present the charge life-span d_{31a} and d_{31b} of the initial sample, fabrication process B, C and D.

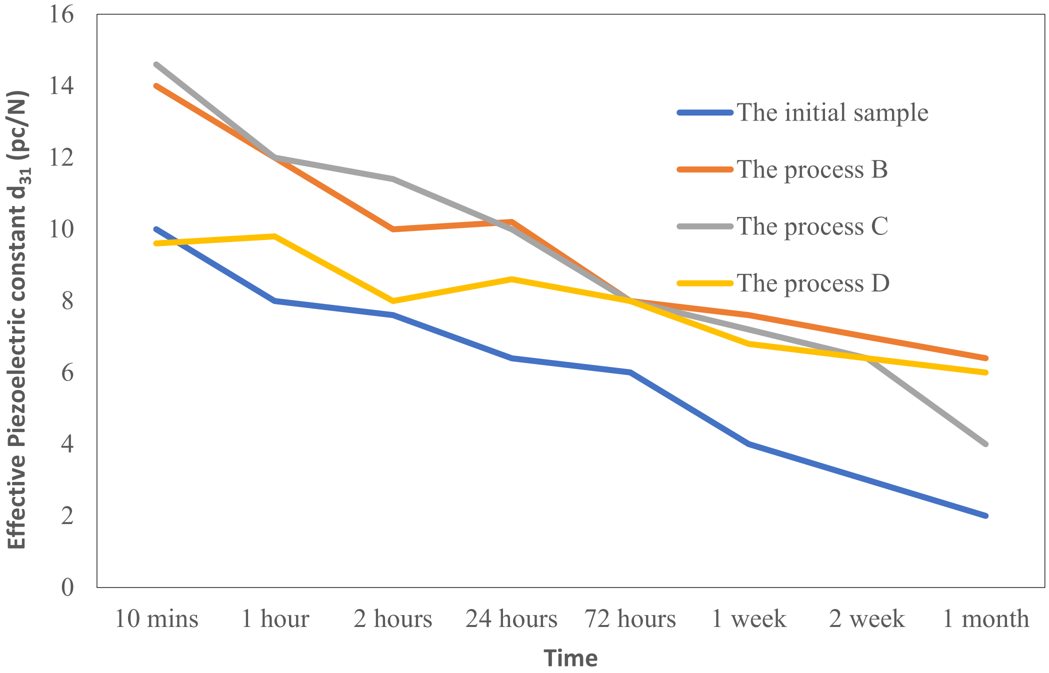

Figure 65. The charge life-span comparison of d_{31a} between 4 fabrication processes

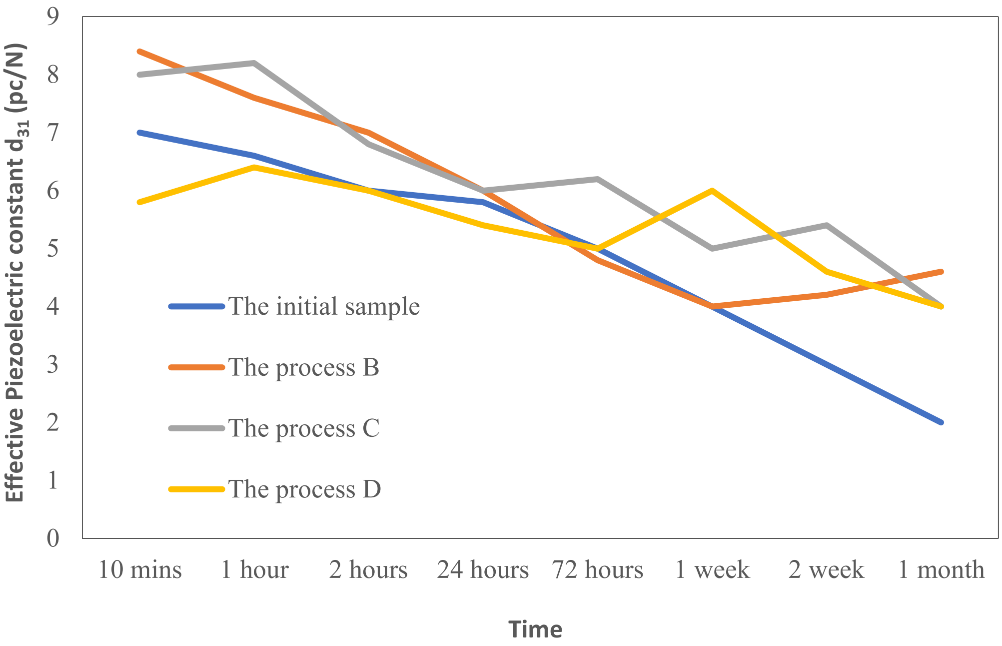

Figure 66. The charge life-span comparison of d_{31b} between 4 fabrication processes

From these two figures, it is clear that the value of measured d_{31} are very low, in the range of 5 to 20 pC/N.

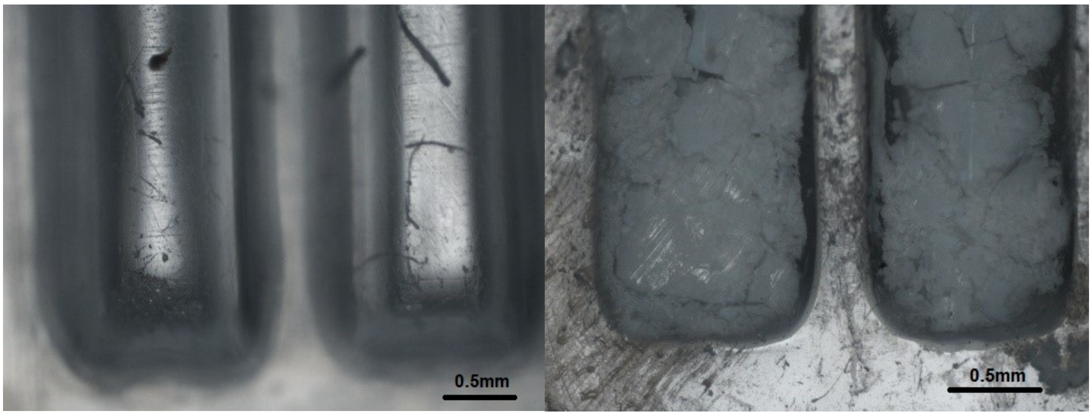

Figure 67. (a) the top view of the PDMS ferroelectret inner void surface (b) the top view of PTFE solution ferroelectret inner void surface

Figure 67 present the top view figure of the PTFE/water solution ferroelectret and PDMS ferroelectret inner void surface. From the surface view, it is obviously easy to see the formed PTFE layer was very fragile and easy to fall off due to there is no binder used between PTFE layer and PDMS layer, it limits long-term application in energy harvesting field. The next research will focus on how to enhance the adhesion between PTFE layer and the gas-polymer interfaces.

5.3.2 Experiment and result for PDMS/PTFE composite layer ferroelectret

As mentioned in last part, the formed PTFE layer was very fragile and easy to fall off in last fabrication process because of there is no binder used. As a result, to enhance the life-span of the samples, PDMS is used as binder to explore the performance.

The fabrication processes are present as below:

A Connex350 TM 3D printer (Stratasys, MN, USA) was used to fabricate the 3D moulds. The 3D printed material is a transparent plastic widely used in 3D printing, but it is hard to clean when PDMS is stuck on the surface. To prevent the PDMS sticking to the mould, they were baked in oven at 80 °C for 24 hours and then exposed to a silane vapour for 1 hour to be coated with a thin layer of trichloro (1H,1H,2H,2H-perfluorooctyl) silane (Sigma Aldrich, MO, USA).

Using the processed moulds, the PDMS ferroelectret can be fabricated. First, liquid PDMS and curing agent (Sylgard 184 from Dow Corning, MI, USA) should be mixed at a 10:1 weight ratio. After that, this mixed gelatinous liquid was degassed in a vacuum desiccator. The prepared degassed PDMS was poured into the moulds and were degassed again and then baked at 80 °C in the oven for two hours. The thickness of the samples is controlled by the level of the PDMS poured into the mould. After curing processing, the polymerized PDMS was detached from the moulds. The polymerized PDMS is prepared for coating next.

A PDMS/PTFE composite layer ferroelectret which composite layer made by PTFE powder mixed evenly with the PDMS gelatinous liquid in the weight ratio of 3:1, A syringe was used to manually deposit a fixed dose (0.1 ml) of the liquid solution onto the void surfaces, after baking in an oven at 80 °C for 1 hour, a thin PDMS/PTFE composite layer is coated in the void surface.

Then an oxygen plasma treatment (Femto Asher, Diener, Germany, 30S at 35-40W) was applied to bond the two parts together (as shown in Figure 70). The bonded device was then baked in oven at 80 °C for 1 hour.

The device is 4 cm × 4 cm square-shaped with several voids inside. The void surfaces are deposited by PDMS/PTFE composite solution. The photograph of the device is shown in Figure 69.

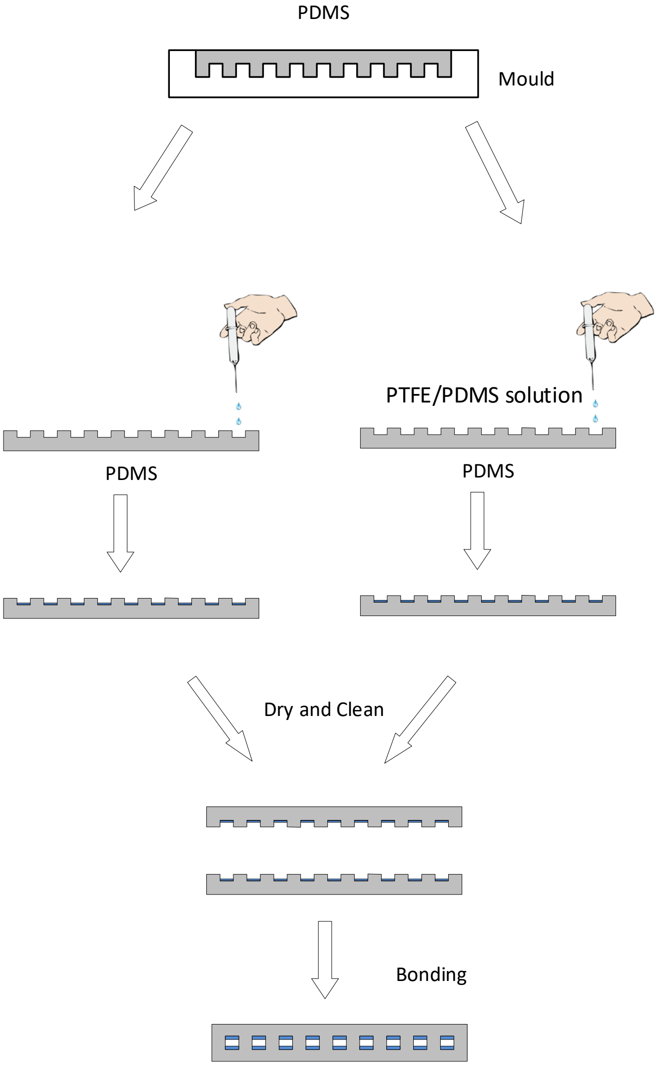

Figure 68. The fabrication process of PDMS/PTFE composite layer ferroelectret

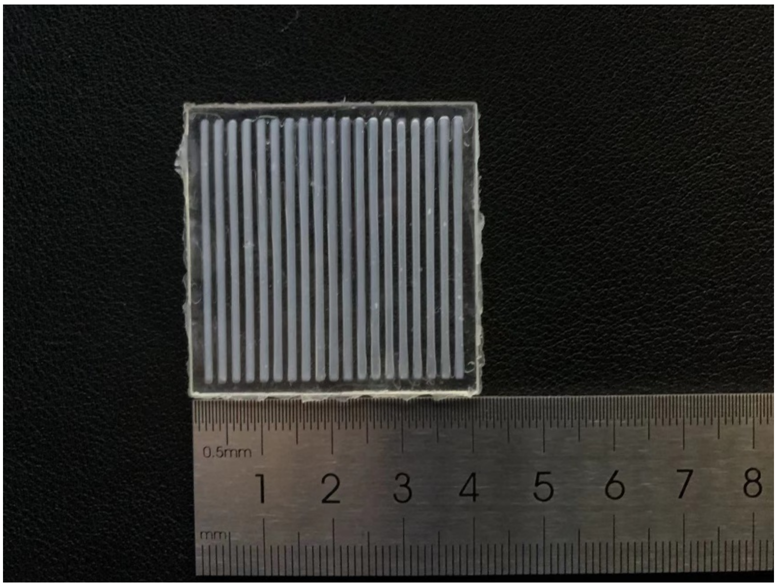

Figure 69. The photograph of the PDMS/PTFE composite layer ferroelectret

Figure 70 shows a comparison of piezoelectric performance between PDMS/PTFE composite layer ferroelectret and pure PDMS ferroelectret. The initial piezoelectric coefficient of PDMS/PTFE composite layer ferroelectret was about 680 pC/N, which is 7 times greater than that of the pure PDMS ferroelectret. The PDMS/PTFE composite layer ferroelectret maintained around 50% of its initial piezoelectric coefficient over 4 months. The d_{33} of pure PDMS drop to below 10 pC/N in one month.

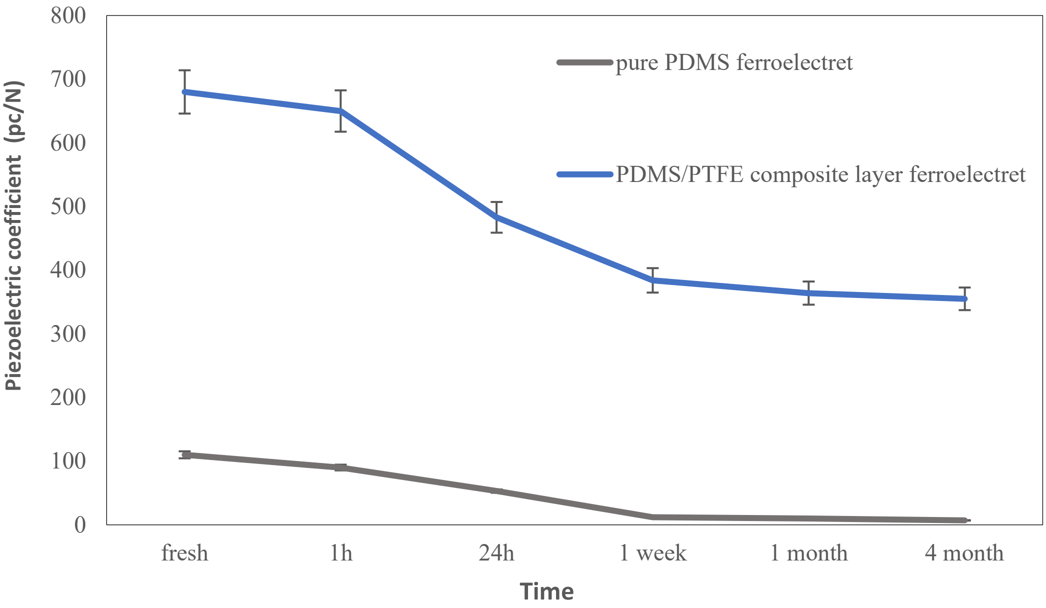

Figure 70. The Piezoelectric coefficient of pure PDMS ferroelectret and composite layer ferroelectret

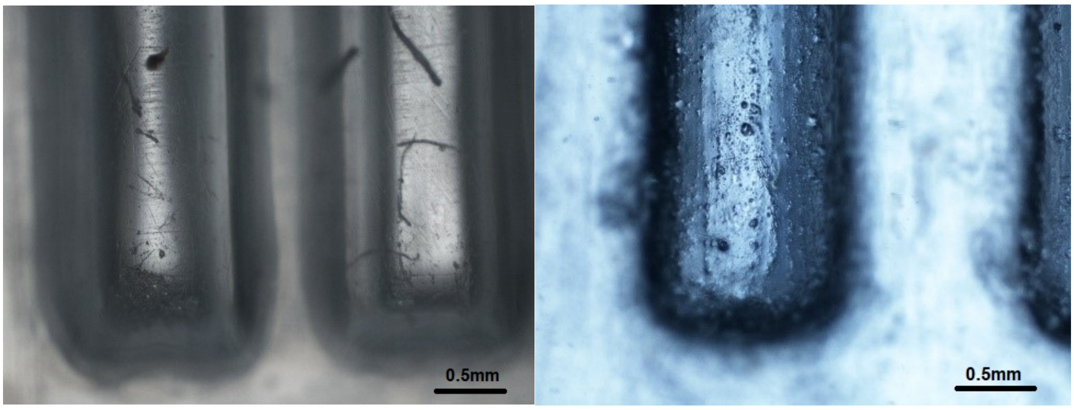

Figure 71. (a) the top view of the PDMS ferroelectret (b) the top view of PDMS/PTFE composite layer ferroelectret

Figure 71 present the top view figure of the PDMS/PTFE composite layer ferroelectret and PDMS ferroelectret inner void surface. The newly formed PDMS/PTFE layer becomes very firmly established on the void surface.

5.3.3 Experiment for PDMS/PTFE composite ferroelectret

The engineered ferroelectret structure is fabricated using PDMS molding techniques to realize a contoured PDMS sheet, two of which are subsequently bonded together to form the sealed voids. A Connex 350 TM 3D printer (Stratasys, MN, USA) was used to fabricate the three-dimensional moulds. To prevent the PDMS sticking to the mould, they were baked in oven at 80 °C for 24 hours and then exposed to a silane vapor for 1 hour which results in a thin coating of trichloro (1H,1H,2H,2H-perfluorooctyl) silane (Sigma Aldrich, MO, USA).

Using the processed moulds, the PDMS ferroelectret can be fabricated. For the standard pure PDMS ferroelectret, liquid PDMS and curing agent (Sylgard 184 from Dow Corning, MI, USA) were mixed at a 10:1 weight ratio and then degassed in a vacuum desiccator. The prepared degassed PDMS was poured into the moulds and were degassed again and then oven baked at 80 °C for 2 hours. The thickness of the samples is controlled by the level of the PDMS poured into the mould. After curing, the polymerized PDMS was peeled away from the moulds. The PTFE coatings can be applied to the void surfaces at this point by applying the PTFE layer to the bottom of the contoured structure as described below and shown in Figure 79. Then an oxygen plasma treatment (Femto Asher, Diener, Germany, 30S at 35-40W) was then used to prepare the surfaces of the two PDMS parts and these are bonded together, and oven baked at 80 °C for 1 hour. The schematic diagram of the cross section view of the pure PDMS ferroelectret is shown in Figure 72(b).

The PDMS/PTFE composite ferroelectret was fabricated using the approach described above but different ratios of PTFE powder were first added to the PDMS. Due to the PTFE content, these two parts cannot be bonded by the plasma treatment, so a thin layer of the PDMS/PTFE composite liquid was used as a glue to bond them together. The bonded assembly was then baked in oven at 80 °C for 1 hour. The schematic diagram of the cross section view of the PDMS/PTFE composite ferroelectret is shown in Figure 72(c).

The PDMS/PTFE composite material was made at different ratios of PTFE powder. The powder was mixed evenly with the gelatinous liquid PDMS in weight ratios of 1:10, 1:5, 1:4, 1:3 and 1:2. A syringe was used to manually deposit a fixed dose (0.1 ml) of the liquid solution onto the void surfaces, after which it was allowed to spread across the surface and settle before being baked in an oven at 80 °C for 1 hour. The schematic diagram of the cross-section view of the PDMS/PTFE composite layer ferroelectret is presented as Figure 72(e).

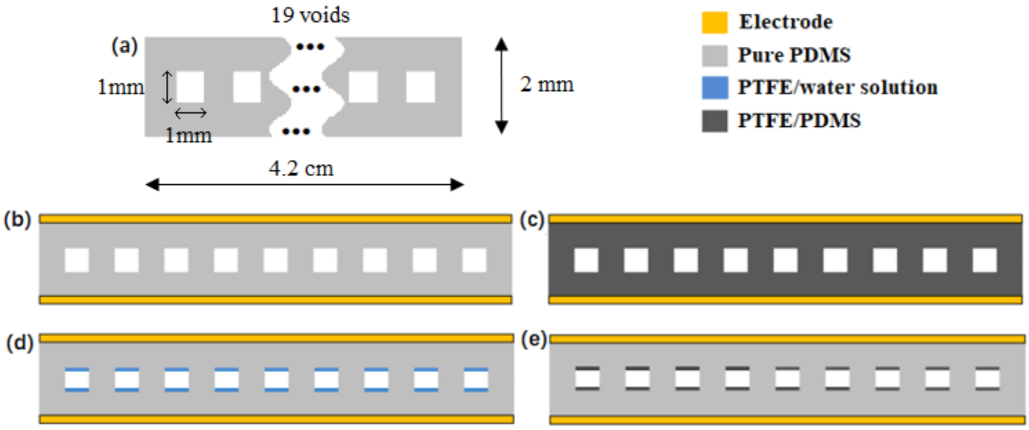

Figure 72. (a) Dimensions of test sample. Schematic cross sectional views of (b) pure PDMS ferroelectret; (c) PDMS/PTFE composite ferroelectret; (d) PTFE/water solution ferroelectret; (e) PDMS/PTFE composite layer ferroelectret.

5.4 Results and discussion

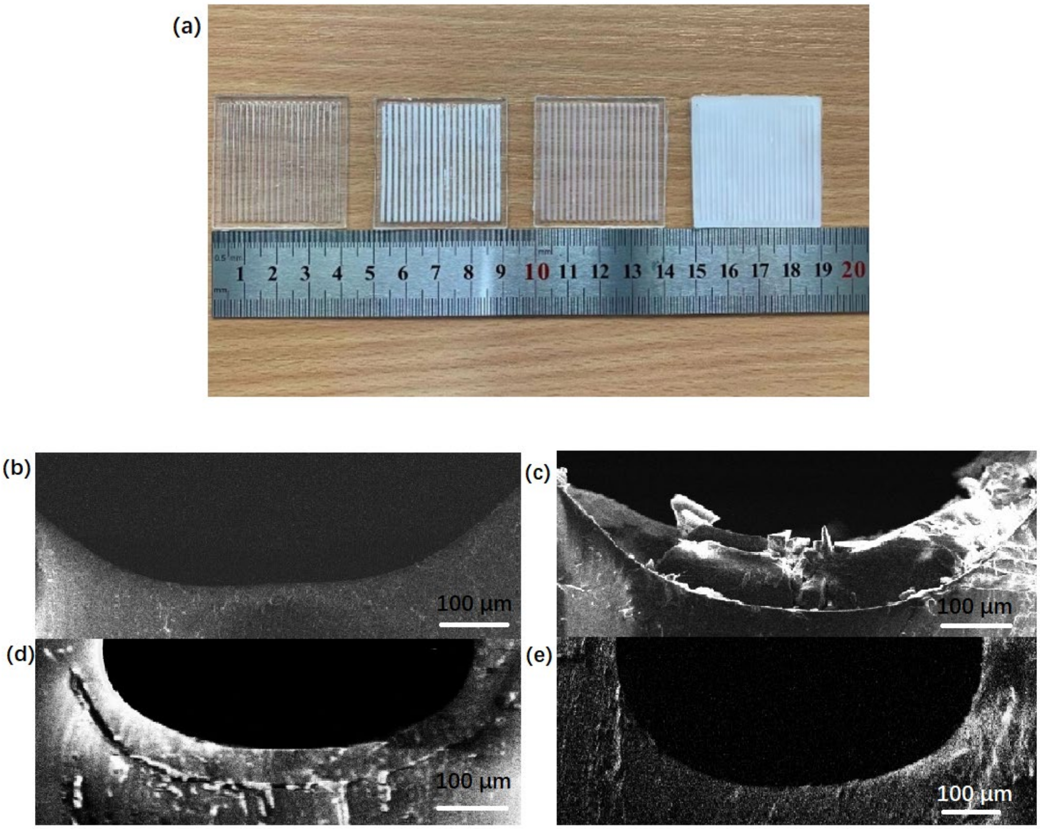

Figure 73. (a) Photo of samples, from left to right: pure PDMS ferroelectret, the PTFE/water solution ferroelectret, the PDMS/PTFE composite layer ferroelectret, and the PDMS/PTFE composite ferroelectret. (b) SEM photo of the cross section view of pure PDMS ferroelectret. (c) SEM photo of the cross section view of PTFE/water solution ferroelectret. (d) SEM photo of the cross section view of PDMS/PTFE composite layer ferroelectret. (e) SEM photo of cross section view of PDMS/PTFE composite ferroelectret

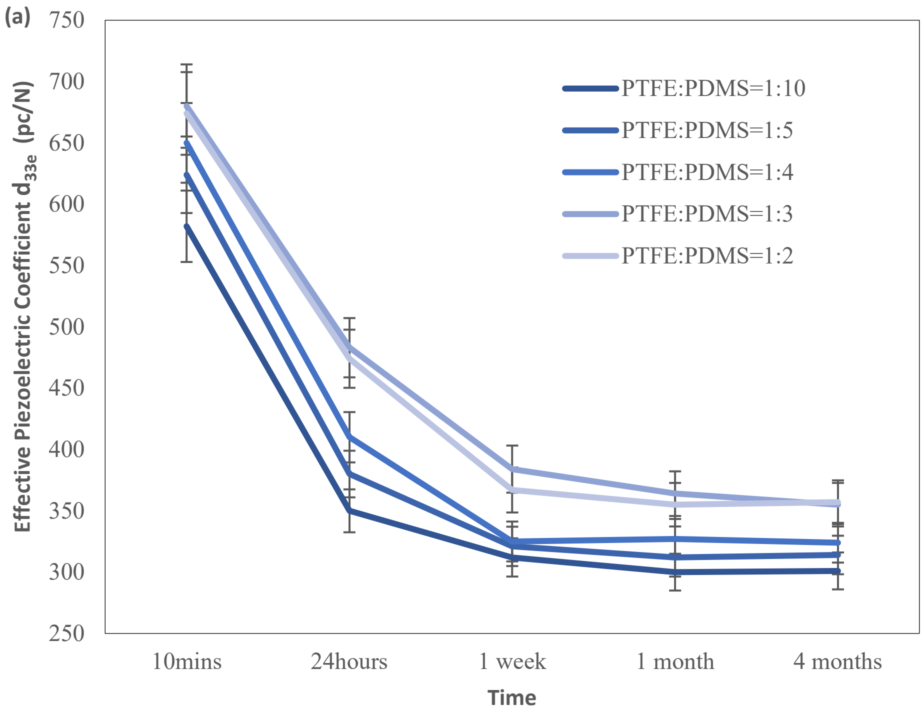
(a)
750
700
650
600
550
500
450
400
350
300
250
Effective Piezoelectric Coefficient d_{33e} (pc/N)
PTFE:PDMS=1:10
PTFE:PDMS=1:5
PTFE:PDMS=1:4
PTFE:PDMS=1:3
PTFE:PDMS=1:2
10mins
24hours
1 week
1 month
4 months
Time

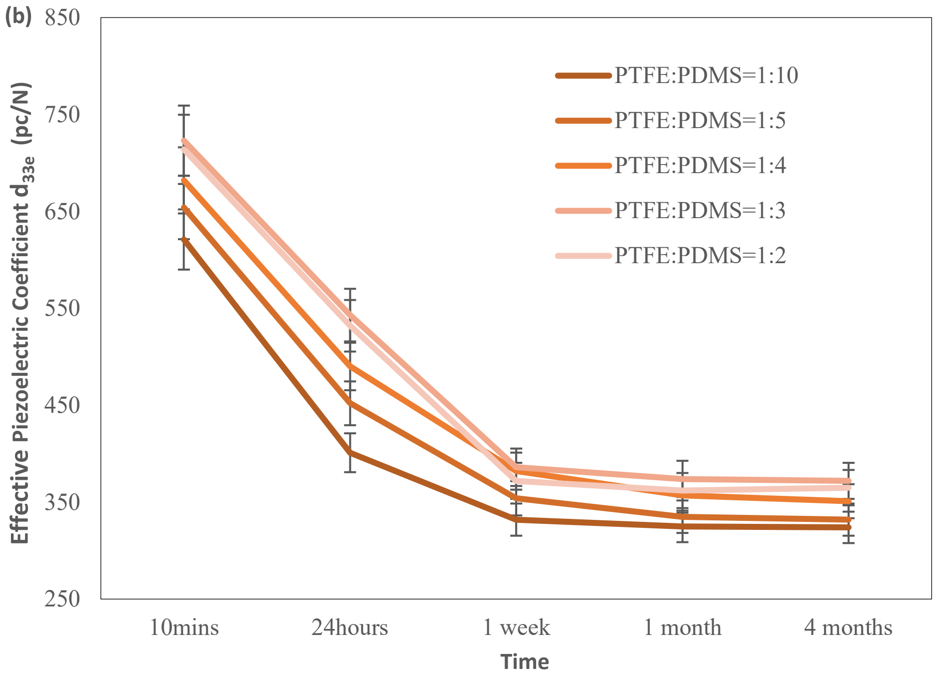
(b)
850
750
650
550
450
350
250
Effective Piezoelectric Coefficient d_{33e} (pc/N)
PTFE:PDMS=1:10
PTFE:PDMS=1:5
PTFE:PDMS=1:4
PTFE:PDMS=1:3
PTFE:PDMS=1:2
10mins
24hours
1 week
1 month
4 months
Time

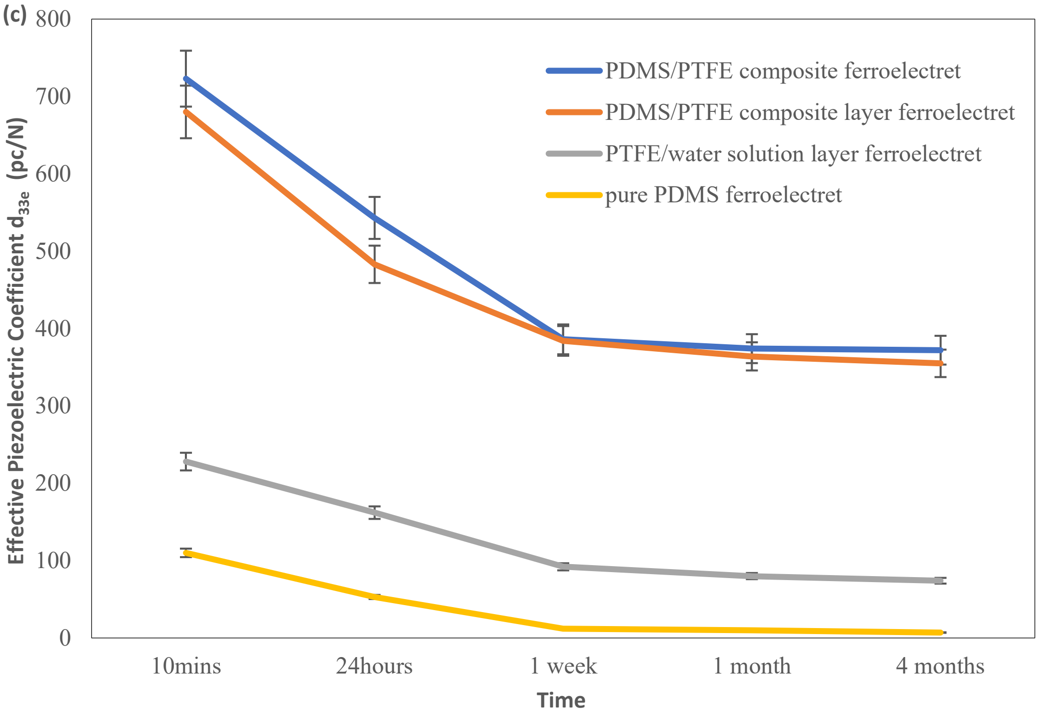

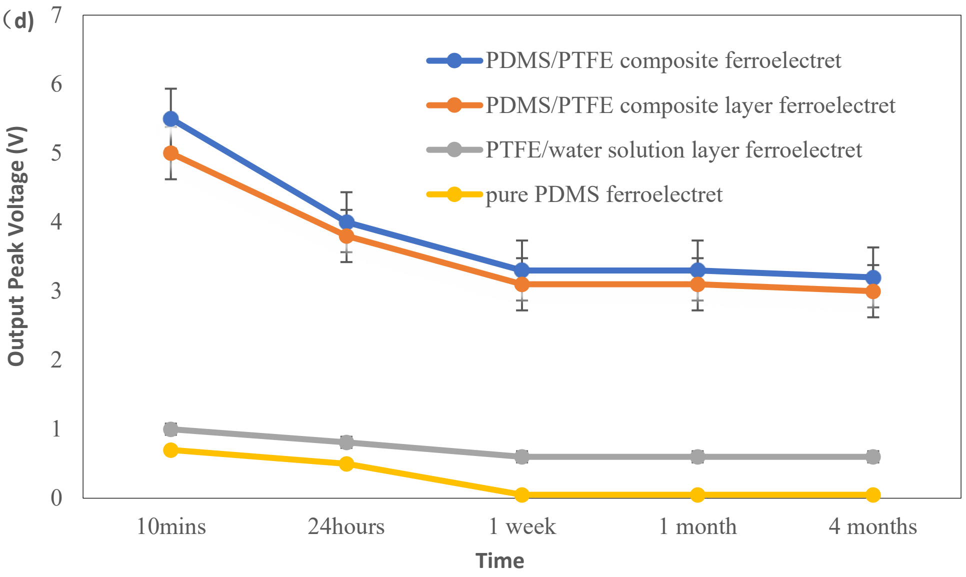

Figure 74. The results of four ferroelectrets. (a) The piezoelectric coefficient value with different weight ratio of PDMS/PTFE composite ferroelectret (b) The effective piezoelectric coefficient d_{33e} value with different weight ratio of PDMS/PTFE composite layer ferroelectret (c) The effective piezoelectric coefficient d_{33e} value of four different types ferroelectret versus time(the PTFE/PDMS weight ratio of PDMS/PTFE composite ferroelectret and PDMS/PTFE composite layer ferroelectret are 1:3) (d) The output peak voltage versus time under compressive force of 500 N (the PTFE/PDMS weight ratio of PDMS/PTFE composite ferroelectret composite ferroelectret and PDMS/PTFE composite layer ferroelectret are 1:3)

As shown in Figures 73(a), all the samples were 4.2 cm × 4.2 cm square-shaped with 19 voids inside. The thickness of the samples was 2mm with a 1mm void thickness. Figure 73(b) is the SEM photo of the cross section view of the pure PDMS ferroelectret. Figure 73(c) is the SEM photo of the cross section view of PTFE/water solution ferroelectret. Figure 73(d) and Figure 73(e) show the SEM photo of the cross section view of PDMS/PTFE composite layer ferroelectret and PDMS/PTFE composite ferroelectret where the white dots are the PTFE powders.

The effect of the different weight ratios of PDMS/PTFE on the PDMS/PTFE composite and PDMS/PTFE composite layer ferroelectrets is shown in Figure 74(a) and 74(b). As the ratio of PTFE particles increases both the amount of internal surface charge and the mechanical stiffness of the composite PDMS increases. The increase in surface charge is offset by the reduced displacement for a given mechanical force and at ratios beyond 1:3 this leads to a reduced effective d_{33e}. The mechanical stiffness of the different materials is presented later.

The corresponding initial effective maximum values of d_{33e} were 723 pC/N and 680 pC/N for the PDMS/PTFE composite and composite layer ferroelectrets respectively. These values are approximately 3 times greater than that of the PTFE/water solution layer ferroelectret (228 pC/N) and 6 times greater than that of the pure PDMS ferroelectret (110 pC/N). Increasing the concentration beyond around a ratio of 1:3 does not result in further increases in the effective piezoelectric coefficient d_{33e}.

Figure 74(c) shows a comparison of the drop in piezoelectric performance over time of the pure PDMS, PTFE solution layer, PDMS/PTFE composite layer and the PDMS/PTFE composite ferroelectrets. The PDMS/PTFE composite layer and PDMS/PTFE composite ferroelectrets maintained around 50% of their initial effective piezoelectric coefficient after 4 months, while the PTFE/water solution ferroelectret only retained around 34%. The effective d_{33e} of the pure PDMS ferroelectret dropped to below 10 pC/N in one month.

The variation in peak output voltage of the four types of ferroelectret under a cyclical compressive force of 500 N (frequency of 1 Hz, averaged from 20 cycles) over time as shown in Figures 74(d). The maximum peak voltages occurred immediately after corona charging being 5.5 V, 5 V, 1 V and 0.7 V for the PDMS/PTFE composite (weight ratio 1:3), PDMS/PTFE composite layer (weight ratio 1:3), PTFE/water solution and pure PDMS ferroelectrets respectively. The maximal peak voltage 4 months after corona charging had fallen to 3.3V, 3V, 0.6 V and 0.05 V respectively. The PDMS/PTFE composite and PDMS/PTFE composite layer ferroelectrets retained approximately 60% of their output voltage after 4 months.

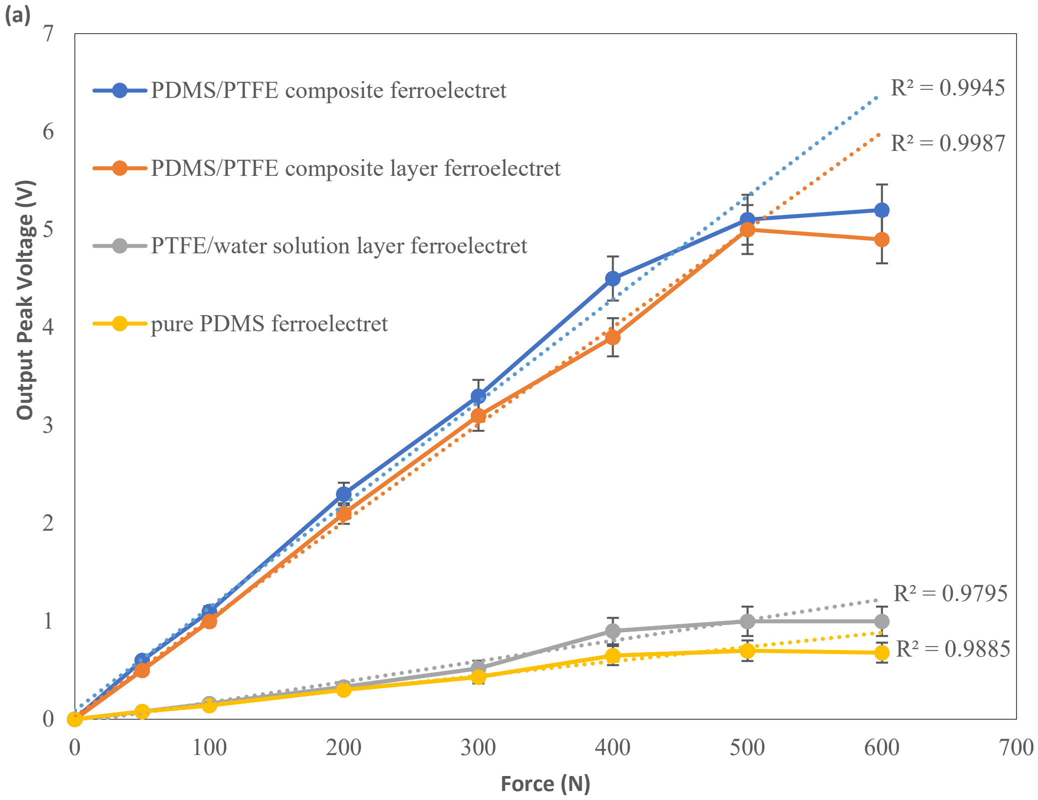

(b)

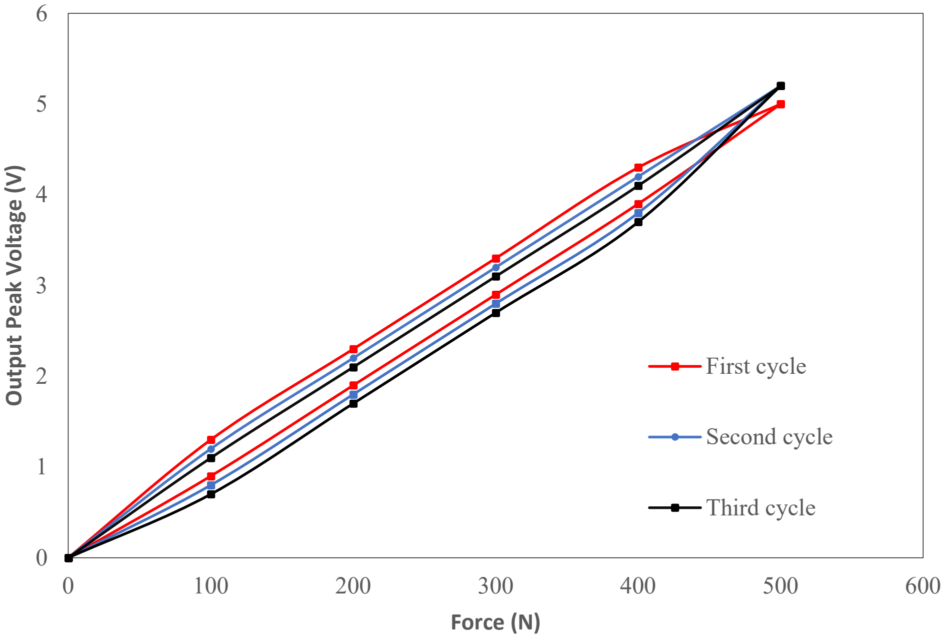
6
5
4
3
2
1
0
Output Peak Voltage (V)
0
100
200
300
400
500
600
Force (N)
First cycle
Second cycle
Third cycle

(c)

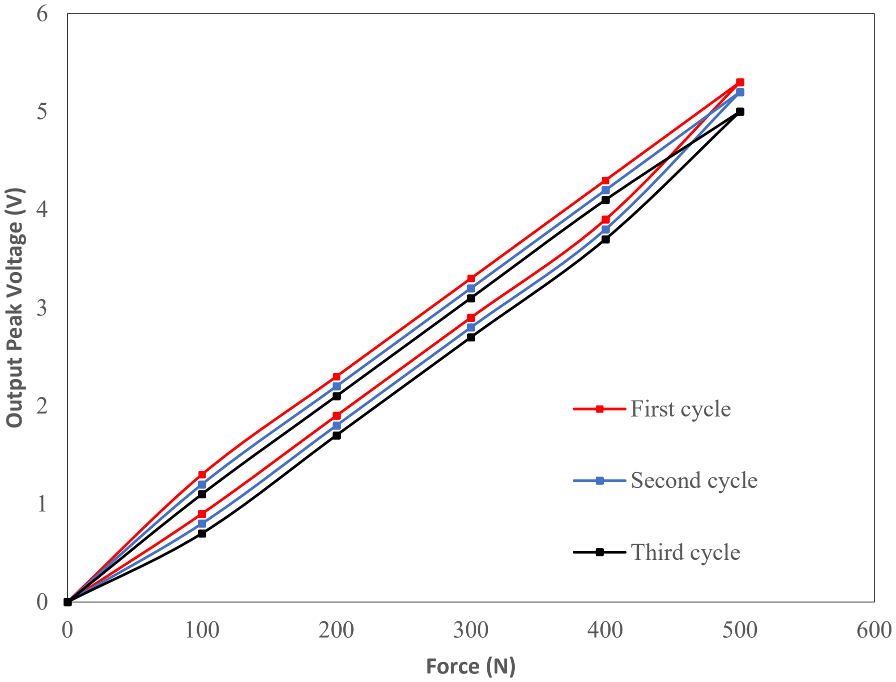
6
5
4
3
2
1
0
Output Peak Voltage (V)
0
100
200
300
400
500
600
Force (N)
First cycle
Second cycle
Third cycle

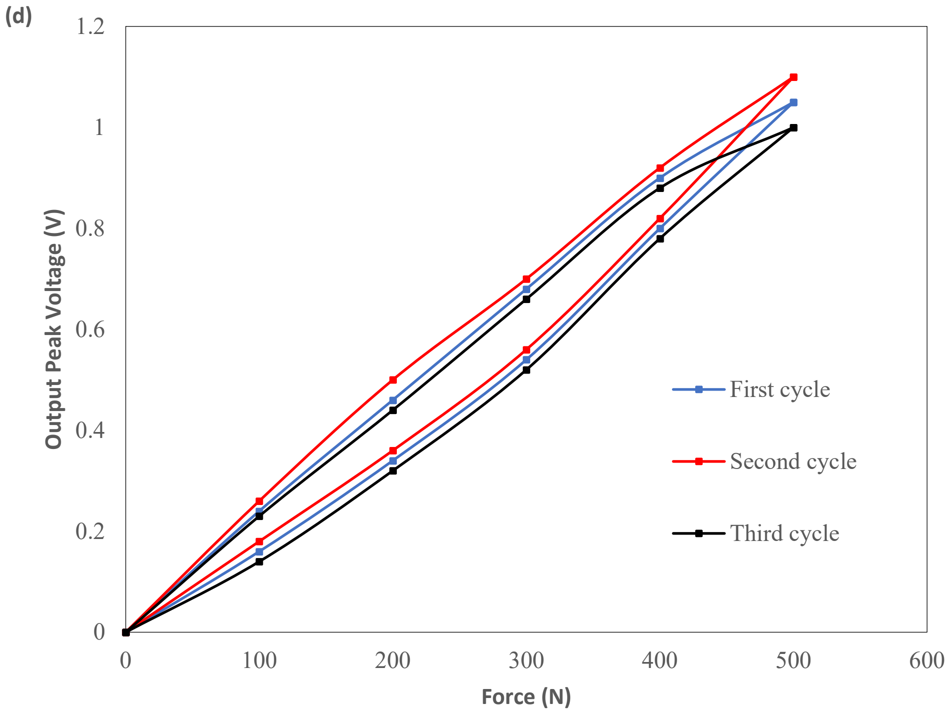

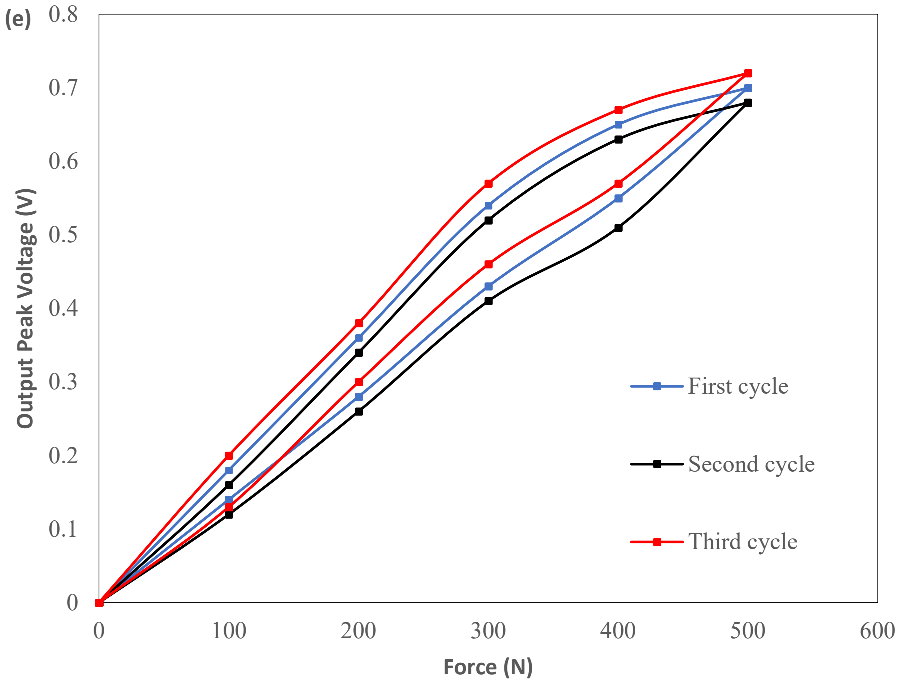

Figure 75. The result of linearity and hysteresis loops. (a) The output peak voltage by different force at a frequency of 1Hz and the fitting curve in the linear region by the least square method (b) The hysteresis loop of the PDMS/PTFE composite ferroelectret (c) The hysteresis loop of the PDMS/PTFE composite

layer ferroelectret (d) The hysteresis loop of the PTFE/water solution ferroelectret (e) The hysteresis loop of the pure PDMS ferroelectret

The peak output voltage of the four types of ferroelectret under different compressive forces ranging from 0 to 600 N (average taken from 20 cycles applied at a frequency of 1 Hz) is shown in Figure 75(a). The output peak voltage initially increases with increasing force but levels off at around 500 N at which point the inner voids of ferroelectret have been fully compressed. The point at which the compression occurs depends upon the fabricated geometries and stiffness of the materials (discussed later). To explore the sensitivity and linearity of each ferroelectret, the least square method was used to form the straight-line approximations shown in Figure 75(a) where each point corresponds to measured values. The sensitivity can be determined from by the slope of the dotted straight-line approximations and are 10.5, 9.9, 2.1, 1.6 mV/N for the PDMS/PTFE composite ferroelectret, the PDMS/PTFE composite layer ferroelectret, the PTFE/water solution ferroelectret and the pure PDMS ferroelectret respectively. The minimum resolution of the ferroelectrets is 0.05N.

The linearity can be characterized by the R^2 (R-squared is a goodness-of-fit measure for linear regression models) or the nonlinearity error. R^2 can be calculated from the straight-line approximations. The closer R^2 is to 1, the better the linearity. The nonlinearity error, δ, can be expressed by Equation (6.1),

$$\delta = \frac{\Delta Y_{max}}{Y} \times 100\% \tag{6.1}$$

where ΔY_{max} is the maximum deviation between measuring results and the straight-line approximations and Y is the full scale of the measured results. The nonlinearity error of the PDMS/PTFE composite ferroelectret, the PDMS/PTFE composite layer ferroelectret, the PTFE/water solution ferroelectret and the pure PDMS ferroelectret is 2.7%, 1.7%, 7% and 8% respectively. The smaller the value of nonlinearity error, the better the linearity. Therefore, the PDMS/PTFE composite ferroelectret, the PDMS/PTFE composite layer ferroelectret have a better linearity than the PTFE/water solution ferroelectret and the pure PDMS ferroelectret, which present the same result from the value of R^2.

The hysteresis loops of the different ferroelectrets are presented in Figures 75(b) to 75(e) with results obtained by incrementally increasing and decreasing the applied force by 100 N. The hysteresis error h' can be calculated by Equation (6.2),

$$h' = \frac{\Delta h_{max}}{Y} \times 100\% \tag{6.2}$$

where Δh_{max} is the maximum difference between the outputs in the increasing and decreasing directions. The hysteresis error of the PDMS/PTFE composite ferroelectret, the PDMS/PTFE composite layer ferroelectret, the PTFE/water solution ferroelectret and the pure PDMS ferroelectret is 5.2%, 6%, 10% and 12.8% respectively. The difference could be explained by the variations in stiffness and the surface energy of the materials which may affect how the surfaces release as the force is removed. The PDMS/PTFE composite layer ferroelectret and the PDMS/PTFE composite ferroelectrets show a higher sensitivity and linearity and smaller hysteresis error than the PTFE/water solution ferroelectret and the pure PDMS ferroelectret, showing improved potential for use in sensing applications.

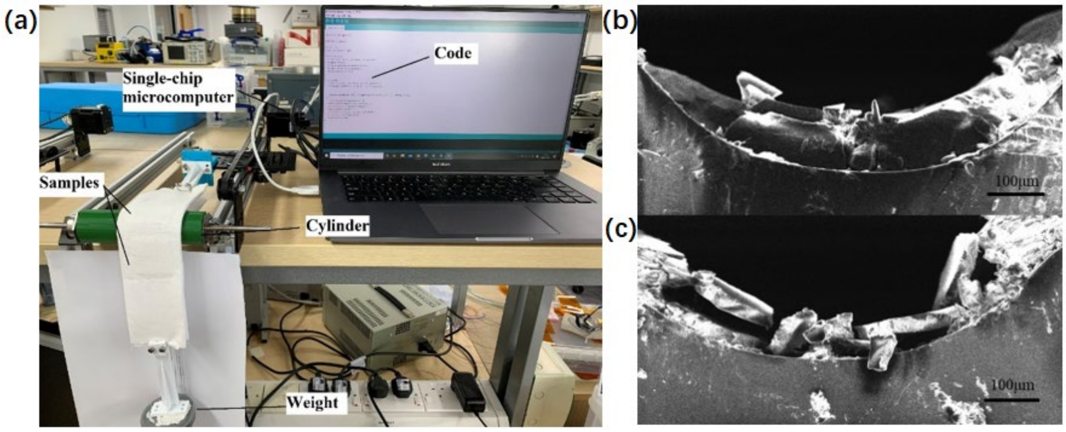

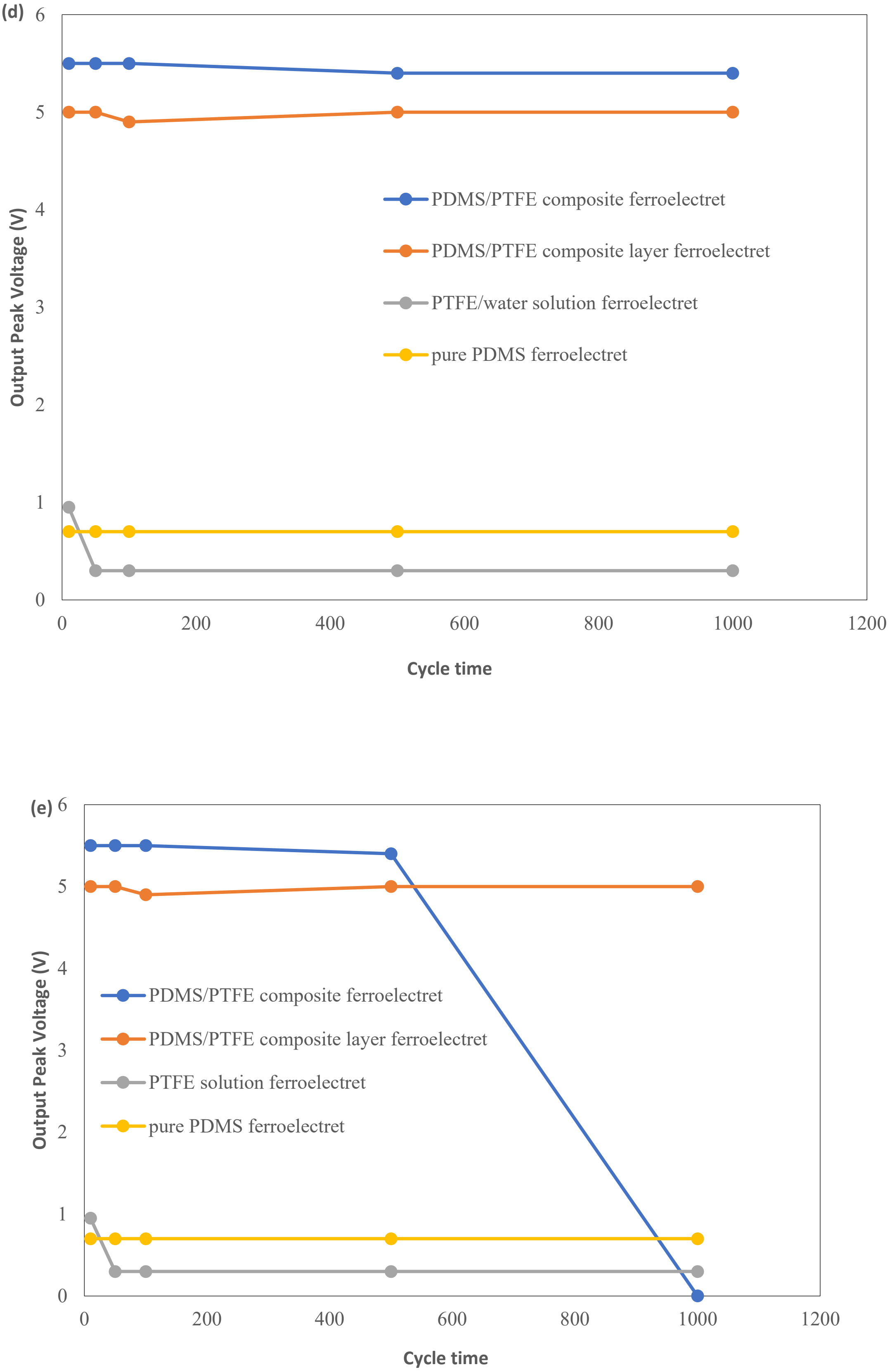

Figure 76. Mechanical robustness test results. (a) The bending test set up. (b) Cross sectional view of

PTFE/water solution layer ferroelectret before compression test and (c) after 50 compressive cycles. (d) Compression test results from different ferroelectret samples under cyclical compressive force of 500N applied at a frequency of 1Hz. (e) Bending test result of different ferroelectret samples.

The mechanical robustness of the samples and the material fatigue resistance are also important considerations for the device and these were tested in the set up shown in Figure 76(a). Figures 76(b) and (c) show the cross-sectional view of the PTFE/water solution layer ferroelectret before and after 50 compressive cycles. It can be seen that the layer formed by PTFE/water solution was destroyed by the mechanical deformation caused by the compressive forces. In the bending test, the PTFE/water solution layer is also destroyed in the first few cycles.

The effects of the cyclical compressive and bending forces on the output voltages from the samples are shown in Figures 76(d) and 76(e). In the case of the compressive tests, the PDMS/PTFE composite ferroelectret, PDMS/PTFE composite layer ferroelectret and pure PDMS ferroelectret show no deterioration in output voltage up to 1000 compressive cycles while the PTFE/water solution layer ferroelectret showed a clear drop in the output voltage after only around 10 to 50 compressive and bending cycles. This is due to the destruction of the PTFE/water layer during the testing process as shown in Figures 76(b) and (c).

The results of the cyclical bending tests shown in Figure 76(e) demonstrate no deterioration in output voltage up to 1000 bending cycles for the pure PDMS and PDMS/PTFE composite layer ferroelectrets. The PTFE/water solution layer ferroelectret again failed between 10 to 50 compressive cycles indicating the dried PTFE layer cannot withstand the lateral strains induced by the bending test. One noticeable difference between the bending and compression test results is for the PDMS/PTFE composite ferroelectret which was damaged after 500 cycles. This is because these samples were assembled using the liquid PDMS bonding process and the level of adhesion is not as high as those bonded by the plasma treatment.

Although the piezoelectric performance of PDMS/PTFE composite ferroelectret is better than that of PDMS/PTFE composite layer ferroelectret, the PDMS/PTFE composite layer ferroelectret is more mechanically robust due to the stronger bond strength. The distribution of the PTFE power in the bulk of the PDMS prevents the plasma bonding process which has a negative effect on the assembled sample's resistance to lateral strains.

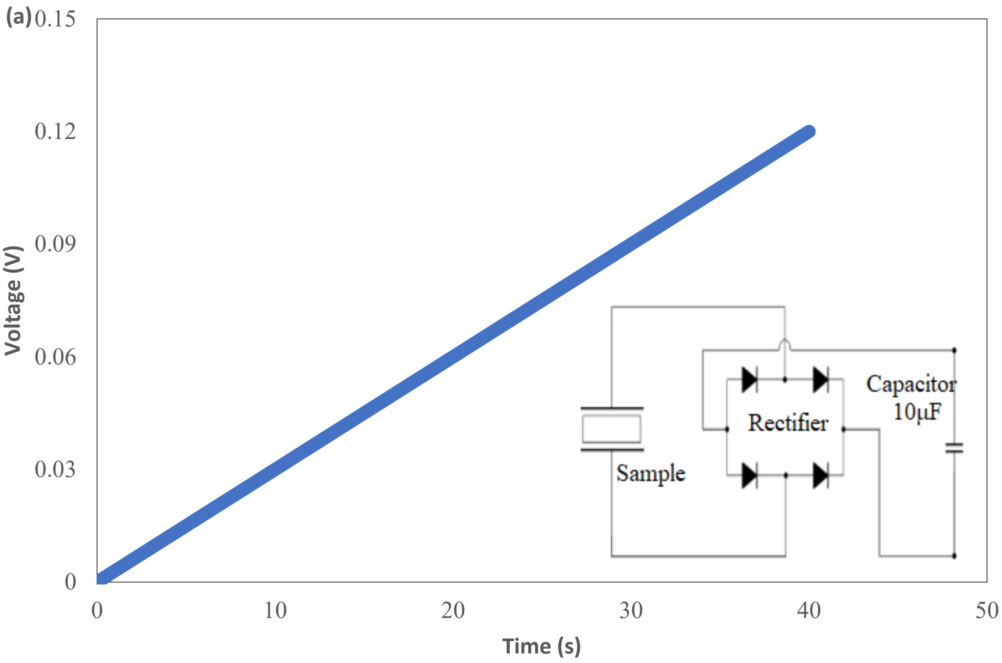

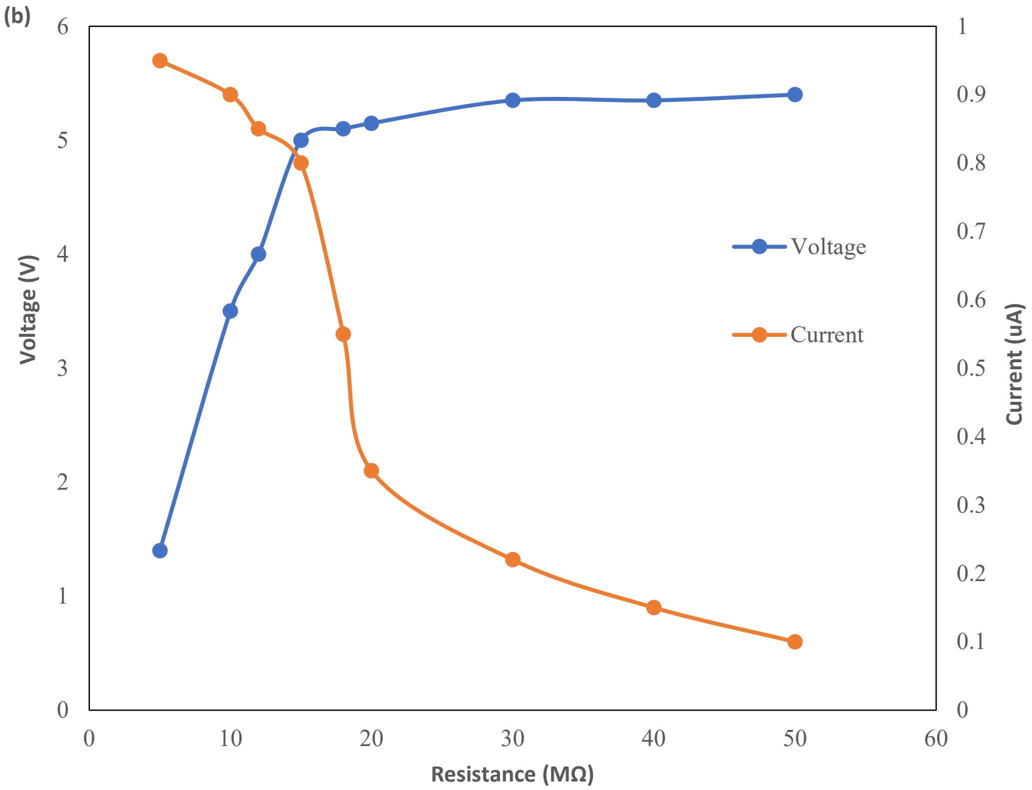

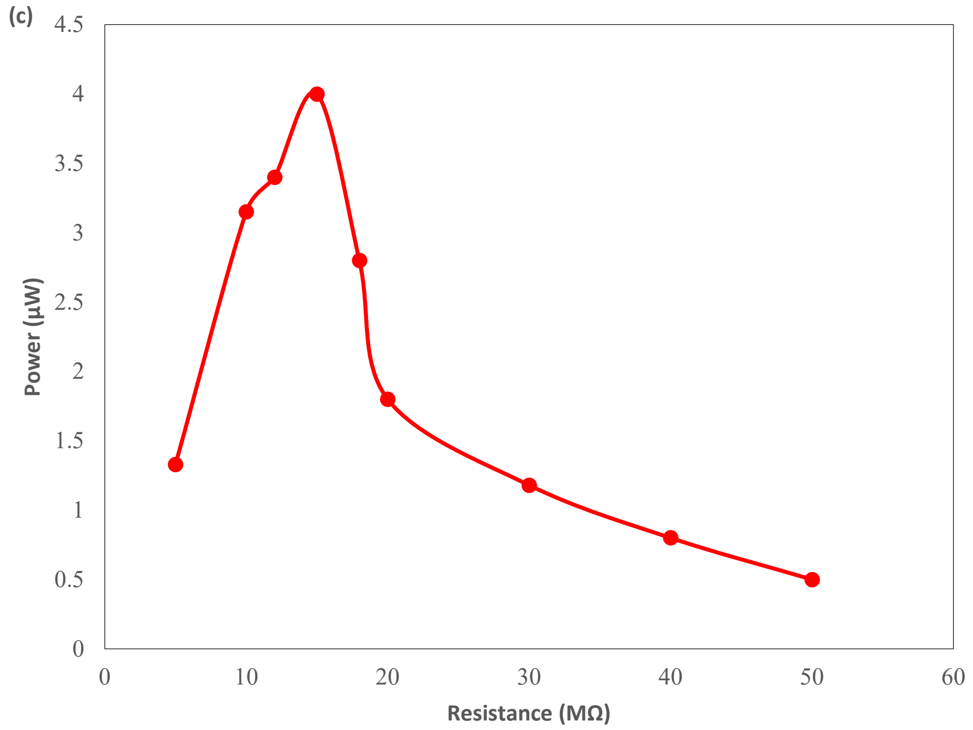

Figure 77. The energy harvesting potential test. (a)The power management circuit and the capacitor charging curve up to 40 s. (b) Current and Voltage as a function of load resistance. (c) Output power as a function of load resistance. For graphs (a) to (c) a compressive force applied of 500 N was applied at 1 Hz.

To explore the practical energy harvesting potential of the ferroelectret samples, the PDMS/PTFE composite ferroelectret with PTFE/PDMS weight ratio of 1:3 (highest piezoelectric performance) was driven by a cyclical mechanical compressive loading of 500 N at 1 Hz for 40 s. The sample was then connected to a 10 µF capacitor via the power management circuit in shown in Figure 77(a). The voltage across the capacitor increases to 0.12 V corresponding to a total energy accumulation after 40 cycles of 0.072 µJ. The average energy stored is 1.8 nJ per cycle which corresponds to an average output power of 1.8 nW. The output current, voltage and power versus resistance are shown in Figure 77(b) and 77(c). Maximum output power occurs at a load resistance of 15 MΩ, with a peak power of 4 µW.

The power delivered to the load is far less than the energy through the rectifier mainly due to the impedance mismatch between the rectifying circuit and the optimal resistive load. In order to improve this, Fengben *et al.* [189] proposed a universal power management strategy for triboelectric harvesters which possess a similarly high output impedance. With the implemented power management module (PMM), about 85% energy from the triboelectric harvesters can be converted and output as a steady and continuous DC voltage to the load resistance. The PMM improves the stored energy by a factor of 128 times (from 18.5 μJ to 2.37 mJ) when charging a 1 mF capacitor compared with a full bridge rectifier alone [189]. Use of a power management circuit with improved impedance matching will be essential for energy harvesting applications.

In order to explore the applicability of different concentrations of PDMS, stress–strain tests were performed on the ferroelectret samples to explore the effect of different PTFE concentrations on the stiffness of the PDMS using the Instron E1000 as shown in Figure 78. Considering the anisotropy of the sample structure, it was chosen to apply strain in the same direction as the voids. The results (Figure 79) show that the pure PDMS and PDMS/PTFE composite layer ferroelectret has the lowest stiffness and the ferroelectret device can withstand strains of up to 100 % without being damaged. The addition of the PTFE particles increases the stiffness of the PDMS and reduces the strain the ferroelectret can withstand. Stiffness increases and the maximum strain decreases with increasing PTFE concentration.

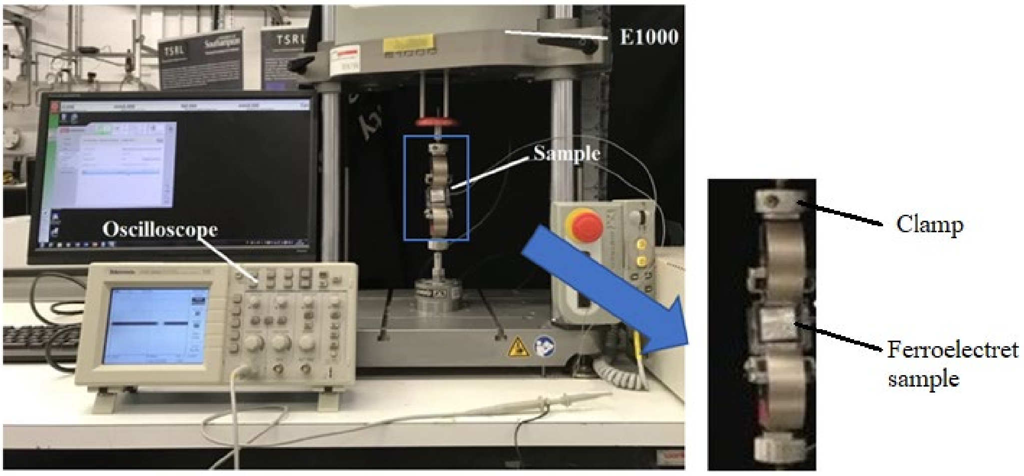

Figure 78. stress–strain tests by the Instron E1000

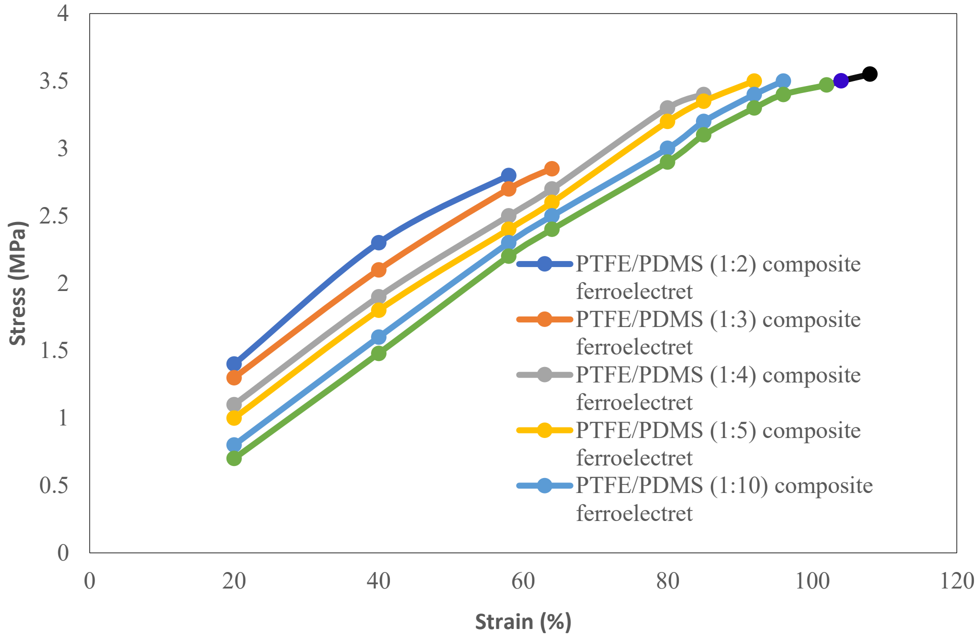

Figure 79. Stress–strain test result for the pure PDMS and composite ferroelectret

5.5 Conclusion

This chapter illustrates and compares approaches to enhancing the surface charge density and stability in PDMS ferroelectrets. Different approaches to adding the PTFE particles to the ferroelectret structure have been explored and the most obvious approach of simply adding the powder directly to the PDMS to form a composite material for the ferroelectret does produce the most active ferroelectret devices. However, the addition of the PTFE prevents the device from being assembled using the plasma bonding process. The alternative liquid PDMS bonding process was found to be weaker under lateral strains leading to failure under cyclical bending. Therefore, the application of the PDMS/PTFE composite as a layer within the standard PDMS ferroelectret device was found to be the preferred fabrication approach since it demonstrates significantly improved activity without compromising the robustness of the ferroelectret device. Different concentration ratios of PTFE powder in PDMS were explored and a PTFE/PDMS weight ratio of around 1:3 was found to achieve the highest effective piezoelectric coefficient d_{33e} value of 680 pC/N which is a 6 times improvement compared to the pure PDMS ferroelectret (110 pC/N). Increasing the amount of PTFE beyond this ratio did not provide any further improvement in device output. The PDMS/PTFE composite layer ferroelectret retained 50% of its initial effective piezoelectric coefficient after 4 months again demonstrating a considerable improvement in charge stability compared with the pure PDMS which reduces to less than 10% of the initial, already inferior, effective piezoelectric coefficient value after just one month. Most of the initial charge decay was found to occur in the first week after poling and the composite layer ferroelectret demonstrates excellent stability beyond this point. Adding a layer of pure PTFE using the water-based PTFE solution to the void surfaces was found not to work well due to the mechanically fragile nature of this film. The energy harvesting potential and sensing performance of the PDMS/PTFE composite layer ferroelectret was explored and achieved an output power of 1.8 nW after rectification and a sensitivity of 9.9 mV/N demonstrating its suitability for sensing applications. The soft, compliant and flexible nature of the PDMS material makes it particularly suitable for wearable applications.

6. A new approach for obtaining PDMS ferroelectrets with random voids

6.1 Introduction

In previous work, PDMS facilitated the synthesis of a ferroelectret via a moulding process which resulted in controlled void layouts and geometries, in contrast to the random voids associated with foam. The connection between the geometry or structure and ferroelectret performance can be quantitatively analysed by the controlled void layouts. However, controlled void layouts limited subsequent ferroelectret structures and increased the complexity of the manufacturing process. Figure 89 displays the piezoelectric PDMS films for MEMS transducers which were fabricated using this method for controlled void layouts. To realize the multi-layer structure within the ferroelectret, it was necessary to manufacture it one layer at a time due to the limitations of this particular process.

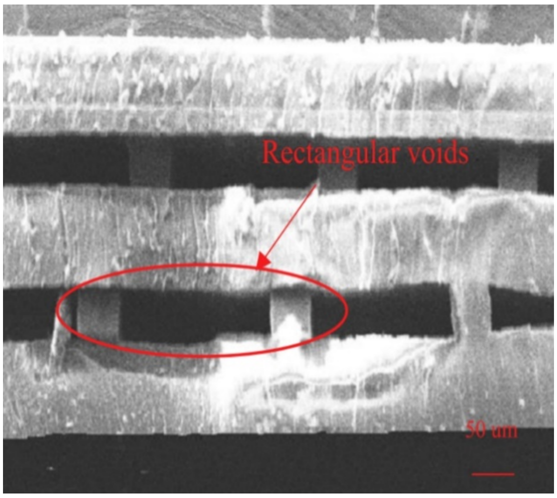

Figure 80. PDMS ferroelectret with controlled void layouts

This chapter proposes a simplified method to synthesize PDMS ferroelectrets which contain a large number of random voids formed by using a high-speed stirring process. Although this technique does not control the geometry of the voids with a high level of precision, it is a nonetheless rapid and convenient way of fabrication and allows the piezoelectric properties to be adjusted by the stirring process and the PDMS curing process.

6.2 Mathematical model

Generally, the piezoelectricity of a charge-implanted, cellular polymer structure is determined by its geometry, elastic modulus and charge density. In order to explore the relationship between these parameters, a model is first built using mathematical methods and the result will compare with the subsequent experimental results.

A simplified model for the piezoelectricity of a charge implanted cellular structure is illustrated in Figure 87, which are used to investigate structures with voids of random size and space distributions. The structure is composed of top and bottom electrodes, and alternating solid and void layers in between.

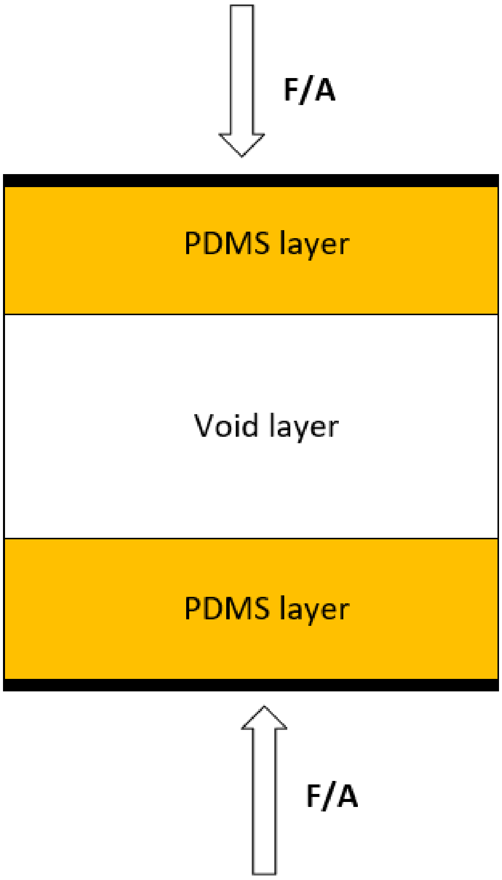

Figure 81. A simplified model of cellular structure

For this simplified model as Figure 87, the electric field in the PDMS layers (E_1) and porous layer (E_2) can be obtained from Gauss'law for the interfaces:

$$E_1 = \frac{\sigma_m}{\varepsilon_1 \varepsilon_0} \text{ and } E_2 = \frac{\sigma_m - \sigma}{\varepsilon_0} \tag{7.1}$$

Where σ_m is the charge density on the electrodes, σ is the charge density on void surfaces, ε_0 and ε_1 are the dielectric constant of air and the relative dielectric constant of PDMS, and the electric potential (V) across the top electrode and bottom electrode can be obtained according to Kirchhoff's second law (Figure 3 have 1 void layer and 2 solid layers):

$$V = \int E\, dx = (n+1)x_1E_1 + nx_2E_2 = 0 \tag{7.2}$$

Where $x_1$and x_2 are the thickness of the solid layer and void layer respectively. Combined equation 1 and 2, the charge density on the electrodes can be described by:

$$\sigma_m = \frac{n\varepsilon_1 \sigma x_2}{[(n+1)x_1 + n\varepsilon_1 x_2]} \tag{7.3}$$

The variation of the charge density on the electrodes $\Delta\sigma_m$ can be illustrated by the function related to the thickness variation Δx_1 and Δx_2:

$$\Delta\sigma_m = \frac{\partial\sigma_m}{\partial x_1}\Delta x_1 + \frac{\partial\sigma_m}{\partial x_2}\Delta x_2 = \frac{-n(n+1)\varepsilon_1\sigma x_2}{[(n+1)x_1 + n\varepsilon_1 x_2]^2}\Delta x_1 + \frac{n(n+1)\varepsilon_1\sigma x_1}{[(n+1)x_1 + n\varepsilon_1 x_2]^2}\Delta x_2 \tag{7.4}$$

Assumed that an external force is applied in the structure surface, and the relationship between stress and strain can be obtained as:

$$\frac{F}{\mathrm{A}} = c_{33}\frac{-\Delta x_1}{x_1} = c_{33}\frac{\Delta x_2}{x_2} \tag{7.5}$$

Where c_{33} is the elastic modulus of material, and A is the area of the surface. Combined equations 3 to 5, the piezoelectricity can be obtained by:

$$d_{33} = \frac{\Delta\sigma_m}{F/A} = \left(\frac{n(n+1)\varepsilon_1\sigma x_2}{[(n+1)x_1 + n\varepsilon_1 x_2]^2}x_1 + \frac{n(n+1)\varepsilon_1\sigma x_1}{[(n+1)x_1 + n\varepsilon_1 x_2]^2}x_2\right)\frac{1}{c_{33}} \tag{7.6}$$

Assumed that k is the cavitation rate, then k should be equal to the ratio of all voids volume to the total volume, which can be described as:

$$k = \frac{nx_2A}{[(n+1)x_1 + nx_2]A} \tag{7.7}$$

$$x_2 = \frac{(n+1)k}{n(1-k)}x_1 \tag{7.8}$$

Combined equations 6 and 8, the piezoelectricity can be obtained by:

$$d_{33} = \frac{\Delta\sigma_m}{F/A} = \frac{2(1-k)\varepsilon_1\sigma k}{(1-k+\varepsilon_1 k)^2}\frac{1}{c_{33}} \tag{7.9}$$

According to equation (9), the piezoelectric coefficient d_{33} of the PDMS ferroelectret structure is determined by the cavitation rate (k), elastic modulus (c_{33}) charge density (σ) and the relative dielectric constant of the cellular material (ε_1). For a given structure, the value of the layer thicknesses can be considered as constant and therefore the d_{33} coefficient only varies with the material properties.

6.3 Experiment work

6.3.1 Fabrication

The engineered ferroelectret structure is fabricated using PDMS molding techniques to realize a contoured PDMS sheet with the size of 2.8cm× 2.8cm× 3mm. A Connex 350 TM 3D printer (Stratasys, MN, USA) was used to fabricate the three-dimensional moulds. To prevent the PDMS sticking to the mould as Figure 82, they were baked in oven at 80 °C for 24 hours and then exposed to a silane vapor for 1 hour which results in a thin coating of trichloro (1H,1H,2H,2H-perfluorooctyl) silane (Sigma Aldrich, MO, USA).

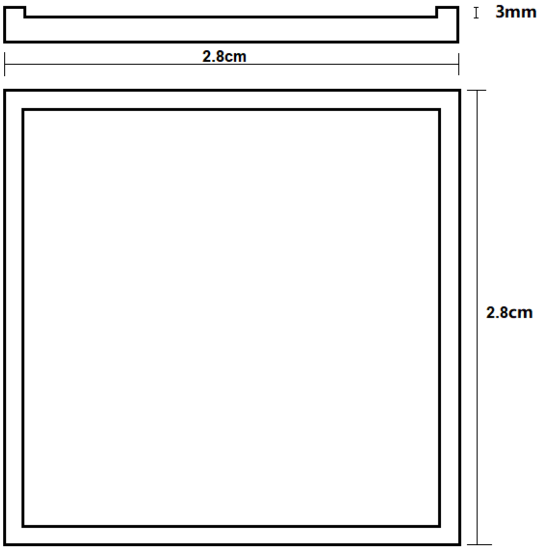

Figure 82. The structure of mould

Using the processed moulds, the PDMS ferroelectret can be fabricated as below: first, the mould and liquid PDMS were initially heated to 80°C for 5 minutes in the oven (Pre-heating can accelerate the forming time of PDMS and reduced the escaping of inside bubbles), then liquid PDMS and curing agent (Sylgard 184 from Dow Corning, MI, USA) were mixed at a 10:1 weight ratio. Second, this mixed gelatinous liquid was stirred at the speed of 2000 rpm by an overhead stirrer for 1 minute. The stirring process have three purposes: firstly, the liquid PDMS and curing agent will be evenly mixed after stirring; secondly, the bubbles generated by the reaction between liquid PDMS and curing agent will evenly distributed in the mixed liquid; lastly, in high-speed stirring, the mixed liquid will absorb more air and therefore generate more bubbles.

When finishing the stirring process, the prepared PDMS mixed liquid was poured into the mould and baked at 150°C in the oven for 30 minutes. After curing, the polymerized PDMS was peeled away from the mould.

6.3.2 Testing

In order to investigate the relationship between cavitation rate and piezoelectric properties, the cavitation rate of samples is calculated by the equation 7.10.

$$\rho_{air} V_m k + \rho_{PDMS} V_m (1-k) = m_m \tag{7.10}$$

Where ρ_{air} and ρ_{PDMS} are the density of the air and PDMS respectively, V_m is the measured volume and m_m is the measured weight of sample, k is the cavitation rate. Based on the measured volume and weight, the cavitation rate can be calculated according to equation 7.10.

To explore the piezoelectrical properties of the PDMS ferroelectret, the sample was polarized using identical corona charging parameters, these being a charging voltage of 25 kV, charging distance of 4 cm and applied for a time of 2 minutes.

Since the surface charge density is directly linked to the effective piezoelectric coefficient d_{33e}, the charge decay over time for the 4 sample has been monitored by measuring the d_{33e} using a PiezoMeter Systems (PM300, Piezotest Ltd). This system provides a direct reading of d_{33e} by clamping the sample in the series with a reference sample and applying a known force to both. The electrical signal from the sample is compared with the built-in reference enabling the d_{33e} value to be calculated. The generated output voltage across the resistive load R can be expressed as given in equation (7.11).

$$V = \frac{\Delta Q}{t} R \qquad (7.11)$$

where R is the output voltage, ΔQ is the variation in charge, and t is the time taken to apply the force.

To evaluate energy harvesting performance, an Instron electrodynamic instrument (ElectroPuls E1000) was used to apply forces to the test samples and the output voltage and voltage across a storage capacitor have been measured.

In order to investigate the durability of these samples, cyclical compressive and bending tests were applied. using The Instron electrodynamic instrument (ElectroPuls E1000) was used to apply a cyclical 300 N compressive force and the change in electrical characteristics of the samples measured after a predetermined number of compressions. In the bending test, the samples were cyclically deformed around a cylinder with diameter of 3 cm equating to a bending radius of 1.5 cm with the weight of 1 kg applied to provide tension in the material.

6.4 Result and discussion

As shown in Figure 82(a), all the samples were 2.8 cm × 2.8 cm square-shaped with thickness of the 3 mm. Schematic illustration of a PDMS ferroelectret with initial heating temperatures of 40ºC, 60ºC, 80ºC and 100ºC with curing temperature of 150ºC is shown in Figure 82. Figure 83(b) present the cross-section view of the sample in Figure 82(a3).

Figure 83 present the cavitation rate by different warm-up and curing temperature with same stirring conditions. Figure 83(a) present the cavitation rate vs initial heating temperatures of 40ºC, 60ºC, 80ºC and 100ºC with a curing temperature of 150ºC (stirring time at 40 seconds and stirring speed at 1000 rpm). As the initial heating temperature gradually increases to 80 ºC, the cavitation rate was increased significantly until it remains at 8.7%, after which there is a small reduction in cavitation rate at 100ºC. Excessive initial heating can cause the mixed PDMS liquid to start solidifying before it has been sufficiently stirred.

Figure 83(b) present the cavitation rate by the initial heating temperature of 80ºC with stirring time of 40 seconds at a speed of 1000 rpm with the curing temperature varied from 80ºC, 120ºC, 150ºC and 180ºC. As the curing temperature gradually increases to 150ºC, the cavitation rate was increased rapidly to 8.7%, after which it will continue to heat up to 180 ºC and there is a small rise in cavitation rate.

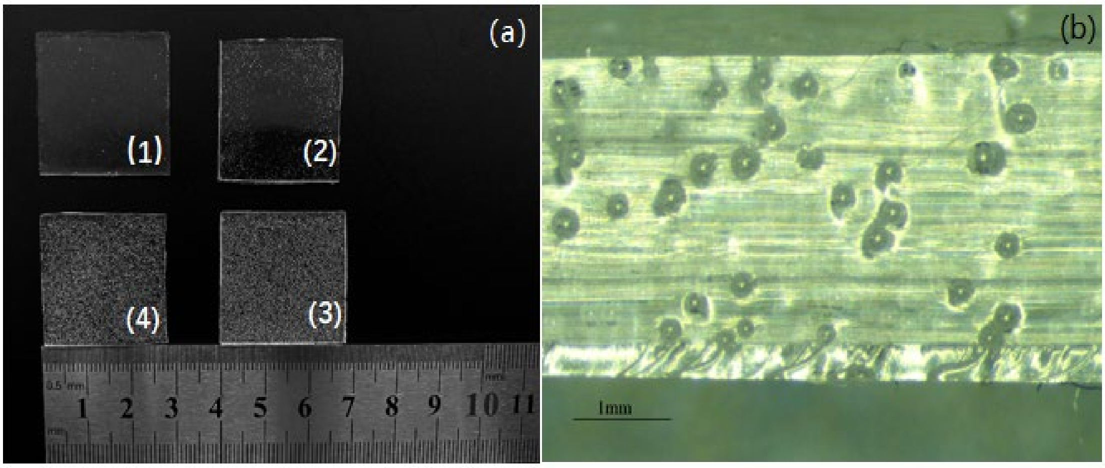

Figure 82. The PDMS ferroelectret (2.8cm × 2.8cm × 3mm) with random voids(a) top view of the PDMS ferroelectrets with warm-up temperature of 40 ºC,60 ºC,80 ºC and 100 ºC with curing temperature of 150 ºC (from (1) to (4)) and (b) cross section view of PDMS ferroelectrets with warm-up temperature of 80 ºC and curing temperature of 150 ºC (the sample in Figure 5(a_3))

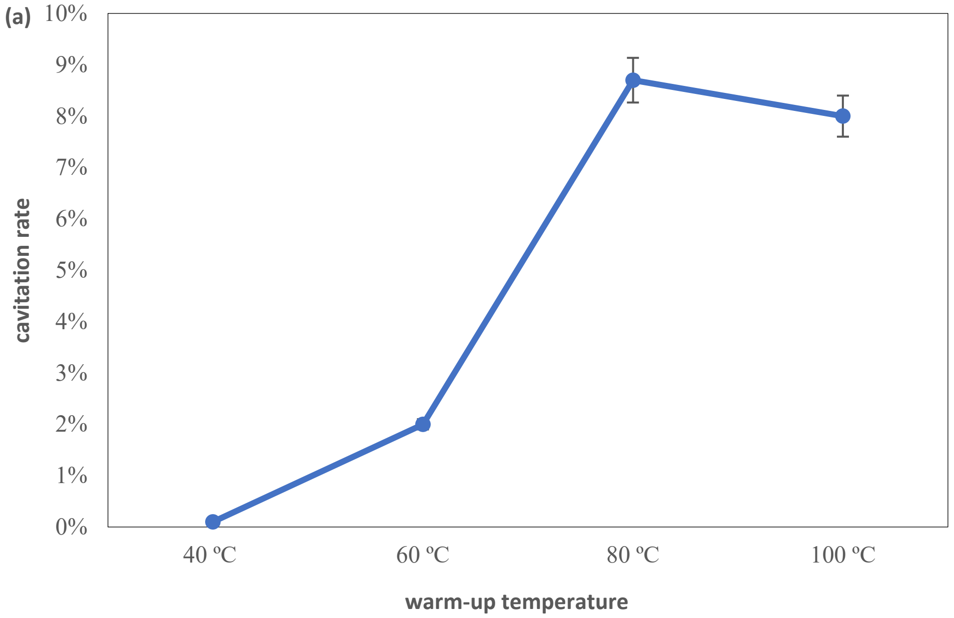

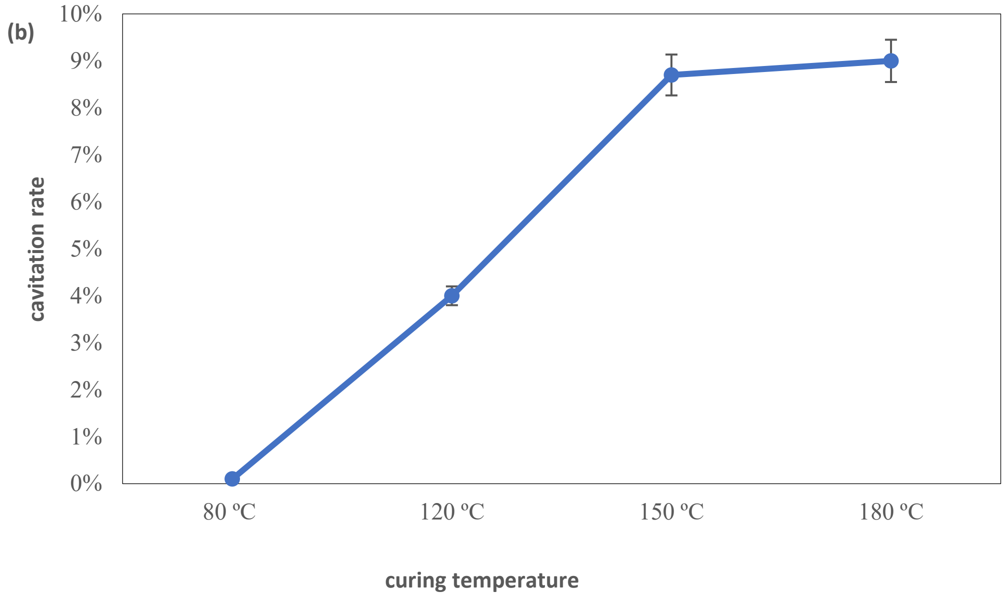

Figure 83. The cavitation rate by different temperature. (a) the warm-up temperature of 40 ºC,60 ºC,80 ºC and 100 ºC with curing temperature of 150 ºC (b) warm-up temperature of 80 ºC with curing temperature of 80 ºC, 120 ºC, 150 ºC, 180 ºC (stirring time at 40 seconds and stirring speed at 1000 rpm)

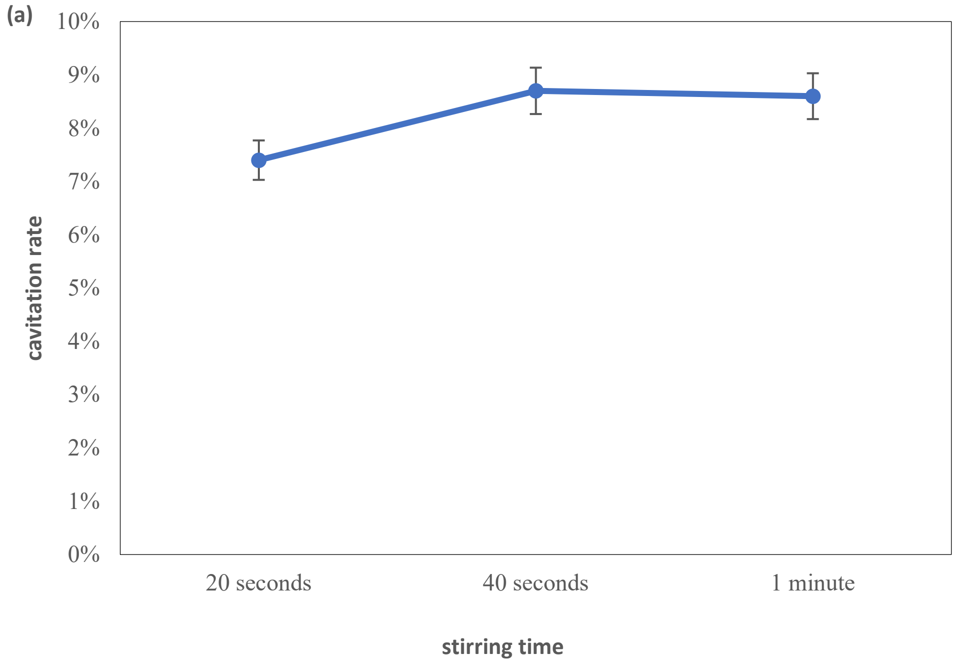

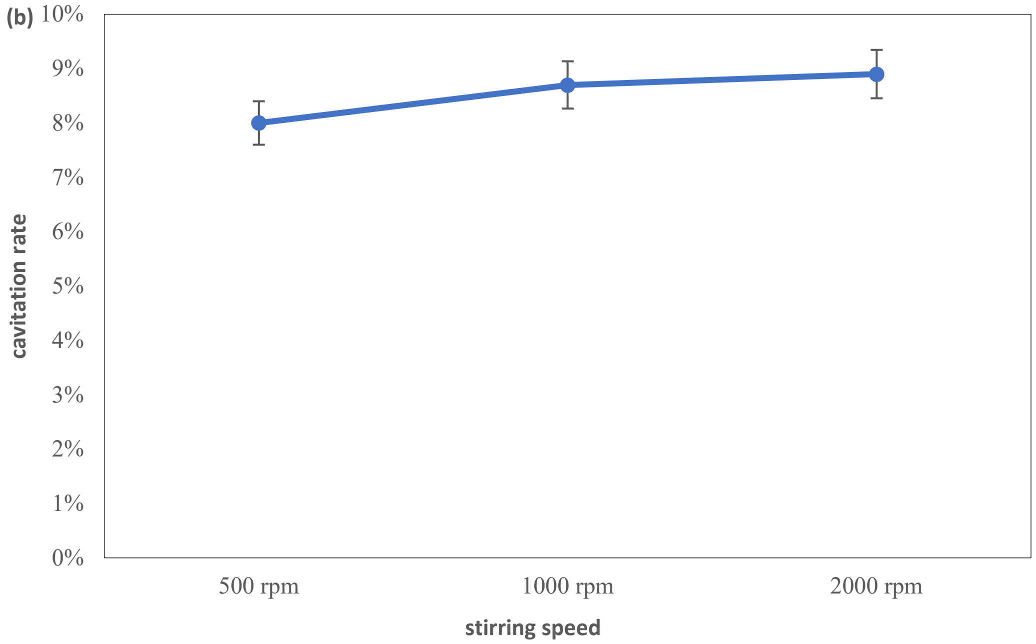

Figure 84. The cavitation rate by stirring conditions. (a) the stirring time of 20 seconds, ,40 seconds and 1 minute with stirring speed of 1000rpm (b) stirring speed of 500rpm, 1000rpm and 2000 rpm with stirring time of 40 seconds (warm-up temperature of 80 ºC and curing temperature of 150 ºC)

Figure 84 presents the influence of stirring time and speed on the cavitation rate. Figure 84(a) presents the results from stirring times of 20 seconds, 40 seconds and 1 minute with a stirring speed of 1000 rpm. Figure 84(b) present the cavitation rate with stirring speeds of 500 rpm, 1000 rpm and 2000 rpm with a stirring time of 40 seconds (warm-up temperature of 80 ºC and curing temperature of 150ºC). After stirring at 1000 rpm for more than 40 seconds, the cavitation rate is basically maintained around 8.7%. The effect of stirring conditions on the cavitation rate is relatively insignificant as seen in Figure 84.

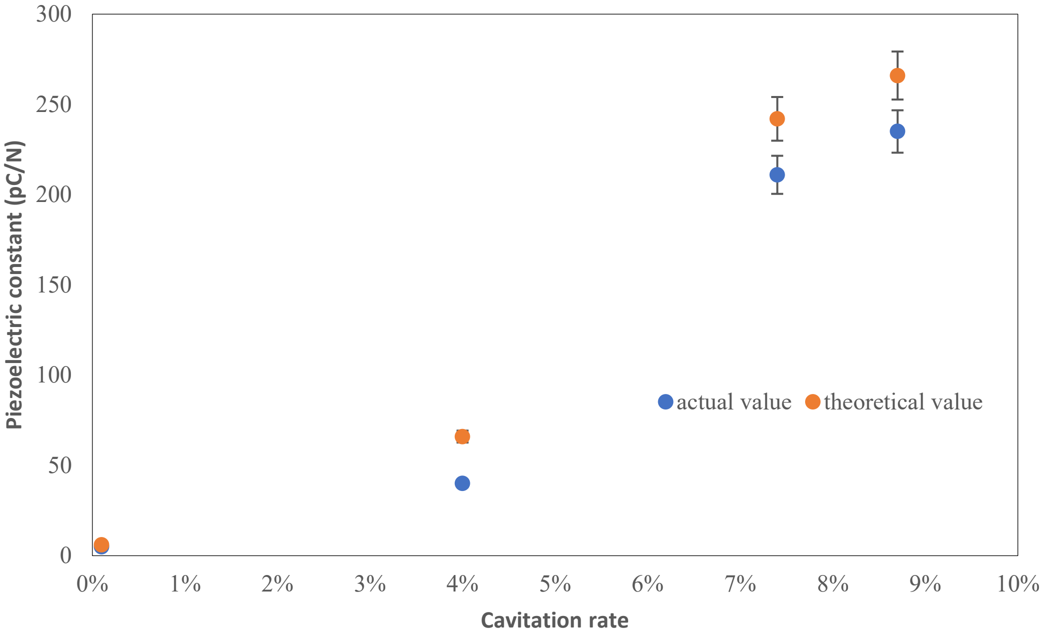

Figure 85. The actual piezoelectric constant value and the simulation value under the different cavitation rate

The actual piezoelectric constant value and the theoretical calculated value by equation 9 of the different cavitation rate of PDMS ferroelectret with random voids are shown in Figure 85. The effective piezoelectric coefficient increases with an increasing cavitation rate up to around 8.7%. The corresponding actual value and the simulation of d_{33e} were 266 pC/N and 235 pC/N respectively. These values are approximately 4 times greater than that value when the cavitation rate is 4% (66 pC/N and 40 pC/N).

The mechanical robustness of the samples and the material fatigue resistance are also important considerations for the device. The PDMS ferroelectret has been tested up to 1000 compressive cycles and bending test cycles and show no deterioration in output result.

(a)

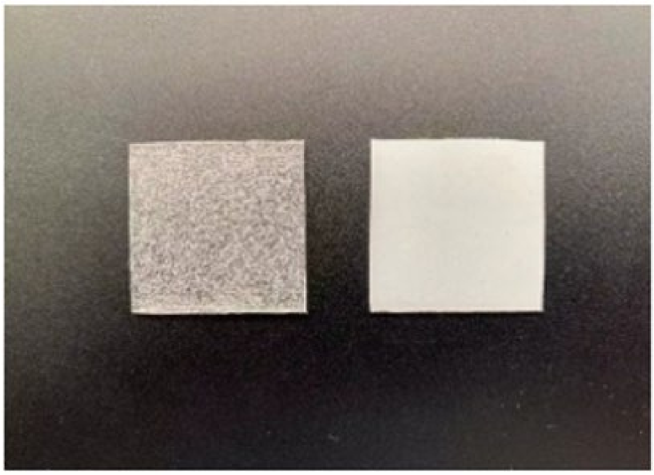

（b）

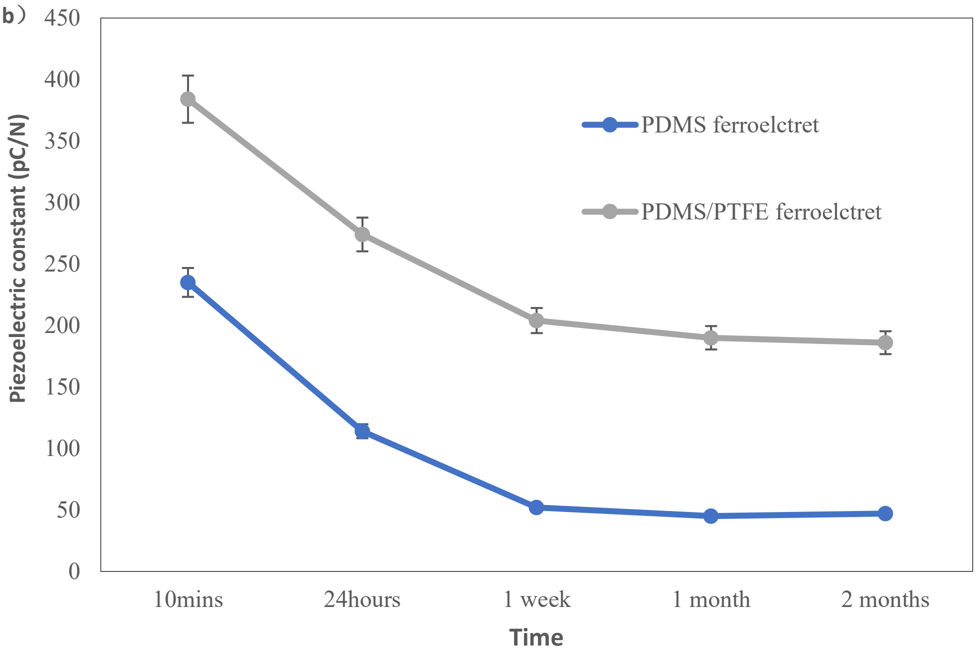
450
400
350
300
250
200
150
100
50
0
Piezoelectric constant (pC/N)
PDMS ferroelctret
PDMS/PTFE ferroelctret
10mins
24hours
1 week
1 month
2 months
Time

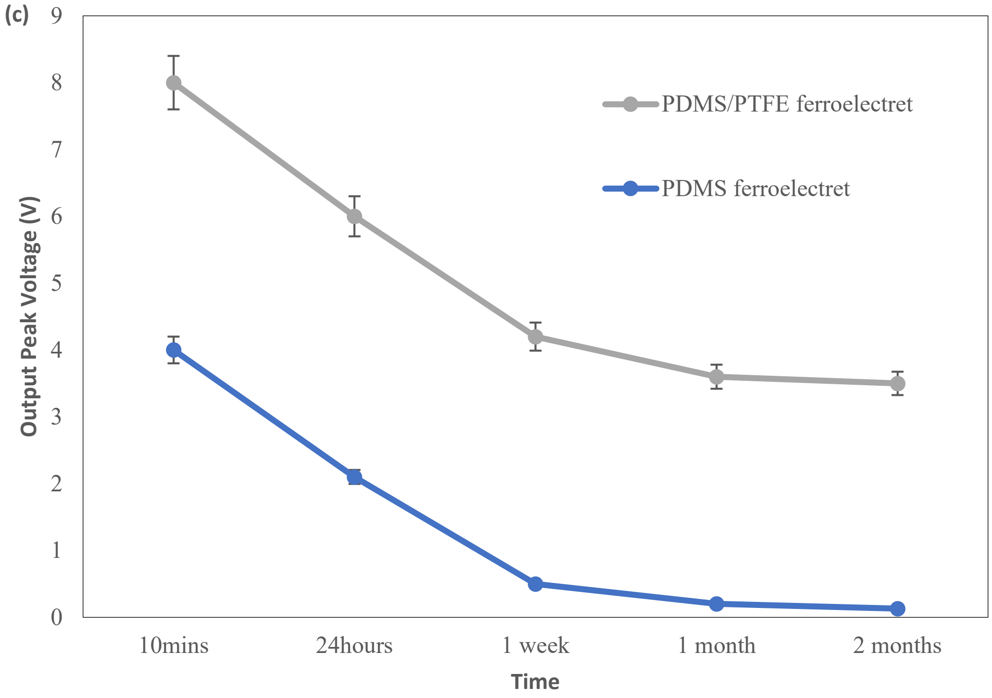

Figure 86. The PDMS ferroelectret and PDMS/PTFE ferroelectret and its property. (a) Photo of samples, from left to right: PDMS ferroelectret, PDMS/PTFE ferroelectret (b) The effective piezoelectric coefficient d_{33e} of PDMS ferroelectret in 2 months (c) The output peak voltage versus time under compressive force of 300 N

PDMS is not a stable electret material and the surface charge stability on the void surfaces of the PDMS is poor, causing the effective piezoelectric coefficient of samples to fall below 50 pC/N from around 235 pC/N in two months, to enhance the charge stability of PDMS ferroelectret, this paper explores measures to combine PTFE in the form of a powder with the PDMS to improve the charge stability in the ferroelectret. Figure 86(a) shows the PDMS ferroelectret and PDMS/PTFE ferroelectret (weight ratio 3:1) and its property (Figure 86(b)). The PDMS/PTFE ferroelectret maintained around 50% of its initial effective piezoelectric coefficient over 2 months, while the PDMS ferroelectret only maintained around 20%. The effective piezoelectric coefficient d_{33e} of this PDMS ferroelectret was about 235 pC/N while the value of PDMS/PTFE ferroelectret was about 384 pC/N just after poling and this value will drop to 47 pC/N and 186 pC/N in 2 months.

The output voltage of the PDMS and PDMS/PTFE ferroelectret under compressive force of 300 N present the voltage pulse as shown in Figures 86(c). The maximal peak voltages measured 1 hour after corona charging for PDMS ferroelectret and PDMS/PTFE ferroelectret were about 4 V and 8V, the maximal peak voltage over 2 months after corona charging for PDMS ferroelectret and PDMS/PTFE ferroelectret were about 0.13 V and 3.5 V respectively.

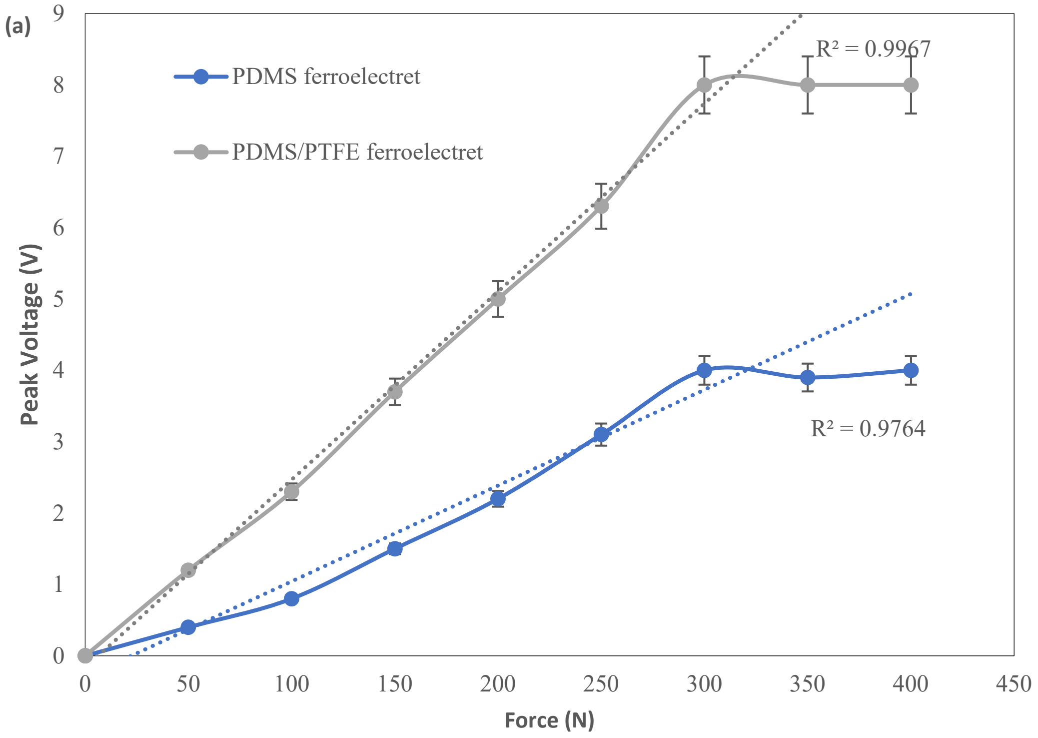

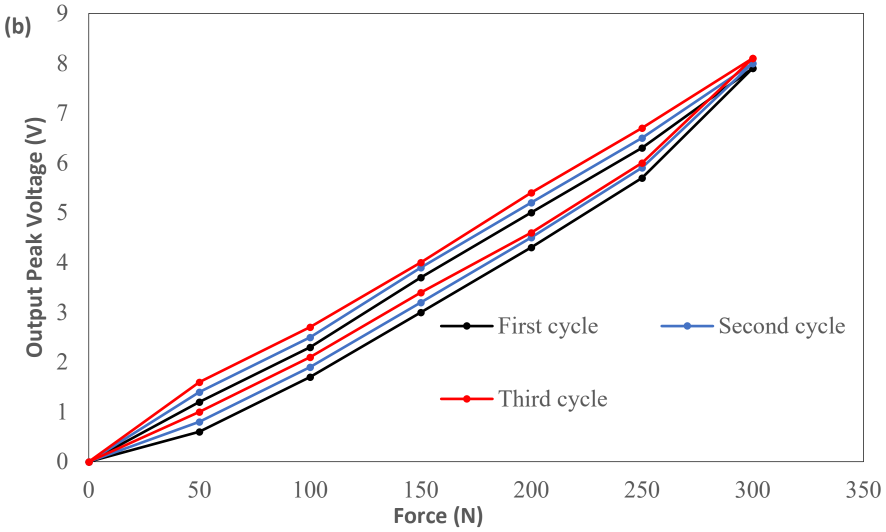

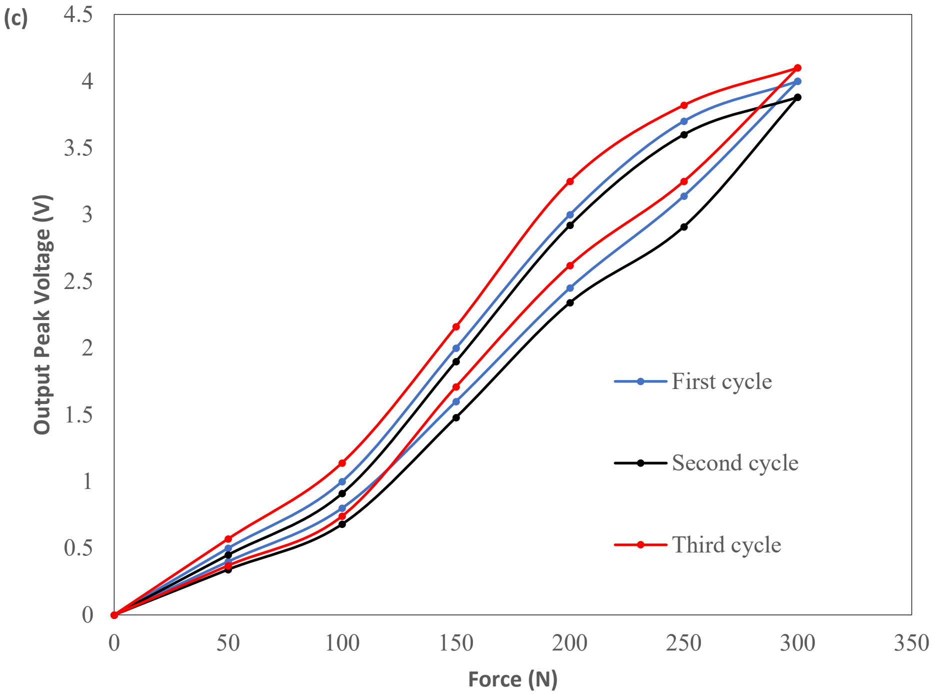

Figure 87. The linearity and hysteresis error. (a) The output peak voltage by different force at a frequency of 1Hz and the fitting curve in the linear region by the least square method (b) The hysteresis loop of the PDMS/PTFE ferroelectret (c) The hysteresis loop of the PDMS ferroelectret

The peak output voltage of the two types of ferroelectret under different compressive forces ranging from 0 to 300 N (average taken from 20 cycles applied at a frequency of 1 Hz) is shown in Figure 87(a). The output peak voltage initially increases with increasing force but levels off at around 300 N at which point the inner voids of ferroelectret have been fully compressed. To explore the sensitivity and linearity of each ferroelectret, the least square method was used to form the straight-line approximations shown in Figure 87(a) where each point corresponds to measured values. The sensitivity can be determined from by the slope of the dotted straight-line approximations and are 25.2, 12.4 mV/N for the PDMS/PTFE ferroelectret and the PDMS ferroelectret respectively. The minimum resolution of the ferroelectrets is 0.05N.

The linearity can be characterized by the R^2 or the nonlinearity error. R^2 can be calculated from the straight-line approximations, which had present in the last chapter. The nonlinearity error of the PDMS/PTFE ferroelectret and the PDMS ferroelectret is 4% and 9.6% respectively.

Therefore, the PDMS/PTFE ferroelectret have a better linearity than the PDMS ferroelectret, which present the same result from the value of R^2.

The hysteresis error of the PDMS/PTFE ferroelectret and the PDMS ferroelectret is 4.2% and 13.8% respectively, the calculation method is described in the previous chapter. The difference of hysteresis error could be explained by the variations in stiffness and the surface energy of the materials which may affect how the surfaces release as the force is removed. The PDMS/PTFE ferroelectret show a higher sensitivity and linearity and smaller hysteresis error than the PDMS ferroelectret, showing improved potential for use in sensing applications.

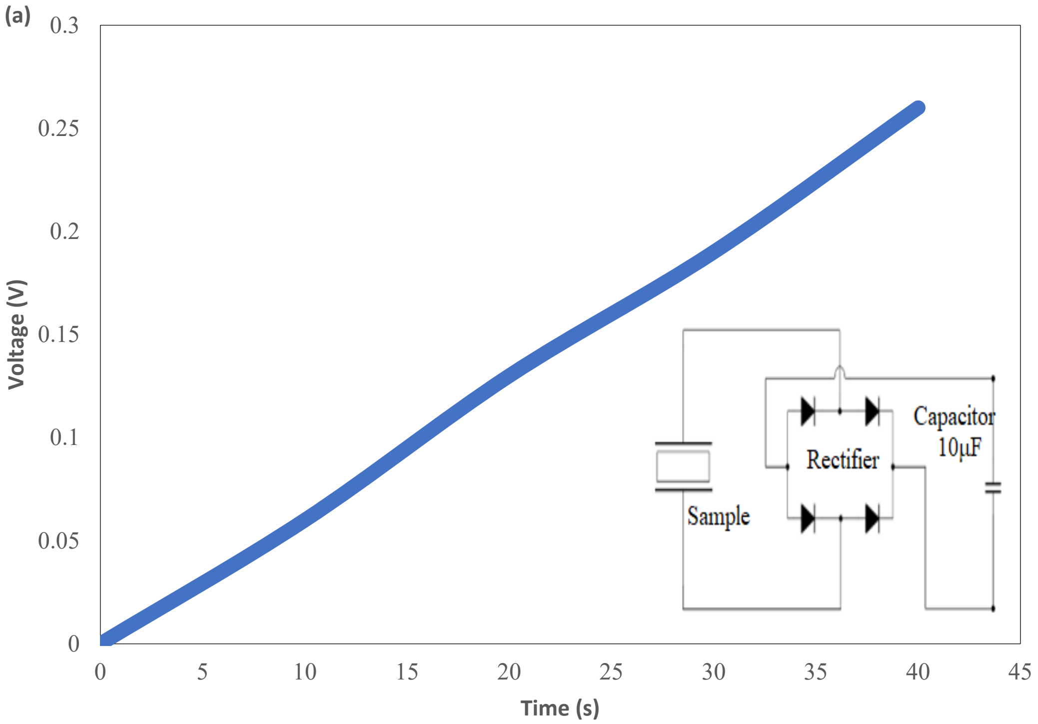

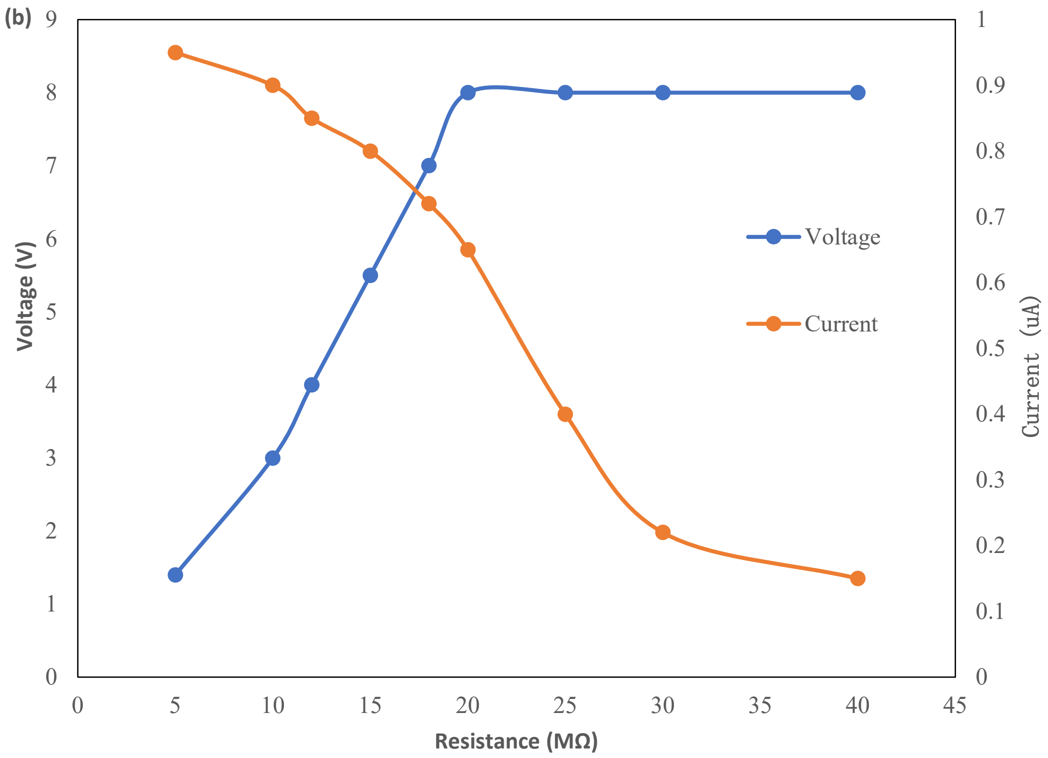

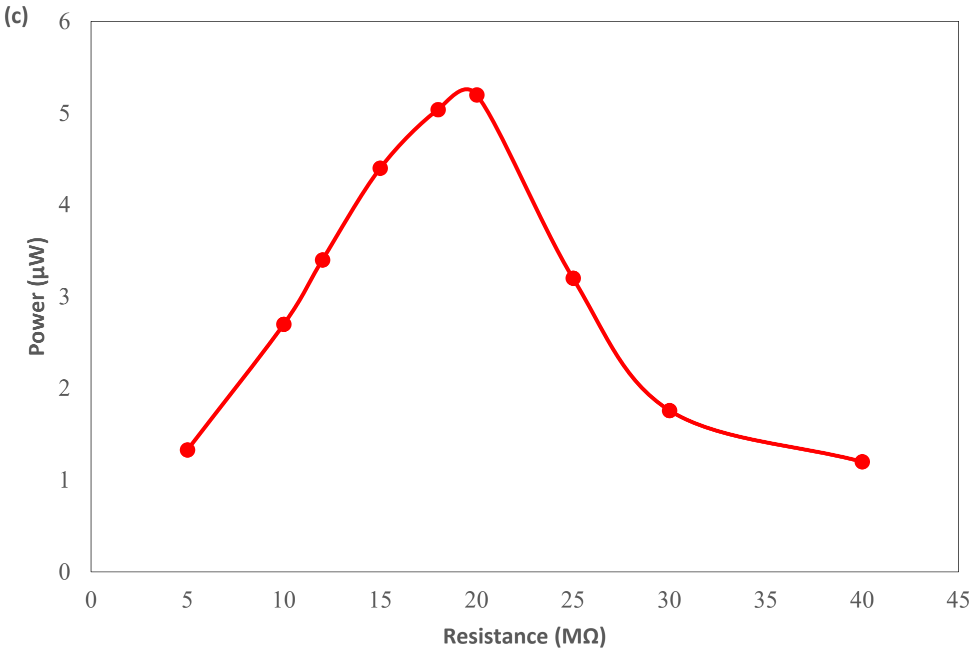

Figure 88. The energy harvesting result. (a) The power management circuit and the capacitor charging curve up to 40 s. (b) Current and Voltage as a function of load resistance. (c) Output power as a function of load resistance. For graphs (a) to (c) a compressive force applied of 300 N was applied at 1 Hz.

To explore the practical energy harvesting potential of the ferroelectret samples, the PDMS/PTFE ferroelectret with PTFE/PDMS weight ratio of 1:3 was driven by a cyclical mechanical compressive loading of 300 N at 1 Hz for 40 s. The sample was then connected to a 10 μF capacitor via the power management circuit in shown in Figure 88(a). The electrical energy generated can be calculated using equation (12).

$$U = \int_{t_1}^{t_2} \frac{V(t)^2}{R} dt \tag{7.14}$$

where R is the output voltage, ΔQ is the variation in charge, and t is the time taken to apply the force.

The voltage across the capacitor increases to 0.26 V corresponding to a total energy accumulation after 40 cycles of 0.338 μJ. The average energy stored is 8.45 nJ per cycle which corresponds to an average output power of 8.45 nW. The output current, voltage and power versus resistance are shown in Figure 88(b) and 88(c). Maximum output power occurs at a load resistance of 20 MΩ, with a peak power of 5.2 μW.

The result comparison between a PDMS/PTFE ferroelectret with controlled void layouts and a PDMS/PTFE ferroelectret with random voids are present as the table 8.

Table 8. The result comparison between a PDMS/PTFE ferroelectret with controlled void layouts and a PDMS/PTFE ferroelectret with random voids

Results	ferroelectret with controlled void layouts	ferroelectret with random voids
Total energy accumulation	0.12 V	0.26V
Average output power	1.8 nW	8.45 nW
Peak power	4 μW	5.2 μW

6.5 Conclusion

This thesis illustrates a simplified method to obtain PDMS ferroelectrets containing a large number of random voids formed using a high-speed stirring process. Although this method does not precisely control the geometry of the voids inside the ferroelectret, it is a very rapid and convenient way of fabrication and allows the piezoelectric properties to be adjusted by the stirring process and the PDMS curing process.

The cavitation rate can be increased significantly by adjusting different warm-up temperature and curing temperature within a certain range, in contrast to changes in stirring conditions which do not have a significant effect on the cavitation rate.

PDMS is not a stable electret material and the surface charge stability on the void surfaces of the PDMS is poor, causing the effective piezoelectric coefficient of samples to fall below 50 pC/N from around 235 pC/N in two months, to enhance the charge stability of PDMS ferroelectret, this paper explores measures to combine PTFE in the form of a powder with the PDMS to improve the charge stability in the ferroelectret. The PTFE powder substantially enhances the charge stability of PDMS ferroelectret, result in PDMS/PTFE ferroelectret maintained around 50% (from 384 pC/N to 186 pC/N) of its initial effective piezoelectric coefficient over 2 months, while the PDMS ferroelectret only maintained around 20% (from 235 pC/N to 47 pC/N).

The energy harvesting potential of the PDMS/PTFE ferroelectret was explored experimentally and found to generate an average output power of 8.45 nW after rectification when compressed at a frequency of 1 Hz. The fabricated PDMS/PTFE ferroelectret and the PDMS ferroelectret were utilized as sensing materials for a pressure sensor with sensitivities of 25.2 and 12.4 mV/N, respectively. The nonlinearity error and the hysteresis error of the PDMS/PTFE ferroelectret and the PDMS ferroelectret is 4%, 9.6% and 4.2%, 13.8% respectively. The PDMS/PTFE ferroelectret show a higher sensitivity and linearity and smaller hysteresis error than the PDMS ferroelectret.

Chapter 7

7. Conclusions and Future Work

7.1 Conclusions

PTFE is characterized by higher mechanical strength, fire resistance, chemical inertness and excellent dielectric properties. What's more important, PTFE has the best charge storage stability and high temperature resistance among the fluorine polymer electrets.

This research established a mathematical model and simulated in ANSYS to reveal the relationship between the geometry of ferroelectret cellular structure and its piezoelectric properties. And finally, both of these two approaches prove that, to achieve a higher piezoelectric property for multilayer ferroelectret cellular material, two geometry parameters should be targeted. The void area should be as large as possible and the value of the ratio of thickness of the solid and void layer t_r should be maintained at 0.4 for 10 or more layers.

In this research, the fabrication procedure for the PDMS ferroelectret is present, the moulds are first made by 3D printing, then a release agent is attached to the surface of the moulds, which can then be used for the manufacture of PDMS ferroelectret. The moulds consist of two parts and eventually the two demolded samples are bonded together and a voids structure ferroelectret is formed.

The related charging conditions are established to optimize the Corona charging conditions. the best charging conditions had been found: the charging voltage is 30 kV, the charging time is 2 minutes and the charging distance is 4 cm.

This research illustrates and compares approaches to enhancing the surface charge density and stability in PDMS ferroelectrets. Different approaches to adding the PTFE particles to the ferroelectret structure have been explored. The most obvious approach of simply adding the powder to the PDMS used to construct the ferroelectret as a whole does produce the most active ferroelectret devices but the addition of the PTFE prevents the device from being assembled using the plasma bonding process. The alternative liquid PDMS bonding process was found to be weaker under lateral strains leading to failure under cyclical bending. Therefore, the application of the PDMS/PTFE blend as a layer within the ferroelectret device is the preferred fabrication approach since it demonstrates significantly improved activity without compromising the robustness of the ferroelectret device. Different concentration ratios of PTFE powder in PDMS were explored and a PTFE/PDMS weight ratio of around 1:3 was found to achieve the highest effective piezoelectric coefficient d_{33e} values. For this ratio, the corresponding initial maximum effective values of d_{33e} was 680 pC/N for the PDMS/PTFE composite layer ferroelectrets demonstrating a 6 times improvement compared to the pure PDMS ferroelectret (110 pC/N). Increasing the amount of PTFE beyond this ratio did not provide any further improvement in device output. The PDMS/PTFE composite layer ferroelectret retained 50% of its initial effective piezoelectric coefficient after 4 months again demonstrating a considerable improvement in charge stability compared with the pure PDMS which reduces to less than 10% of the initial, already inferior, effective piezoelectric coefficient value after just one month. Most of the initial charge decay was found to occur in the first week after poling and the composite layer ferroelectret demonstrates excellent stability beyond this point. Adding a layer of pure PTFE using the water-based PTFE solution to the void surfaces was found not to work well due to the mechanically fragile nature of this film. The PDMS/PTFE composite layer ferroelectret show a higher sensitivity and linearity and smaller hysteresis error than the PTFE/water solution ferroelectret and the pure ferroelectret, also the PDMS/PTFE composite layer ferroelectret device shows good sensitivity to mechanical forces demonstrating its suitability for sensing applications. The soft, compliant and flexible nature of the PDMS material makes it particularly suitable for wearable applications.

This research also illustrates a simplified method to obtain PDMS ferroelectrets containing a large number of random voids formed using a high-speed stirring process. Although this method does not precisely control the geometry of the voids inside the ferroelectret, it is a very rapid and convenient way of fabrication and allows the piezoelectric properties to be adjusted by the stirring process and the PDMS curing process. The cavitation rate can be increased significantly by adjusting different warm-up temperature and curing temperature within a certain range, in contrast to changes in stirring conditions which do not have a significant effect on the cavitation rate.

7.2 Outlook

The main purpose of this project is use different approaches to extend the charge stability of existing ferroelectret materials or find a novel ferroelectret material suitable for achieving a high level of activity over a large period of time. From the current results, the charge stability needs to be further increased.

In attention, the relationship between different parameters of cellular structure and the piezoelectric constant d_{31} should be explored. Different size and structure of samples will be attempted to enhance the value of d_{31}.

The energy harvesting potential of the PDMS/PTFE composite layer ferroelectret had been explored and found to generate an average output power of 1.8 nW after rectification when compressed at a frequency of 1 Hz. This is a relatively low figure and is due to the high impedance of the PDMS material and lack of impedance matching with the power management circuit. In order to improve this, there is a universal power management strategy for triboelectric harvesters which possess a similarly high output impedance. Use of a power management circuit with improved impedance matching will be essential for energy harvesting applications.

In the research of the simplified method to obtain PDMS ferroelectret with random voids, the cavity rate can only vary from a few values due to the experimental method, and the next step could be to improve the experimental method to control the exact value of the cavity rate so that performance can be maximized.

Bibliography

[1] Meyer, J., Bischoff, R. and Feltrin, G., 2009. Microelectromechanical systems (MEMS). Encyclopedia of structural health monitoring.

[2] Spearing, S.M., 2000. Materials issues in microelectromechanical systems (MEMS). Acta materialia, 48(1), pp.179-196.

[3] Cook-Chennault K A, Thambi N and Sastry A M. Powering MEMS portable devices: a review of non-regenerative and regenerative power supply systems with special emphasis on piezoelectric energy harvesting systems. Smart Materials and Structures, 2008, 17(4): 0431001.

[4] Kimball J W, Kuhn B T, Balog R S. A System Design Approach for Unattended Solar Energy Harvesting Supply. IEEE, 2009, 24(4): 952-960.

[5] Harb A. Energy harvesting: state-of-the-art. Renewable energy, 2010: 1-14.

[6] Erturk, A. and Inman, D.J., 2011. Piezoelectric energy harvesting. John Wiley & Sons.

[7] Rahman, A., Farrok, O., Islam, M.R. and Xu, W., 2020. Recent progress in electrical generators for oceanic wave energy conversion. IEEE Access, 8, pp.138595-138615.

[8] Panda, P.K. and Sahoo, B., 2015. PZT to lead free piezo ceramics: a review. Ferroelectrics, 474(1), pp.128-143.

[9] Murayama, N., Nakamura, K., Obara, H. and Segawa, M., 1976. The strong piezoelectricity in polyvinylidene fluroide (PVDF). Ultrasonics, 14(1), pp.15-24.

[10] T. T. Wang, J. M. Herbert, and A. M. Glass, The Applications of Ferroelectric Polymers, Chapman & Hall, New York, USA, 1998, ch. Introduction.

[11] Bauer, S., Gerhard-Multhaupt, R. and Sessler, G.M., 2004. Ferroelectrets: Soft electroactive foams for transducers.

[12] Qaiss, A., Saidi, H., Fassi-Fehri, O. and Bousmina, M., 2012. Cellular polypropylene-based piezoelectric films. Polymer Engineering & Science, 52(12), pp.2637-2644.

[13] Wang, J.J., Hsu, T.H., Yeh, C.N., Tsai, J.W. and Su, Y.C., 2011. Piezoelectric polydimethylsiloxane films for MEMS transducers. Journal of Micromechanics and Microengineering, 22(1), p.015013.

[14] Wegener, M. and Bauer, S., 2005. Microstorms in cellular polymers: A route to soft piezoelectric transducer materials with engineered macroscopic dipoles. ChemPhysChem, 6(6), pp.1014-1025.

[15] Bauer, S., 2006. Piezo-, pyro-and ferroelectrets: soft transducer materials for electromechanical energy conversion. *IEEE Transactions on Dielectrics and Electrical Insulation, 13*(5), pp.953-962.

[16] Zhang, X., von Seggern, H., Sessler, G.M. and Kupnik, M., 2020. Mechanical energy harvesting with ferroelectrets. *IEEE Electrical Insulation Magazine*, *36*(6), pp.47-58.

[17] Qiu, X., Xia, Z. and Wang, F., 2007. Piezoelectricity of single-and multi-layer cellular polypropylene film electrets. *Frontiers of Materials Science in China*, *1*(1), pp.72-75.

[18] Mohebbi, A., Mighri, F., Ajji, A. and Rodrigue, D., 2018. Cellular polymer ferroelectret: a review on their development and their piezoelectric properties. *Advances in Polymer Technology*, *37*(2), pp.468-483.

[19] Chien, C.C., Hsu, Y.H., Lee, C.K. and Tang, W.C., 2020, May. Analysis and development of a ferroelectret cellular PP film. In *Behavior and Mechanics of Multifunctional Materials IX* (Vol. 11377, pp. 51-56). SPIE.

[20] Luo, Z., Zhu, D., Shi, J., Beeby, S., Zhang, C., Proynov, P. and Stark, B., 2015. Energy harvesting study on single and multilayer ferroelectret foams under compressive force. *IEEE Transactions on Dielectrics and Electrical Insulation, 22*(3), pp.1360-1368.

[21] Jaffe, H., 1958. Piezoelectric ceramics. *Journal of the American Ceramic Society*, *41*(11), pp.494-498.

[22] Katzir, S., 2006. The discovery of the piezoelectric effect. In *The beginnings of piezoelectricity* (pp. 15-64). Springer, Dordrecht.

[23] Berlincourt, D., 1981. Piezoelectric ceramics: Characteristics and applications. *The Journal of the Acoustical Society of America*, *70*(6), pp.1586-1595.

[24] Bera, B. and Sarkar, M.D., 2016. Piezoelectric effect, piezotronics and piezophototronics: a review. *Imperial Journal of Interdisciplinary Research (IJIR)*, *2*(11), pp.1407-1410.

[25] Liu, W. and Ren, X., 2009. Large piezoelectric effect in Pb-free ceramics. *Physical review letters*, *103*(25), p.257602.

[26] Shamos, M.H., Lavine, L.S. and Shamos, M.I., 1963. Piezoelectric effect in bone. *Nature*, *197*(4862), pp.81-81.

[27] Sessler, G.M. and Shahi, K., 1980. Electrets, Topics in Applied Physics. *Journal of The Electrochemical Society, 127*(12), pp.530C-530C.

[28] Wintle, H.J., 1973. Introduction to electrets. The Journal of the Acoustical Society of America, 53(6), pp.1578-1588.

[29] Kestelman, V.N., Pinchuk, L.S. and Goldade, V.A., 2000. Electrets in engineering: fundamentals and applications. Springer Science & Business Media.

[30] B. Hilczer and J. Malecki. *Electrets*, Elsevier, 1986.

[31] Sessler, G.M., 2006. Bernhard Gross and electret research: his contributions, our collaboration, and what followed. *IEEE transactions on dielectrics and electrical insulation*, *13*(5), pp.942-952.

[32] Sessler, G.M., 2001. Electrets: recent developments. *Journal of Electrostatics*, *51*, pp.137-145.

[33] Kressmann, R., Sessler, G.M. and Gunther, P., 1996. Space-charge electrets. *IEEE Transactions on Dielectrics and Electrical Insulation*, *3*(5), pp.607-623.

[34] Eberle, G., Schmidt, H. and Eisenmenger, W., 1996. Piezoelectric polymer electrets. *IEEE transactions on dielectrics and electrical insulation*, *3*(5), pp.624-646.

[35] Sessler, G.M. and West, J.E., 1973. Electret transducers: a review. *The Journal of the*

Acoustical Society of America, *53*(6), pp.1589-1600.

[36] Goel, M., 2002, October. An integrated view of applications of electret technology in energy and health sectors. In *Proceedings. 11th International Symposium on Electrets* (pp. 169-172). IEEE.

[37] Suzuki, Y., 2011. Recent progress in MEMS electret generator for energy harvesting. *IEEJ Transactions on Electrical and Electronic Engineering*, *6*(2), pp.101-111.

[38] Goel, M., 2003. Electret sensors, filters and MEMS devices: New challenges in materials research. *Current science*, *85*(4), pp.443-453.

[39] Li, X., Wang, Y., Xu, M., Shi, Y., Wang, H., Yang, X., Ying, H. and Zhang, Q., 2021. Polymer electrets and their applications. *Journal of Applied Polymer Science*, *138*(19), p.50406.

[40] Kestelman, V.N., Pinchuk, L.S. and Goldade, V.A., 2000. *Electrets in engineering: fundamentals and applications*. Springer Science & Business Media.

[41] Mikolajick, T., Schroeder, U. and Slesazeck, S., 2020. The past, the present, and the future of ferroelectric memories. *IEEE Transactions on Electron Devices*, *67*(4), pp.1434-1443.

[42] Chen, X., Han, X. and Shen, Q.D., 2017. PVDF‐based ferroelectric polymers in modern flexible electronics. *Advanced Electronic Materials*, *3*(5), p.1600460.

[43] Raukola, J.I., 1998. *A new technology to manufacture polypropylene foam sheet and biaxially oriented foam film* (Vol. 361). Technical Research Centre of Finland.

[44] Bauer, S., 2006. Piezo-, pyro-and ferroelectrets: soft transducer materials for electromechanical energy conversion. *IEEE Transactions on Dielectrics and Electrical Insulation*, *13*(5), pp.953-962.

[45] Bauer, S., Gerhard, R. and Sessler, G.M., 2004. Ferroelectrets: Soft electroactive foams for transducers.

[46] Bauer, S., 2006. Piezo-, pyro-and ferroelectrets: soft transducer materials for electromechanical energy conversion. *IEEE Transactions on Dielectrics and Electrical Insulation*, *13*(5), pp.953-962.

[47] Mohebbi, A., Mighri, F., Ajji, A. and Rodrigue, D., 2018. Cellular polymer ferroelectret: a review on their development and their piezoelectric properties. *Advances in Polymer Technology*, *37*(2), pp.468-483.

[48] Zhang, Y., Bowen, C.R., Ghosh, S.K., Mandal, D., Khanbareh, H., Arafa, M. and Wan, C., 2019. Ferroelectret materials and devices for energy harvesting applications. *Nano Energy*, *57*, pp.118-140.

[49] Zhang, X., von Seggern, H., Sessler, G.M. and Kupnik, M., 2020. Mechanical energy harvesting with ferroelectrets. *IEEE Electrical Insulation Magazine*, *36*(6), pp.47-58.

[50] Hamdi, O., Mighri, F. and Rodrigue, D., 2018. Piezoelectric cellular polymer films: Fabrication, properties and applications. *AIMS Mater. Sci*, *5*(5), pp.845-869.

[51] Altafim, R.A.C., Basso, H.C., Neto, L.G., Lima, L., Altafim, R.A.P. and de Aquino, C.V., 2005, October. Piezoelectricity in multi-air voids electrets. In *CEIDP'05. 2005 Annual Report Conference on Electrical Insulation and Dielectric Phenomena, 2005.* (pp. 669-672). IEEE.

[52] Altafim, R.A.P., Qiu, X., Wirges, W., Gerhard, R., Altafim, R.A.C., Basso, H.C., Jenninger, W. and Wagner, J., 2009. Template-based fluoroethylenepropylene piezoelectrets with tubular channels for transducer applications. *Journal of Applied Physics*, *106*(1), p.014106.

[53] Zhang, X., Hillenbrand, J. and Sessler, G.M., 2006. Thermally stable fluorocarbon ferroelectrets with high piezoelectric coefficient. *Applied Physics A*, *84*(1), pp.139-142.

[54] Zhang, X., Pondrom, P., Sessler, G.M. and Ma, X., 2018. Ferroelectret nanogenerator with large transverse piezoelectric activity. *Nano energy*, *50*, pp.52-61.

[55] Zhang, X., Cao, G., Sun, Z. and Xia, Z., 2010. Fabrication of fluoropolymer piezoelectrets by using rigid template: Structure and thermal stability. *Journal of Applied Physics*, *108*(6), p.064113.

[56] Zhang, X., Sessler, G.M., Xue, Y. and Ma, X., 2016. Audio and ultrasonic responses of laminated fluoroethylenepropylene and porous polytetrafluoroethylene films with different charge distributions. *Journal of Physics D: Applied Physics*, *49*(20), p.205502.

[57] Zhang, X., Hillenbrand, J., Sessler, G.M., Haberzettl, S. and Lou, K., 2012. Fluoroethylenepropylene ferroelectrets with patterned microstructure and high, thermally stable piezoelectricity. *Applied Physics A*, *107*(3), pp.621-629.

[58] Zhang, X., Sessler, G.M. and Wang, Y., 2014. Fluoroethylenepropylene ferroelectret films with cross-tunnel structure for piezoelectric transducers and micro energy harvesters. *Journal of applied physics*, *116*(7), p.074109.

[59] Li, Y. and Zeng, C., 2013. Low-Temperature CO2-Assisted Assembly of Cyclic Olefin Copolymer Ferroelectrets of High Piezoelectricity and Thermal Stability. *Macromolecular Chemistry and Physics*, *214*(23), pp.2733-2738.

[60] Li, Y. and Zeng, C., 2013. Low-Temperature CO2-Assisted Assembly of Cyclic Olefin Copolymer Ferroelectrets of High Piezoelectricity and Thermal Stability. *Macromolecular Chemistry and Physics*, *214*(23), pp.2733-2738.

[61] Kachroudi, A., Basrour, S., Rufer, L., Sylvestre, A. and Jomni, F., 2015. Dielectric properties modelling of cellular structures with PDMS for micro-sensor applications. *Smart Materials and Structures*, *24*(12), p.125013.

[62] Zhong, J., Zhong, Q., Zang, X., Wu, N., Li, W., Chu, Y. and Lin, L., 2017. Flexible PET/EVA-based piezoelectret generator for energy harvesting in harsh environments. *Nano Energy*, *37*, pp.268-274.

[63] Rychkov, D., Altafim, R.A.P. and Gerhard, R., 2014, October. Unipolar ferroelectrets-Following the example of the electret microphone more closely. In *2014 IEEE Conference on Electrical Insulation and Dielectric Phenomena (CEIDP)* (pp. 860-862). IEEE.

[64] Ma, X., Zhang, X., Sessler, G.M., Chen, L., Yang, X., Dai, Y. and He, P., 2019. Energy harvesters based on fluorinated ethylene propylene unipolar ferroelectrets with negative charges. *AIP Advances*, *9*(12), p.125334.

[65] Shi, J., Zhu, D. and Beeby, S.P., 2014, November. An investigation of PDMS structures for optimized ferroelectret performance. In *Journal of physics: conference series* (Vol. 557, No. 1, p. 012104). IOP Publishing.

[66] Ge, C. and Zhai, W., 2018. Cellular thermoplastic polyurethane thin film: preparation, elasticity, and thermal insulation performance. *Industrial & Engineering Chemistry Research*, *57*(13), pp.4688-4696.

[67] Xu, B.X., von Seggern, H., Zhukov, S. and Gross, D., 2013. Continuum modeling of charging process and piezoelectricity of ferroelectrets. *Journal of Applied Physics*, *114*(9), p.094103.

[68] Zhukov, S. and Von Seggern, H., 2007. Breakdown-induced light emission and poling dynamics of porous fluoropolymers. *Journal of applied physics*, *101*(8), p.084106.

[69] Sappati, K.K. and Bhadra, S., 2018. Piezoelectric polymer and paper substrates: a review. *Sensors*, *18*(11), p.3605.

[70] Zhang, X., Hillenbrand, J. and Sessler, G.M., 2004. Piezoelectric d 33 coefficient of cellular polypropylene subjected to expansion by pressure treatment. *Applied physics letters*, *85*(7), pp.1226-1228.

[71] Mellinger, A., Wegener, M., Wirges, W., Mallepally, R.R. and Gerhard-Multhaupt, R., 2006. Thermal and temporal stability of ferroelectret films made from cellular polypropylene/air composites. *Ferroelectrics*, *331*(1), pp.189-199.

[72] Zhang, X., Zhang, X., Sessler, G.M. and Gong, X., 2013. Quasi-static and dynamic piezoelectric responses of layered polytetrafluoroethylene ferroelectrets. *Journal of Physics D: Applied Physics*, *47*(1), p.015501.

[73] Basso, H.C., Altafim, R.A.P., Altafim, R.A.C., Mellinger, A., Fang, P., Wirges, W. and Gerhard, R., 2007, October. Three-layer ferroelectrets from perforated Teflon®-PTFE films fused between two homogeneous Teflon®-FEP films. In *2007 Annual Report-Conference on Electrical Insulation and Dielectric Phenomena* (pp. 453-456). IEEE.

[74] Zhang, X., Hillenbrand, J., Sessler, G.M., Haberzettl, S. and Lou, K., 2012.

Fluoroethylenepropylene ferroelectrets with patterned microstructure and high, thermally stable piezoelectricity. *Applied Physics A*, *107*(3), pp.621-629.

[75] Wegener, M., Paajanen, M., Voronina, O., Schulze, R., Wirges, W. and Gerhard-Multhaupt, R., 2005, September. Voided cyclo-olefin polymer films: Ferroelectrets with high thermal stability. In *2005 12th International Symposium on Electrets* (pp. 47-50). IEEE.

[76] Fang, P., Qiu, X., Wirges, W., Gerhard, R. and Zirkel, L., 2010. Polyethylene-naphthalate (PEN) ferroelectrets: cellular structure, piezoelectricity and thermal stability. *IEEE Transactions on Dielectrics and Electrical Insulation*, *17*(4), pp.1079-1087.

[77] Wegener, M., Wirges, W., Dietrich, J.P. and Gerhard-Multhaupt, R., 2005, September. Polyethylene terephthalate (PETP) foams as ferroelectrets. In *2005 12th International Symposium on Electrets* (pp. 28-30). IEEE.

[78] Wang, J.J., Hsu, T.H., Yeh, C.N., Tsai, J.W. and Su, Y.C., 2011. Piezoelectric polydimethylsiloxane films for MEMS transducers. *Journal of Micromechanics and Microengineering*, *22*(1), p.015013.

[79] Wang, S., Shao, H.Q., Liu, Y., Tang, C.Y., Zhao, X., Ke, K., Bao, R.Y., Yang, M.B. and Yang, W., 2021. Boosting piezoelectric response of PVDF-TrFE via MXene for self-powered linear pressure sensor. *Composites Science and Technology*, *202*, p.108600.

[80] Wang, F.P., Xia, Z.F., Wu, Y.H. and Qiu, X.L., 2004. The piezoelectricity of P (VDF-TFE-HFP)/PTFE double-layer electret films. *Acta Physica Sinica*, *53*(5), pp.1534-1539.

[81] Xia, Z., Gerhard-Multhaupt, R., Künstler, W., Wedel, A. and Danz, R., 1999. High surface-charge stability of porous polytetrafluoroethylene electret films at room and elevated temperatures. *Journal of Physics D: Applied Physics*, *32*(17), p.L83.

[82] Huiming, X., Gangjin, C., Xumin, C. and Zhi, C., 2017. A flexible electret membrane with persistent electrostatic effect and resistance to harsh environment for energy harvesting. *Scientific reports*, *7*(1), pp.1-8.

[83] Patel, I., 2011. Ceramic based intelligent piezoelectric energy harvesting device. *InTech China*, pp.133-150.

[84] Sun, H., Yin, M., Wei, W., Li, J., Wang, H. and Jin, X., 2018. MEMS based energy harvesting for the Internet of Things: a survey. *Microsystem Technologies*, *24*(7), pp.2853-2869.

[85] Junior, O.A., Maran, A.L.O. and Henao, N.C., 2018. A review of the development and applications of thermoelectric microgenerators for energy harvesting. *Renewable and Sustainable Energy Reviews*, *91*, pp.376-393.

[86] Mateu, L. and Moll, F., 2005, June. Review of energy harvesting techniques and applications for microelectronics. In *VLSI Circuits and Systems II* (Vol. 5837, pp. 359-373). SPIE.

[87] Safaei, M., Sodano, H.A. and Anton, S.R., 2019. A review of energy harvesting using piezoelectric materials: state-of-the-art a decade later (2008–2018). *Smart Materials and Structures*, *28*(11), p.113001.

[88] Anton, S.R. and Farinholt, K.M., 2012, March. An evaluation on low-level vibration energy harvesting using piezoelectret foam. In *Active and Passive Smart Structures and Integrated Systems 2012* (Vol. 8341, pp. 162-171). SPIE.

[89] Umeda, M., Nakamura, K. and Ueha, S., 1996. Analysis of the transformation of mechanical impact energy to electric energy using piezoelectric vibrator. *Japanese Journal of Applied Physics*, *35*(5S), p.3267.

[90] Anton, S.R. and Farinholt, K.M., 2012, March. An evaluation on low-level vibration energy harvesting using piezoelectret foam. In *Active and Passive Smart Structures and Integrated Systems 2012* (Vol. 8341, pp. 162-171). SPIE.

[91] Pondrom, P., Hillenbrand, J., Sessler, G.M., Bös, J. and Melz, T., 2015. Energy harvesting with single-layer and stacked piezoelectret films. *IEEE Transactions on Dielectrics and Electrical Insulation*, *22*(3), pp.1470-1476.

[92] Pondrom, P., Hillenbrand, J., Sessler, G.M., Bös, J. and Melz, T., 2014. Vibration-based energy harvesting with stacked piezoelectrets. *Applied physics letters*, *104*(17), p.172901.

[93] Ray, C.A. and Anton, S.R., 2017. Multilayer piezoelectret foam stack for vibration energy harvesting. *Journal of Intelligent Material Systems and Structures*, *28*(3), pp.408-420.

[94] Sessler, G.M., Pondrom, P. and Zhang, X., 2016. Stacked and folded piezoelectrets for vibration-based energy harvesting. *Phase Transitions*, *89*(7-8), pp.667-677.

[95] Zhang, X., Wu, L. and Sessler, G.M., 2015, May. Energy scavenging from vibration with two-layer laminated fluoroethylenepropylene piezoelectret films. In *2015 Joint IEEE International Symposium on the Applications of Ferroelectric (ISAF), International Symposium on Integrated Functionalities (ISIF), and Piezoelectric Force Microscopy Workshop (PFM)* (pp. 24-27). IEEE.

[96] Zhang, X., Pondrom, P., Sessler, G.M. and Ma, X., 2018. Ferroelectret nanogenerator with large transverse piezoelectric activity. *Nano energy*, *50*, pp.52-61.

[97] Ma, X., Zhang, X., Sessler, G.M., Chen, L., Yang, X., Dai, Y. and He, P., 2019. Energy harvesters based on fluorinated ethylene propylene unipolar ferroelectrets with negative charges. *AIP Advances*, *9*(12), p.125334.

[98] Ben Dali, O., Pondrom, P., Sessler, G.M., Zhukov, S., Von Seggern, H., Zhang, X. and Kupnik, M., 2020. Cantilever-based ferroelectret energy harvesting. *Applied Physics Letters*, *116*(24), p.243901.

[99] Li, W., Zhao, S., Wu, N., Zhong, J., Wang, B., Lin, S., Chen, S., Yuan, F., Jiang, H., Xiao, Y. and Hu, B., 2017. Sensitivity-enhanced wearable active voiceprint sensor based on cellular polypropylene piezoelectret. *ACS applied materials & interfaces*, *9*(28), pp.23716-23722.

[100] Williams, C.B. and Yates, R.B., 1996. Analysis of a micro-electric generator for microsystems. *sensors and actuators A: Physical*, *52*(1-3), pp.8-11.

[101] Kymissis, J., Kendall, C., Paradiso, J. and Gershenfeld, N., 1998, October. Parasitic power harvesting in shoes. In *Digest of papers. Second international symposium on wearable computers (Cat. No. 98EX215)* (pp. 132-139). IEEE.

[102] Li, W., Zhao, S., Wu, N., Zhong, J., Wang, B., Lin, S., Chen, S., Yuan, F., Jiang, H., Xiao, Y. and Hu, B., 2017. Sensitivity-enhanced wearable active voiceprint sensor based on cellular

polypropylene piezoelectret. *ACS applied materials & interfaces*, *9*(28), pp.23716-23722.

[103] Yan, C., Deng, W., Jin, L., Yang, T., Wang, Z., Chu, X., Su, H., Chen, J. and Yang, W., 2018. Epidermis-inspired ultrathin 3D cellular sensor array for self-powered biomedical monitoring. *ACS applied materials & interfaces*, *10*(48), pp.41070-41075.

[104] Wu, N., Chen, S., Lin, S., Li, W., Xu, Z., Yuan, F., Huang, L., Hu, B. and Zhou, J., 2018. Theoretical study and structural optimization of a flexible piezoelectret-based pressure sensor. *Journal of Materials Chemistry A*, *6*(12), pp.5065-5070.

[105] Wu, N., Jiang, H., Li, W., Lin, S., Zhong, J., Yuan, F., Huang, L., Hu, B. and Zhou, J., 2017. Output enhanced compact multilayer flexible nanogenerator for self-powered wireless remote system. *Journal of Materials Chemistry A*, *5*(25), pp.12787-12792.

[106] Tajitsu, Y., Takarada, J., Hiramoto, M., Nakatsuji, T., Nakiri, T., Imoto, K., Kaimori, S. and Shikata, Y., 2019. Application of piezoelectric electrets to an energy-harvesting system. *Japanese Journal of Applied Physics*, *58*(SL), p. SLLD05.

[107] Chen, G., 2010. A new model for surface potential decay of corona-charged polymers. *Journal of Physics D: Applied Physics*, *43*(5), p.055405.

[108] Kindersberger, J. and Lederle, C., 2008. Surface charge decay on insulators in air and sulfurhexafluorid-part I: simulation. *IEEE Transactions on Dielectrics and Electrical Insulation*, *15*(4), pp.941-948.

[109] Kindersberger, J. and Lederle, C., 2008. Surface charge decay on insulators in air and sulfurhexafluorid-part II: measurements. *IEEE Transactions on Dielectrics and Electrical Insulation*, *15*(4), pp.949-957.

[110] Gao, Y. and Du, B., 2012. Effect of gamma-ray irradiation on surface charge decaying characteristic of epoxy resin. *Gaodianya Jishu/ High Voltage Engineering*, *38*(4), pp.824-830.

[111] Gao, Y., 2009. *Dynamic behavior of surface charge on polymer insulating materials* (Doctoral dissertation).

[112] Serkan, M., Kirkici, H. and Koppisetty, K., 2006, May. Surface flashover characteristics

of nano-composite dielectric materials under DC and pulsed signals in partial vacuum. In *Conference Record of the 2006 Twenty-Seventh International Power Modulator Symposium* (pp. 90-92). IEEE.

[113] Kumara, S., Ma, B., Serdyuk, Y.V. and Gubanski, S.M., 2012. Surface charge decay on HTV silicone rubber: effect of material treatment by corona discharges. *IEEE Transactions on Dielectrics and Electrical Insulation*, *19*(6), pp.2189-2195.

[114] Wang, B., Zhang, G.X., Wang, Q., Li, J.Z. and Tang, H., 2011. Analysis of Surface Charge Decay Process on Insulators in SF sub (6) and Air. *Gaodianya Jishu/ High Voltage Engineering*, *37*(1), pp.99-103.

[115] Feng, W.A.N.G., Zhi, F.A.N.G. and Yuchang, Q.I.U., 2005. Study of charge accumulation on insulator surface in HVDC gas-insulated switchgear. *Proceedings of the CSEE*, *25*(3), pp.105-109.

[116] Alam, S., Serdyuk, Y.V. and Gubanski, S.M., 2014, September. Contribution of gas neutralization to the potential decay on silicon rubber surfaces at different ambient pressures. In *2014 ICHVE International Conference on High Voltage Engineering and Application* (pp. 1-4). IEEE.

[117] Elkhodary, S.M. and Hackam, R., 1993, October. Generation of surface charges on an insulator in SF/sub 6/gas. In *Proceedings of IEEE Conference on Electrical Insulation and Dielectric Phenomena-(CEIDP'93)* (pp. 336-342). IEEE.

[118] Wang, B., Zhang, G.X., Wang, Q., Li, J.Z. and Tang, H., 2011. Analysis of Surface Charge Decay Process on Insulators in SF sub (6) and Air. *Gaodianya Jishu/ High Voltage Engineering*, *37*(1), pp.99-103.

[119] Liu, Y.Q., An, Z.L., Cang, J., Zhang, Y.W. and Zheng, F., 2012. Influence of fluorination time on surface charge accumulation on epoxy resin insulation. *Acta Phys. Sin*, *61*, p.158201.

[120] Rychkov, D., Kuznetsov, A. and Rychkov, A., 2011. Electret properties of polyethylene and polytetrafluoroethylene films with chemically modified surface. *IEEE Transactions on Dielectrics and Electrical Insulation*, *18*(1), pp.8-14.

[121] Gao, Y. and Du, B., 2012. Effect of gamma-ray irradiation on surface charge decaying characteristic of epoxy resin. *Gaodianya Jishu/ High Voltage Engineering*, *38*(4), pp.824-830.

[122] Shao, T., Yang, W., Zhang, C., Niu, Z., Yan, P. and Schamiloglu, E., 2014. Enhanced surface flashover strength in vacuum of polymethylmethacrylate by surface modification using atmospheric-pressure dielectric barrier discharge. *Applied Physics Letters*, *105*(7), p.071607.

[123] Lewis, T.J., 1994. Nanometric dielectrics. *IEEE Transactions on Dielectrics and Electrical Insulation*, *1*(5), pp.812-825.

[124] Tanaka, T., 2005. Dielectric nanocomposites with insulating properties. *IEEE Transactions on Dielectrics and Electrical Insulation*, *12*(5), pp.914-928.

[125] Li, C., Ding, L., Lu, J. and Liang, Y., 2007. Traping and de-traping process resulting in the alumina surface flashover in vacuum. *PROCEEDINGS-CHINESE SOCIETY OF ELECTRICAL ENGINEERING*, *27*(9), p.1.

[126] Du, B.X. and Xiao, M., 2014. Influence of surface charge on DC flashover characteristics of epoxy/BN nanocomposites. *IEEE Transactions on Dielectrics and Electrical Insulation*, *21*(2), pp.529-536.

[127] Xia, Z., 1991. Corona charging and charge decay of Teflon-PFA. *IEEE transactions on electrical insulation*, *26*(6), pp.1104-1111.

[128] Zhongfu, X. and Jian, J., 1991. Corona charged Aclar PCTFE film electrets. *Vacuum*, *42*(16), p.1086.

[129] Ambrosy, A. and Holdik, K., 1984. Piezoelectric PVDF films as ultrasonic transducers. *Journal of Physics E: Scientific Instruments*, *17*(10), p.856.

[130] Qiu, X., Xia, Z., Wang, F., Wu, Y. and Zhang, Y., 2002, October. The electret behavior of poly (vinylidenefluoride/chlorotrifluorethylene) film. In *Proceedings. 11th International Symposium on Electrets* (pp. 322-325). IEEE.

[131] Lu, X., Schirokauer, A. and Scheinbeim, J., 2000. Giant electrostrictive response in poly (vinylidene fluoride-hexafluoropropylene) copolymers. *IEEE transactions on ultrasonics, ferroelectrics, and frequency control*, *47*(6), pp.1291-1295.

[132] Gorokhovatsky, Y.A., Boitzov, V.G. and Rychkov, D.A., 2002, October. Thermal stability of polarization structures in corona-charged P (VDF-HFP) copolymer films. In *Proceedings. 11th International Symposium on Electrets* (pp. 134-137). IEEE.

[133] Wang, F., Xia, Z., Qiu, X., Shen, J., Zhang, X. and An, Z., 2006. Piezoelectric properties and charge dynamics in poly (vinylidene fluoride-hexafluoropropylene) copolymer films with different content of HEP. *IEEE transactions on dielectrics and electrical insulation*, *13*(5), pp.1132-1139.

[134] Bai, Y., Jantunen, H. and Juuti, J., 2018. Energy harvesting research: the road from single source to multisource. *Advanced materials*, *30*(34), p.1707271.

[135] Xia, Z., Wedel, A., & Danz, R. (2003). Charge storage and its dynamics in porous polytetrafluoroethylene (PTFE) film electrets. *IEEE transactions on dielectrics and electrical insulation*, 10(1), 102-108.

[136] Kulah, H., Goksu, N. and Beker, L., 2017. *Energy harvesting cochlear implant*. U.S. Patent 9,630,007.

[137] Cascetta, F., Schiavo, A.L., Minardo, A., Musto, M., Rotondo, G. and Calcagni, A., 2018. Analysis of the energy extracted by a harvester based on a piezoelectric tile. *Current Applied Physics*, *18*(8), pp.905-911.

[138] H.W. Kim, S. Priya, . Piezoelectric energy harvesting under high pre-stressed cyclic vibrations. *Journal of Electroceramics*, 2005, 15:27-34.

[139] H.W. Kim, A. Batra, S. Priya, . Energy harvesting using a piezoelectric "cymbal" transducer in dynamic environment.*Japanese Journal of Applied Physics*, 2004, 43:6178-6183.

[140] Sunghwan Kim. Low power energy harvesting with piezoelectric generators [PhD Dissertation]. U.S.A: University of Pittsburgh, 2002.

[141] Morel, A., Pillonnet, G. and Badel, A., 2017. Regenerative synchronous electrical charge extraction for highly coupled piezoelectric generators. *interface*, *4*, p.6.

[142] Wang, X., Niu, S., Yi, F., Yin, Y., Hao, C., Dai, K., Zhang, Y., You, Z. and Wang, Z.L., 2017. Harvesting ambient vibration energy over a wide frequency range for self-powered electronics. *ACS nano*, *11*(2), pp.1728-1735.

[143] S. Roundy, E. S. Leland, J. Baker, et al. Improving power output for vibration-based energy scavengers. *IEEE Pervasive Computing*, 2005, 4: 28-36.

[144] Henry A. Sodano, Gyuhae Park, et al. Model of piezoelectronic power harvesting beam. *Proceedings of IMECE'03,* 2003:1-10.

[145] Yaowen Yang, Lihua Tang, Hongyun Li. Vibration energy harvesting using Macro-fiber composites. *Smart Material structure*, 2009, 18:5025-5033.

[146] Jeon Y, Sood R, et al. MEMS power generator with transverse mode thin film PZT. *Sensors & Actuators: A. Physical*, 2005, 122 (1): 16-22.

[147] Renaud M. et al. Piezoelectric harvesters and MEMS technology: fabrication, modeling and measurements solid-state sensors, *Actuators and microsystems conference*, 2007: 891-894.

[148] Shen D N, Park J H, Ajitsaria J, Choe S Y, Wikle III H C and Kim D J. The design, fabrication and evaluation of a MEMS PZT cantilever with an integrated Si proof mass for vibration energy harvesting. *Journal of Micromechanics and Microengineering*. 2008,18(5): doi:10.1088/0960-1317/18/5/055017

[149] Shen D N, Park J H, Noh J H, et al. Micromachined PZT cantilever based on SOI structure for low frequency vibration energy harvesting. *Sensors Actuators A : Physical*. 2009, 155(1): 103-108.

[150] B S Lee, S C Lin, W J Wu, et al. Piezoelectric MEMS generators fabricated with an aerosol deposition PZT thin film. *Journal of Micromechanics and Microenoineering.*

2009,19:065014-21.

[151] M. Marzencki, Y. Ammar, and S. Basrour. Integrated Power Harvesting System Including a MEMS Generator and a Power Management Circuit. Transducers International Conference in Solid-State Sensors, *Actuators and Microsystems*, 2007: 887-890.

[152] Yen T T, Hirasawa T, et al. Corrugated aluminum nitride energy harvesters for high energy converstion effectiveness. *Journal of Micromechanics and Microenoineering.* 2016, 21(8):085037.

[153] Liu J Q, Fang H B, Xu Z Y, et al. A MEMS-based piezoelectric power generator array for vibration energy harvesting. *Microelectronics Journal.* 2013, 39(5): 802-806.

[154] Ottman G K, Hofmann H F, Bhatt A C, et al. Adaptive Piezoelectric Energy Harvesting Circuit for Wireless Remote Power Supply. *IEEE Transactions on Power Electronics, 2002, 17*(5):669-676.

[155] Shu Y C, Lien I C. Analysis of power output for piezoelectric energy harvesting systems. *Smart Materials and Structures, 2006, 15*(6): 1499-1512.

[156] Taylor G W, Burns J R, Kammann S A, et al. The energy harvesting Eel: a small subsurface ocean/river power generator. *IEEE Journal of Oceanic Engineering, 2001, 26*(4): 539-547.

[157] Lefeuvre E, Badel A, Richard C, et al. A comparison between several vibration-powered piezoelectric generators for standalone systems. *Sensors and Actuators, 2005, 126*(2):405-416.

[158] Garbuio L, Lallart M, Guyomar D, et al. Mechanical Energy Harvester With Ultralow Threshold Rectification Based on SSHI Nonlinear Technique. *IEEE Transactions on Industrial Electronics*, 2009, 56(4): 1048-1056.

[159] Ottman G K, Hofmann H F, Lesieutre G A. Optimized Piezoelectric Energy Harvesting Circuit Using Step-Down Converter in Discontinuous Conduction Mode. *IEEE Transactions on*

Power Electronics, 2003, 18(2): 696-703.

[160] Lallart M, Richard C, Petit L, et al. High efficiency, wide load bandwidth piezoelectric energy scavenging by a hybrid nonlinear approach. *Sensors and Actuators A*, 2011, 165(2): 294-302.

[161] Guan M J and Liao W H. Characteristics of Energy Storage Devices in Piezoelectric Energy Harvesting Systems. *Journal of Intelligent Material Systems and Structures*, 2008, 19(6): 671-680.

[162] Challa V R, Prasad M G, Shi Y, et al. A vibration energy harvesting device with bidirectionalresonance frequency tenability. *Smart Materials and Structures*, 2008, 17(1):015035-035044.

[163] Peters C, Maurath D, Schock W, et al. Novel electrically tunable mechanical resonator for energy harvesting. *Procedings of PowerMEMS*, 2008: 253-258.

[164] Guyomar D, Lallart M, Monnier T. Stiffness Tuning Using a Low-Cost Semiactive Nonlinear Technique. *IEEE/ASME Transactions on Mechatronics*, 2008, 13(5):604-607.

[165] Lallart M, Anton S R, Inman D J. Frequency Self-tuning Scheme for Broadband Vibration Energy Harvesting. *Journal of Intelligent Material Systems and Structures*, 2010, 21(9):897-906.

[166] Leland E S, Wright P K. Resonance tuning of piezoelectric vibration energy scavenging generators using compressive axial preload. *Smart Materials and Structure*, 2006, 15(5): 1413-20.

[167] Eichhorn C, Goldschmidtboeing F and Woias P. A frequency piezoelectric energy convert based on a cantilever beam. *Procedings of PowerMEMS*, 2008: 309-312.

[168] Xia, Z., Wedel, A. and Danz, R., 2003. Charge storage and its dynamics in porous polytetrafluoroethylene (PTFE) film electrets. *IEEE transactions on dielectrics and electrical insulation, 10*(1), pp.102-108.

[169] Wang, Chen, and Jie-Rong Chen. "Studies on surface graft polymerization of acrylic

acid onto PTFE film by remote argon plasma initiation." *Applied Surface Science 253.10 (2007):* 4599-4606.

[170] Feipeng Wang. Piezoelectric properties and charge dynamics in poly (vinylidene-fluoride-hexafluoropropylene) copolymer films with different content of hfp[J]. *IEEE Transactions on Dielectrics and Electrical Insulation. 2006, 13(5)*:1132-1139.

[171] Gorokhovatsky Y.A. et al. Thermal stability of polarization structures in corona-charged P(VDF-HFP) copolymer films[C]. 11th *International Symposium on Electrets. 2002.* pp.134-137.

[172] Preparation and assessment of piezo- and pyroelectric poly(vinylidene fluoride-hexafluoropropylene) copolymer films[J]. *Applied Physics. 2001, 73(5):*641-645.

[173] Takumi Tsutsumino, Yuji Suzuki, Nobuhide Kasagi, Yoshihiko Sakane. Seismic power generator using high-performance polymer electret[C]. Istanbul: *19th IEEE International Conference on Micro Electro Mechanical Systems, 2006:*98-101.

[174] His-wen Lo, Yu-Chong Tai. Parylene-based electrets power generators[J]. *Journal of Micromechanics and Microengineering. 2008,* 18:8.

[175] YI Jin-gang et al. A PVDF-Based Deformation and Motion Sensor: Modeling and Experiments[J]. *IEEE Sensors Journal. 2008, 8*(4):384-391.

[176] Okubo, Masaaki, et al. "Preparation of PTFE film with adhesive surface treated by atmospheric-pressure nonthermal plasma graft polymerization." *IEEE transactions on industry applications 46.5 (2010):* 1715-1721.

[177] Wu, Xing-Long, et al. "Enhanced working temperature of PEO-based polymer electrolyte via porous PTFE film as an efficient heat resister." *Solid State Ionics 245 (2013):* 1-7.

[178] Onodera, Tasuku, et al. "Structure and function of transfer film formed from PTFE/PEEK polymer blend." *The Journal of Physical Chemistry C 121.27 (2017):* 14589-14596.

[179] Yu, Chung-Hao, et al. "PTFE/polyamide thin-film composite membranes using PTFE films modified with ethylene diamine polymer and interfacial polymerization: Preparation and

pervaporation application." *Journal of colloid and interface science 336.1 (2009):* 260-267.

[180] Zhang, M. C., et al. "Surface modification of aluminum foil and PTFE film by graft polymerization for adhesion enhancement." *Colloids and Surfaces A: Physicochemical and Engineering Aspects 176.2-3 (2001):* 139-150.

[181] Ji, L. Y., et al. "Oxidative graft polymerization of aniline on PTFE films modified by surface hydroxylation and silanization." *Langmuir* 18.23 (2002): 9035-9040.

[182] Gerard, M., Christopher R. Bowen, and Fayek H. Osman. "Processing and properties of PTFE-FEP-PTFE ferroelectret Films." *Ferroelectrics* 422.1 (2011): 59-64.

[183] Basso, Heitor Cury, et al. "Three-layer ferroelectrets from perforated Teflon®-PTFE films fused between two homogeneous Teflon®-FEP films." 2007 Annual Report-Conference on Electrical Insulation and Dielectric Phenomena. IEEE, 2007.

[184] Zhang, Xiaoqing, Joachim Hillenbrand, and Gerhard M. Sessler. "Thermally stable fluorocarbon ferroelectrets with high piezoelectric coefficient." *Applied Physics A* 84.1 (2006): 139-142.

[185] Mohebbi, Abolfazl, et al. "Cellular polymer ferroelectret: a review on their development and their piezoelectric properties." *Advances in Polymer Technology* 37.2 (2018): 468-483.

[186] Zhang, X., J. Hillenbrand, and G. M. Sessler. "Ferroelectrets with improved thermal stability made from fused fluorocarbon layers." *Journal of Applied Physics* 101.5 (2007): 054114.

[187] Zhang, Yan, et al. "Ferroelectret materials and devices for energy harvesting applications." *Nano Energy* 57 (2019): 118-140.

[188] Zhukov, S., Fedosov, S. and von Seggern, H., 2011. Piezoelectrets from sandwiched porous polytetrafluoroethylene (ePTFE) films: influence of porosity and geometry on charging properties. Journal of Physics D: Applied Physics, 44(10), p.105501.

[189] Xi, F., Pang, Y., Li, W., Jiang, T., Zhang, L., Guo, T., Liu, G., Zhang, C. and Wang, Z.L., 2017. Universal power management strategy for triboelectric nanogenerator. Nano Energy, 37, pp.168-176.